INVESTIGATION OF GENE DELIVERY CAPABILITY OF SELENIUM NANOPARTICLES COMPARED TO FUNCTIONALIZED SINGLE WALL CARBON NANOTUBES IN *ARABIDOPSIS THALIANA*

by

Gülnur ŞENER

Submitted to the Graduate School of Engineering and Natural Sciences in partial fulfillment of the requirements for the degree of Master of Science

Sabancı University

June 2024

ABSTRACT

INVESTIGATION OF GENE DELIVERY CAPABILITY OF SELENIUM NANOPARTICLES COMPARED TO FUNCTIONALIZED SINGLE WALL CARBON NANOTUBES IN *ARABIDOPSIS THALIANA*

GÜLNUR ŞENER

Molecular Biology, Genetics and Bioengineering

MSc Thesis, June 2024

Thesis Supervisor: Asst. Prof. Stuart James Lucas

Keywords: plant biotechnology, gene delivery efficiency, selenium nanoparticles, carbon nanotubes, toxicity

As an ancient method, plant breeding is not enough to meet growing quality food demand. Genetic engineering stands out in plant biotechnology as a supportive and new approach. Effective gene editing is possible with an effective gene delivery. Gene delivery methods have been expanded by using nanomaterials for several decades. The cell walls, unlike other living cells, are the limiting factor in the transfer of genetic material in plants. One of the most widely used nanomaterials on this subject is carbon nanotube (CNT) and its functionalized versions; however, it has toxicity in plant tissues. On the other hand, selenium nanoparticles (SeNPs) are preferred in therapeutic applications for mammalians for gene

transfer, because of their additional benefits, yet they have never been used in plant biotechnology. In this study, SeNPs were synthesized chemically (about 20 nm). Then, SeNPs and polyethyleneimine functionalized single-walled CNTs (PEI-SWNTs) were characterized and applied to the model plant organism *Arabidopsis thaliana* from leaves and roots. As a result of the observations, it has been understood that SeNPs are 100 times less phytotoxicity than PEI-SWNTs. Furthermore, the gene transfer efficiencies of these two nanomaterials have been investigated with the help of plasmids and linear GFP DNA. According to the expression levels of GFP in applied tissues, the SeNPs were 45% more effective in linear DNA transport compared to PEI-SWNTs, and PEI-SWNTs have been found to be more effective in carrying plasmid DNA than SeNPs. However, SeNPs is a promising nanoparticle for approaches to linear DNA or RNA transfer in plants because of its less toxic effect in plants. With further studies, the adequacy of SeNPs for plant gene engineering studies can be investigated in other plant species as well.

ÖZET

ARABİDOPSİS THALİANA BİTKİSİNDE SELENYUM NANOPARÇACIKLARININ FONKSİYONELLEŞTİRİLMİŞ TEK DUVARLI CARBON NANOTÜPLERİNE KIYASLA GEN AKTARIM KAPASİTESİSİN ARAŞTIRILMASI

GÜLNUR ŞENER

Moleküler Biyoloji, Genetik ve Biyomühendislik
Yüksek Lisans Tezi, Haziran, 2024

Tez Danışmanı: Dr. Öğr. Üyesi Stuart James Lucas

Anahtar Kelimeler: bitki biyoteknolojisi, gen aktarımı, selenium nanopartikül, karbon nanotüp, toksik etki

Eski bir method olan bitki ıslahı, artan kaliteli gıda talebine karşılamak için yeterli değildir. Destekleyici ve yeni bir yaklaşım olarak, bitki biyoteknolojisinde genetik mühendisliği öne çıkıyor. Etkili gen düzenleme, etkili bir gen iletimi ile mümkündür. Gen iletim yöntemleri, nanomalzemeler kullanılarak birkaç on yıldır daha da genişletilmiştir. Bitki hücrelerinin diğer canlı hücrelerden farklı olarak sahip olduğu hücre duvarı genetik materyalin aktarılması konusunda sınırlayıcı faktördür. Bu konuda yürütülen çalışmalarda en çok kullanılan gen aktarım yöntemlerinden biri karbon nanotüp (CNT) ve onun foksiyonelleştirilmiş versiyonlarıdır. Fakat bitki

dokularında sebep olduğu toksik etki sınırlayıcı bir faktördür. Metalik nanopartiküllerden biri olan ve biyomedikal gibi alanlarda birçok yararlı etkisi sebebiyle tercih edilen ve gen aktarımı için kullanılan Selenyum nanopartiküller (SeNPs), bitki biyoteknolojisinde gen aktarım amacıyla hiç kullanılmamıştır. Bu çalışmada kimyasal yöntemle SeNPs (yaklaşık 20 nm) sentezlenmiştir. Sentezlenen SeNPs ve polietilenimin ile fonksiyonelleştirilmiş tek duvarlı CNT (PEI-SWNTs) karakterize edilerek model bitki organizması olan *Arabidopsis thaliana*'ya yaprak ve kökten uygulanmıştır. Elde edilen gözlemler sonucunda SeNPs' nin PEI-SWNTS den 100 kat daha az fitotoksik etki bıraktığı anlaşılmıştır. Ayrıca, bu iki nanomateryalin gen aktarım verimlilikleri, GFP plasmit ve doğrusal DNA'lar yardımıyla araştırılmıştır. Yapılan çalışmalar sonucunda GFP ışıması uygulama yapılmış dokularda saptanmıştır ve GFP geninin ekspresyon seviyesindeki değerleri incelenerek doğrusal DNA taşıma konusunda SeNPs'nin, PEI-SWNTS'ye kıyasla %45 daha etkili iken, PEI-SWNTS plasmid DNA taşımada SeNPs den daha etkili olduğu saptanmıştır. Fakat sentezlenen SeNPs'nin daha az toksik etkisi sebebiyle, SeNPs'nin bitkilerde doğrusal DNA yahut RNA aktarımı planlanan yaklaşımlar için umut vaat eden bir nanopartiküldür. İleri çalışmalar ile başka bitki türlerinde de SeNPs'nin bitki gen mühendisliği çalışmaları için yeterliliği araştırılabilir.

ACKNOWLEDGEMENTS

I want to sincerely thank everyone who supported me along the way while I pursued my master's degree. Additionally, I want to express my gratitude to Nihal Öztolan Erol and Stuart James Lucas, my advisors, for their knowledge and guidance on this study. I would like to express my sincere gratitude to Zehra Çobandede, who supported me in every way during this study and my graduate adventure at Sabancı University. Their extensive knowledge base, guidance, and academic acumen have greatly enhanced and directed my comprehension of the subject. Additionally, I am grateful to Ravzanur Yazıcıoğlu, Kadriye Kahraman, Gülce Güralp, Serap Sakarya and the entire 'SJL Lab' team for their help and support during my thesis work. My sincere gratitude to my lovely family and dear friends, Sümeyye Narin, Aybüke Büşra Özer, Cemile Uslu, Ahmet Baki Şahin, Büşra Elif Kıvrak, and Gülşah Yıldız, for their unwavering support, understanding, and encouragement throughout the entire master adventure. I consider myself lucky to have received your support in finishing this master's thesis.

In conclusion, Tübitak 1004 Project LIGNONANO is to be thanked for the research funding and scholarship it has given.

To my past self …

TABLE OF CONTENTS

LIST OF TABLES

LIST OF FIGURES

LIST OF ABBREVIATONS

° Degree

°C Degree Celsius

BSA Bovine Serum Albumin

cm centimeter

CNT Carbon Nanotube

CNT-COOH carboxylic group being single walled carbon nanotube.

Cp cycle number

dNTP Nucleotide mix

E. coli Escherichia coli

GFP Green Fluorescent Protein

gr gram

H_2O_2 Hydrogen peroxide

HCl Hydrochloric acid solution

L Liter

M Molar

mg milligram

min minute

mL milliliter

mm millimeter

mM millimolar

mRNA messenger RNA

NM nanomaterials

nm nanometer

NP nanoparticles

PBS Phosphate-Buffered Saline

PCR Polymerase Chain Reaction

PEI polyethyleneimine

PEI-SWNTS polyethyleneimine functionalized single walled carbon nanotube.

qPCR quantitative Polymerase Chain Reaction

Se Selenium

SeNPs Selenium Nanoparticle

uL microliter

1.INTRODUCTION

1.1. Genetic Engineering and Gene Delivery in Plant Systems

Climate change and global warming is one of the biggest threats to the world and human civilization. Problems that occur due to global warming such as high rises in average temperatures, alterations of climatic conditions, declining water resources, extreme weather conditions, and soil salinization adversely affect agricultural production and productivity, food safety and quality while the food demand is constantly increasing with the world population [2, 3]. In the face of this threat, the necessity of innovations in agricultural production increases to produce good quality and safe food.

Traditional plant breeding is a method performed in the past to enhance overall crop productivity [4]. However, the breeding methods are time-consuming and don't allow the introduction of new desired characteristics to a plant that it was lacking before. It's time-consuming because, since the flowering cycle of perennial plants is long, achieve the targeted feature, many years are required. Alternatively, plant genetic engineering is accepted as a potential supplement to regular breeding methods to help meet the rising food demand [5, 6]. Genetic engineering could be performed to enable plants to provide higher yields even under severe biotic and abiotic stress conditions [7], to make them resistant to insects and pathogens [8], to improve their nutritional profile or to introduce new properties [9]. Genetic engineering approaches in plant systems include the process of introducing new genes of interest or manipulating existing genes into the genome of the host plant to generate plants with modified genotypes and eventually phenotypes. These approaches generally rely on efficient gene delivery. By delivering a gene, genetic manipulation is made possible via genetic engineering tools such as CRISPR/Cas9. Thus, the main base of genetic engineering of plants is delivery of genetic materials.

Various ways exist to deliver genetic materials to plant systems. Among the approaches developed for nucleic acid delivery in plants, there are several different ways such as the use of *Agrobacterium* species, biolistic particle bombardment, polyethylene glycol (PEG)-

mediated transfection, viral transfection, and microinjection [10, 11]. These are listed in table 1 with their merits and limitations.

Table 1: The merits and limitations of several delivery methods used in plant genetic engineering.

Traditional Delivery Methods	Merits	Limitations	Ref.
Agrobacterium	introduces DNA segments into the genome of the host plant through natural infection. Well-established protocols available, low cost and widely used	Genotype and species dependent; narrow host range, limited cargo type, poor gene transfer efficiency	[12, 13]
Particle bombardment	promising in terms of mitochondrial and chloroplast genome engineering, appropriate for all cargos	Causes random insertions, tissue- type dependent delivery, host genome damage, sophisticated equipment needed	[14, 15]
Microinjection	Direct injection of desired DNA into cells using a fine needle or micropipette	Limited cargo-carrying capacity, low efficiency, applicable only for large cells	[16]
PEG	High efficiency in protoplast, appropriate for all cargos	Time-consuming, only in protoplast cell, inefficient regeneration, polyploid formation	[17]
Plant virus	Genotype independent, provide high level of transient expression	limited cargo size, plant species restrictions, safety concern in crop yield	[18, 19]

Agrobacterium-mediated gene delivery is accepted as the predominant method in plant genetic engineering[13]. Nonetheless, there are several significant drawback of utilizing *Agrobacterium* for plant transformation relating to its specificity to particular hosts and restricted range of compatible species, leading to diminished transformation levels in certain plants[20]. Furthermore, about delivery and regeneration, *Agrobacterium* species often manifest insufficient transformation efficiency in monocotyledonous compared to

dicotyledonous plants. In addition, *Agrobacterium* prompts random DNA integration, which may lead to disruption or insertion of critical genes into regions of the genome with inconsistent or poor expression [13]. Other physical methods like particle bombardment or electroporation require sophisticated devices which cause high cost for operation, which clearly restrict their worldwide usage [21]. Besides, these kinds of techniques generally leads deterioration of the target plant tissue, and possess several restrictions such as limited cargo types while their efficiency is quite inferior [16].

In many economically notable plant or crop species, the desired genetic transformation protocol has not yet been established or only results with poor transformation efficiency have been obtained, despite years of scientific advancements in the field of plant genetic engineering [22]. The dense, multilayered cell wall of plant cells, which is made of cellulose microfibrils is the most serious obstacle to gene transfer to plants. Therefore, research on protoplasts—plant cells lacking a cell wall—has been performed to improve the efficacy of gene transfer. However, for many types of plants there are no entirely optimal strategies for the sustainability and maintenance of protoplast culture as well as the regeneration of new plantlets from protoplasts [23]. Therefore, delivering biomolecules that can lead to the desired transformation through plant cell walls and eventually into plant cells as a genetic engineering approach is a significant hindrance for effective and successful genetic engineering in plants [24]. Despite all the advancements achieved in the field, plant biotechnology today still lacks a method for passively transferring desired forms of biomolecules to a wide range of plant species without the necessity of external force leading to tissue damage.

1.2. Nanoparticles for Gene Delivery in Plant System

1.2.1. Nanoparticles and Applications

Nanoparticles (NPs) include materials ranging in size from 1 to 100 nanometers (nm), possessing either inorganic or organic compositions [25]. Among advancements in nanotechnology, the utilization of NPs as delivery agents within living systems bears certain significance [26]. NP mediated delivery can provide efficient manipulation at the subcellular level, affording remarkable control over exogenous interactions with biological entities [27].

This capability renders them original substances for drug delivery and gene transfer into different kind of living systems.

Based on their forms, shapes, sizes, composition, chemical and physical characteristics, nanoparticles could be divided into many different groups. Nanoparticles are often categorized into three main types: (1) organic NPs such as liposomes, micelles, dendrimers, or compact polymers; (2) inorganic NPs such as metal (gold, silver, etc.) nanoparticles, quantum dots, and (3) carbon-based NPs such as carbon nanotubes (CNT), fullerenes, and carbon nanofibers. Nanoparticles' capability to synthesized with physical features such as high surface area to volume ratio, distinctive structures, electromagnetic properties, shape, and size, as well as chemical characteristics like cation exchange capacity, raised reactivity, significant ion adsorption ratio, and catalytic properties provide wide utilization in distinct scientific fields. Besides, they demonstrate biological functionalities including antimicrobial activity, interactions with cellular components, and effects on toxicity, rendering them requisite across a plethora of disciplines [28]. Notably, some NPs exhibit characteristics of non-viral vectors as like as being biocompatible and non-cytotoxic, facilitating their efficient transportation of several biomolecules into living cells [29]. Their small size, versatile physical and chemical properties, and diverse functions further underscore their phenomenal utility in bioengineering applications over decades.

1.2.2. Nanoparticle Applications on Plant Science

The application of nanomaterials has been extended to plant science and been employed to improve agronomic characteristics of plants, in many research studies [30, 31]. Within this framework, nanoparticles (NPs) have been applied as nano-fertilizers [32], pesticides, herbicides, carriers enhancing the controlled release of agrochemicals [33] ,and nutrients proposed to improve crop yield [34]. Moreover, particular investigated nanomaterials have been established to accelerate plant acclimatization to climate change stressors, thereby improving stress tolerance [35, 36]. Furthermore, research has stated that nanomaterials can lead to significant enhancements in plant tissue culture stages, including callus induction, somatic embryogenesis, organogenesis, and the production of secondary metabolites [37].

1.2.3. Nanoparticle Uptake on Plant System

Many investigations about NP utilization in plant systems suggest that NPs have the ability to penetrate plant cell wall, although the exact mechanism of NPs uptake remains insufficiently characterized. It is assumed that the uptake and transport of nanoparticles by plants relies on the particle size, surface charge, concentration, exposure time of the nanoparticle and plant type. Nanoparticles may enter the plant system via distinct pathways including stomata, root tips, and microcavities on leaf surfaces. Figure 1 illustrates the leaf and root uptake routes schematically. After penetration, NPs may move into the plant system via diffusion from the apoplast, bulk flow, and phloem loading. Similar to their penetration mechanism, the transport of nanoparticles through plant systems is affected by various factors such as size and morphology, surface characteristics, solution pH, and the existence of other ions or compounds in the solution [38].

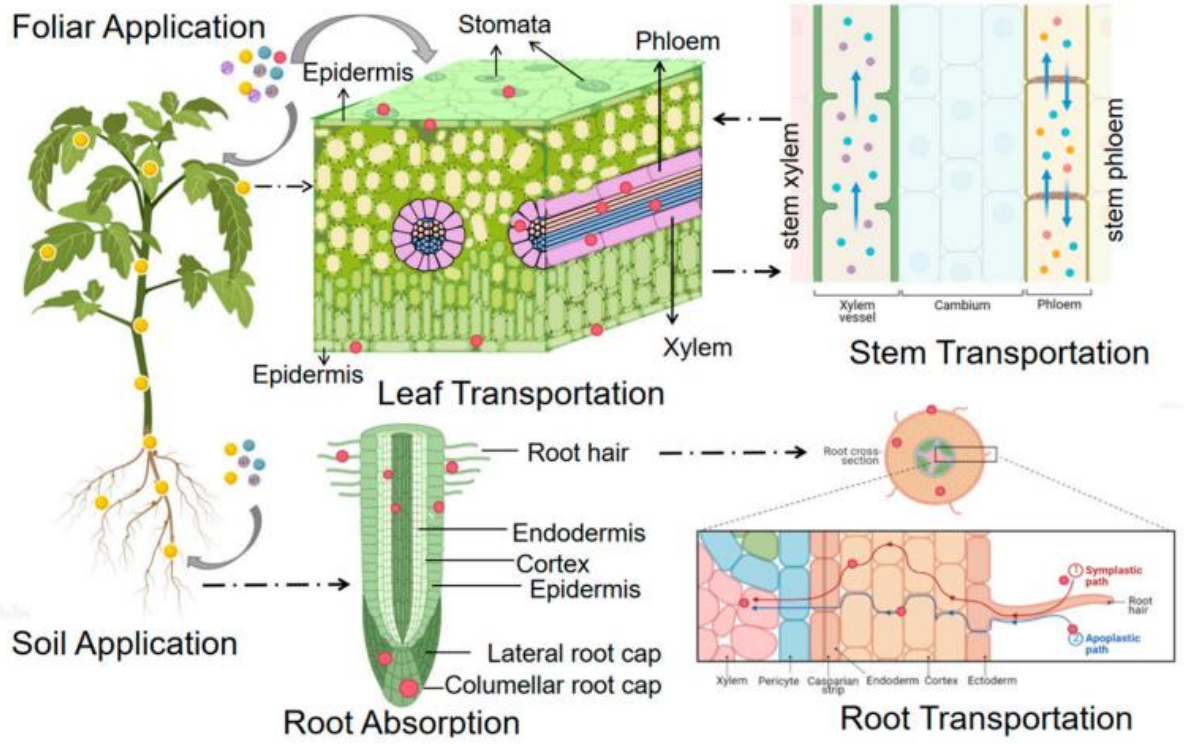

Figure 1 : İllustration of uptake and translocation pathways of NPs in plants through foliar and root applications. [38]

For NP uptake from mature plant leaves some natural barriers exist such as the waxy cuticle of the leaf epidermis that is mainly made up of wax, cutin, and pectin [39]. This configuration reduces water loss during growth. However, uptake of NPs though plant leaf is restricted due to limited size of pore channels in the cuticle structure. In some research

studies, applied NPs have been accumulated in leaf epidermis and vascular tissue. In contrast, in many studies, it has been reported that NPs are able to translocate to other plant parts. According to these studies, it has been stated that the stomatal pathway could be an uptake mechanism of NPs through plant leaves. The stomata size is typically 10–100 μm, which varies in the size and density of the stomata in different plant species. The precise size exclusion limit (SEL) of the stomatal aperture for nanoparticle diffusion remains unclear because of the distinct geometric structure and physiological role of stomata [40]. Many plant species demonstrate stomata solely on the lower epidermis of leaves, whereas a few have stomata on both upper and lower epidermal surfaces. In occasions where stomata exist in both sides of leaves, dicotyledonous plants typically demonstrate approximately 1.4 times more stomata on the lower epidermis compared to the upper epidermis [41]. Thus, for NPs application from leaves, preferring abaxial application is more logical to enhance NPs uptake.

For root applications of NPs, firstly NPs are absorbed via root hairs. Roots hairs secrete some chemical substances that are negatively charged, this is thought to be an enhancing factor for the uptake of positively charged NPs [33]. Moreover, lateral roots generation provides another absorption surface for NPs, this also rises possibility of NPs penetration through the root column [42]. In comparison root epidermis and leaf epidermis are similar, however, the root tips epidermis and hair surface of roots are not completely generated. Thus, in applications of NPs from roots, possibly they directly interfere and uptake [43].

Penetrating plant tissue does not mean entering the plant cell. Nanoparticles that have penetrated plant tissue can enter plant cells though several pathways. These include endocytosis, ion pathways or by generating physical damage on cell membrane proteins [33]. Nanoparticle entry to the plant cell is thought to be the main limiting factor because of the rigid plant cell wall. Yong et al. (2023) stated that 50 nm is the threshold for size of nanoparticles that can enter plant pollen cells [44]. It has been established in previous studies that NPs should be smaller than 20 nm at least in one dimension to be absorbed by plant cells [45]. Additional characteristics of nanomaterials, such as their shape and zeta potential - a physical property of particles that manipulate its electrostatic interactions in dispersions- also affect their capability to penetrate plant cells. Nano-delivery systems demonstrate high efficiency when applied NPs have zeta potential values over +30 mV. This is attributed to thought that tendency for low zeta potential values to prompts aggregation, whereas higher zeta potential values contribute to enhanced stability of the delivery system [46, 47]. Zhang and colleagues performed several different shapes and sizes of gold nanoparticles (AuNPs),

including spheres and bars forms, to administer RNA interference (RNAi) into *Nicotiana benthamiana* leaves. Bar-shaped AuNPs demonstrated superior transferring efficiency compared to spherical AuNPs [48].

To this date, it has been exhibited that dicotyledon and monocotyledon plants display varying degrees of direct uptake of many different type of NP types such as mesoporous silica nanoparticles [49], carbon nanotubes (CNTs) [50], quantum dots [51], and metal/metal oxide NPs [52, 53]. Some NPs, which are taken in through different routes and degrees after application, display phytotoxic effects in the form of cellular level, oxidative stress, or structural damage to DNA [54]. On the contrary, it has been shown that some NPs facilitate root development and chloroplast generation [55]. The complex reasons why different NO dosages may have phytotoxic effects or result in growth enhancement when applied to a plant species require further investigation to complete our understanding. To improve plant genetic engineering via NPs, these kinds of gaps must be closed. However, results where NP uptake is proven have opened inspiring avenues for nanomaterial-based DNA delivery in plants [56]. Since nanoparticles are small in size, they can deliver biomolecules with them into plant cells while protecting them from degradation [57].

1.2.4. Nanoparticle Mediated Gene Delivery on Plant System

In 2007, Torney and co-researchers documented a pioneering study that investigated nanoparticle-mediated simultaneous delivery of DNA to *Nicotiana tabacum* plants using biolistic delivery of 100–200-nm- gold-capped mesoporous silica nanoparticles (MSN) [58]. In this research, a chemical expression stimulant was loaded into pores measuring approximately 3 nanometers across in mesoporous silica nanoparticles (MSN). Subsequently, these MSNs were capped with gold nanoparticles (NPs) in a covalent manner. The capped MSNs then have been coated with Green Fluorescent Protein (GFP) plasmids and applied into *Nicotiana tabacum* cotyledons via a gene gun. By uncapping and release of the GFP plasmid the GFP expression was initiated [58]. This work proves that DNA can be delivered via NPs in plant systems. However, because many factor-dependent structure-function parameters of nanoparticles have not yet been entirely optimized to passively transit through the plant cell wall, many delivery strategies still require an external force such as a gene gun, electromagnetic field, or PEG transfection (osmotic pressure) in protoplast transformation applications [59-62]. Although they are penetrating with help of chemical or

physical assistance, the usage of NPs with the advantages of small sizes and high surface area still gave superior performance than traditional methods which was also confirmed by another MSN study conducted by Torney and colleagues. In this research they achieved transgene expression with 1000 times less amount of DNA than the hundreds of micrograms of DNA that is typically necessary for conventional PEG transfection in protoplasts [58]. Nevertheless, recent research has documented promising outcomes regarding the use of NP-mediated delivery on plants without any external force, both in laboratory settings (*in vitro*) [63, 64] and in living organisms (*in vivo*) [65, 66]. Figure 2 indicates some achieved nanoparticle mediated gene delivery approaches in plants. For instance, successful delivery has been demonstrated in *N. tabacum* protoplasts [64] and *Arabidopsis thaliana* roots [67]. These types of studies demonstrate the possibility of delivering nanoparticles passively to plants with high efficiency and low toxicity. Although additional research is required to improve the characteristics and functionalization of NPs, the initial findings are encouraging for the continued investigation of NPs as a means of delivering biomolecules to plants, which can also overcome the restrictions of traditional approaches.

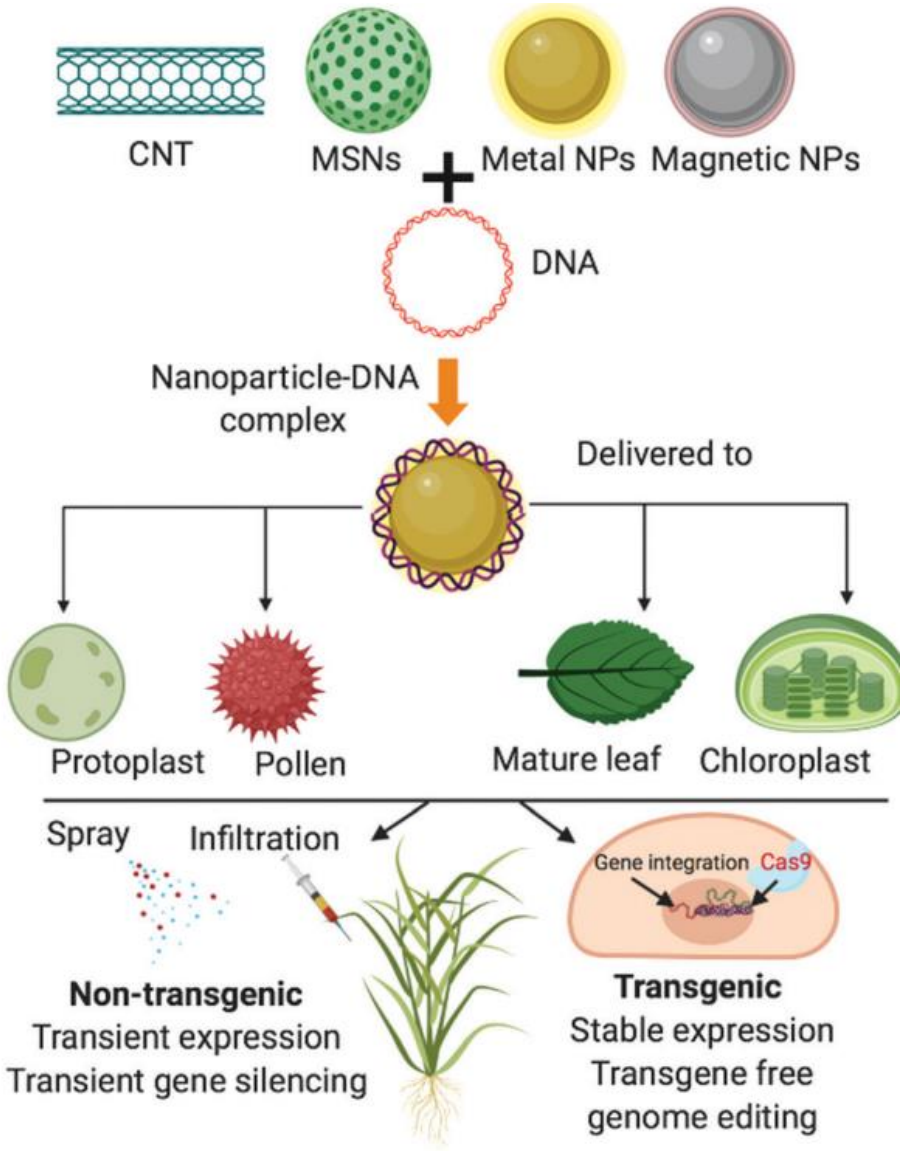

Figure 2 : Schematic illustration of delivery of DNA cargo to some part of plant via some nanomaterials [10]

1.3. Carbon Nanotubes

With conspicuous physicochemical and structural features, including noteworthy electrical and thermal conductivity, the presence of a hollow cavity, and remarkable tensile strength, carbon nanotubes (CNT) are a prominent type of nanomaterial [68]. Due to these particular characteristics, CNTs are valuable tools in the biotechnology fields such as biomedical engineering [69], and drug delivery. CNTs can be classified into 2 distinct groups: multiwalled carbon nanotubes (MWNTs) and single-walled carbon nanotubes (SWNTs).

MWNTs are comprised of many coaxially aligned cylinders. Every cylinder is made up of a solitary graphene sheet surrounding a hollow core [70]. MWNTs external diameters are ranging from 2 to 100 nm and an inner diameters of 1 to 3 nm [71]. The length of MWNTs ranges from 1 to several micrometers. However, SWNTs are comprised of a solitary graphene cylinder with a diameter ranging from 0.4 to 2 nm [72]. SWNTs are able to exhibit either metallic or semiconducting properties depending on their helicity and diameter [73]. SWNTs typically form in hexagonal, close-packed bundles, bound together by van der Waals forces.

SWNTs can be generated in a way that results in their smallest size being around 1 nanometer. This size is smaller than the limit at which plants can exclude particles, which is approximately 20 nanometers [45]. Additionally, SWNTs have a significantly large surface area. Hence, the consequently substantial surface area to volume ratio is optimal for the swift loading of a significant amount of biological cargo. The diameter of SWNTs is smaller than 5 nm enabling them to penetrate the plant's cell wall [74].

1.3.1. Modifications on Carbon Nanotubes

CNTs can be functionalized with some proteins, nucleic acids, medicines, and polymers. Covalent functionalization enhances the biocompatibility of CNTs [75]. The following are some examples of materials that are utilized in the functionalization of CNTs: Poly-3-aminobenzenesulfonic acid (PABS) [76], Fluorescein- polyethylene glycol (Fluor-PEG)[77], cellulase [78], chitosan [79], aliphatic amine group[80], arginine [81] and, polyethylenimine [82]. Functionalization of CNTs can decrease their toxicity to both plant and mammalian cells. However, studies have established that functionalized SWCNTs do not induce any adverse effects on cells or tissues when applied at concentrations lower than 10 mg L^{-1} [83]. In addition, functionalization of CNTs leads to superior dispersibility in solutions, enabling their efficient utilization for biological purposes.

1.3.2.PEI Functionalization of CNT

Polyethyleneimine (PEI) is a synthetic polymer that can be linear, branched, or dendrimer. It consists of repeating units that comprise amine groups and a spacer constructed of two

carbons aliphatic CH_2CH_2 groups [84]. PEI is a water-soluble compound that has been widely preferred in various fields because of its polycationic properties. These applications include cell culture [85], gene transfer, transfection and delivery [86, 87]. Demirer and colleagues utilized PEI for functionalization of carboxylated SWNTs for the purpose of gene transfer in a plant system [83]. This functionalization provides positive surface charge, and it allows them making interaction with DNA which is negatively charged biomolecules. This is illustrated in Figure 3. PEI functionalization aids in neutralizing the negative charge of DNA, due to its strong positive charge.

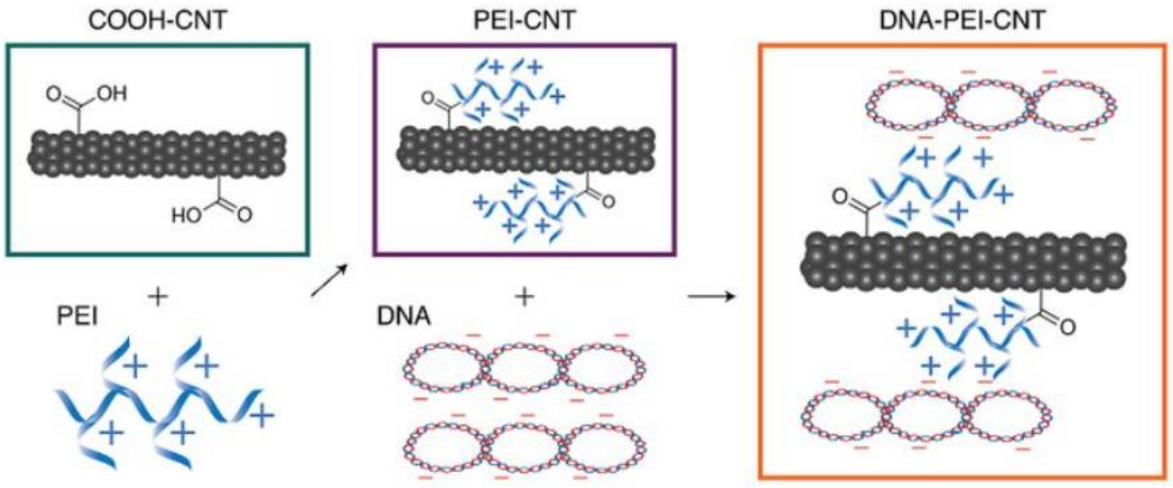

Figure 3 : PEI modifications of CNTs provide positive charge and enhance DNA binding.[46]

Additionally, this modification is thought to safeguard the DNA against endosomal destruction by the ‘proton sponge’ effect. In the photon sponge effect, PEI's buffering capacity causes osmotic swelling and rupture of endosomes. This results in the release of the cargo into the cytoplasm [87]. Demirer and coworkers have utilized PEI functionalized SWNT to passively transport DNA plasmids and protected siRNA. This resulted in successful transient GFP expression in *Eruca sativa* (arugula) leaves and transient suppression of constitutively produced GFP in transgenic *Nicotiana benthamiana* leaves [46]. This study also established that CNTs can be utilized to temporarily express GFP in *Triticum aestivum* (wheat). These suggest that by PEI functionalization SWNTs could deliver their cargo with minimal toxicity in both model and crop species. Figure 4 illustrates the delivery of PEI-SWNTs-GFP plasmid and obtaining GFP proteins in plant cells.

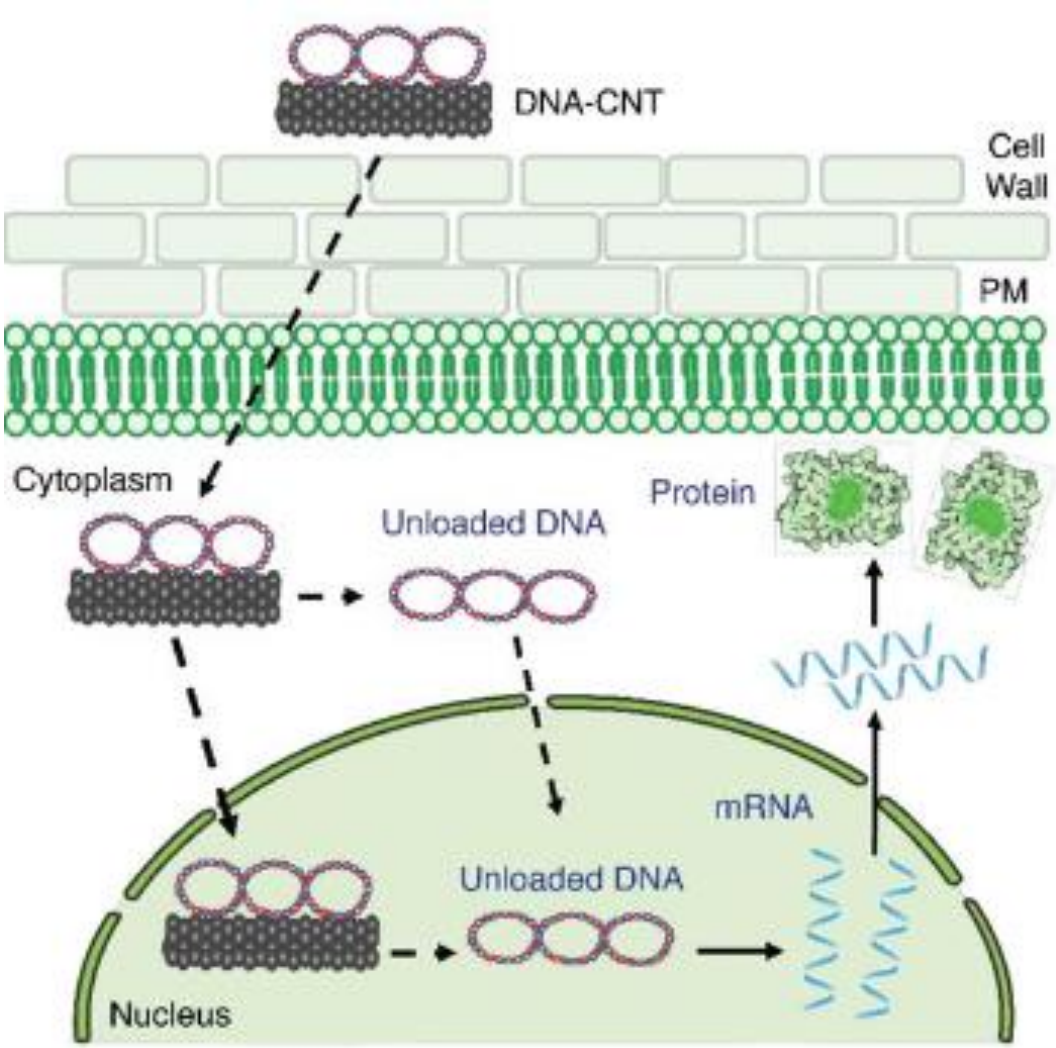

Figure 4: Schematic İllustration of DNA bound PEI-SWNT uptake from plant cells and following GFP gene expression [46].

1.4. Selenium Nanoparticles

Selenium is an element that found in group 16 of the periodic table. It exhibits semi-metallic characteristics and is commonly present in the soil in many inorganic forms, such as elemental Se (Se^0), selenide (Se^{2-}), selenate (SeO_4^{2-}), and selenite (SeO_3^{2-}). Selenium can also be found in organic forms such as seleno-methionine (SeMet) and selenocysteine (SeCys). Due to its exceptional ability to migrate to various oxidation states, it is

distinguished from the other elements in the same group [88]. In the past, Se was regarded as a toxic element; however, now it is categorized as an element that conducts out essential roles in various organisms, including mammals, bacteria, some insects and nematodes, archaea, and algae [89, 90]. The employment of Selenium (Se) has been emphasized in various scientific fields, including agriculture, food technology, and particularly in the medical and pharmaceutical field due to its distinctive physical, chemical, and biological characteristics [91-94]. Se is regarded as a beneficial element for plant as an antioxidant agent. It regulates the production and quenching of reactive oxygen species (ROS) [95]. However, high concentrations of inorganic Se able to trigger Se-amino acids generation that cause toxic effect in plant [96]. However, low dosages of inorganic Se can ensure various beneficial effects such as an antioxidant, antimicrobial, or stress-modulating agent. Additionally, it has been discovered that the element selenium functions as a component of antioxidant enzymes that may control the production and elimination of reactive oxygen species (ROS) in plants. [97-99]. Thus, its benefits to plants depend on factors such as its concentration, available form, application method, and the species and growth stage of the plant. The ability of Se to promote growth, improve crop quality, and lessen the negative effects of biotic and abiotic stressors are among its key plant-related characteristics. [95, 100, 101]. Toxic effects of Se and SeNPs are different also for plant applications. One possibility for reducing this negative effect and improving its biological properties has been found: selenium nanoparticles, or SeNPs. [96]. The cytotoxic effect of Se forms and SeNPs are illustrated in Figure 5.

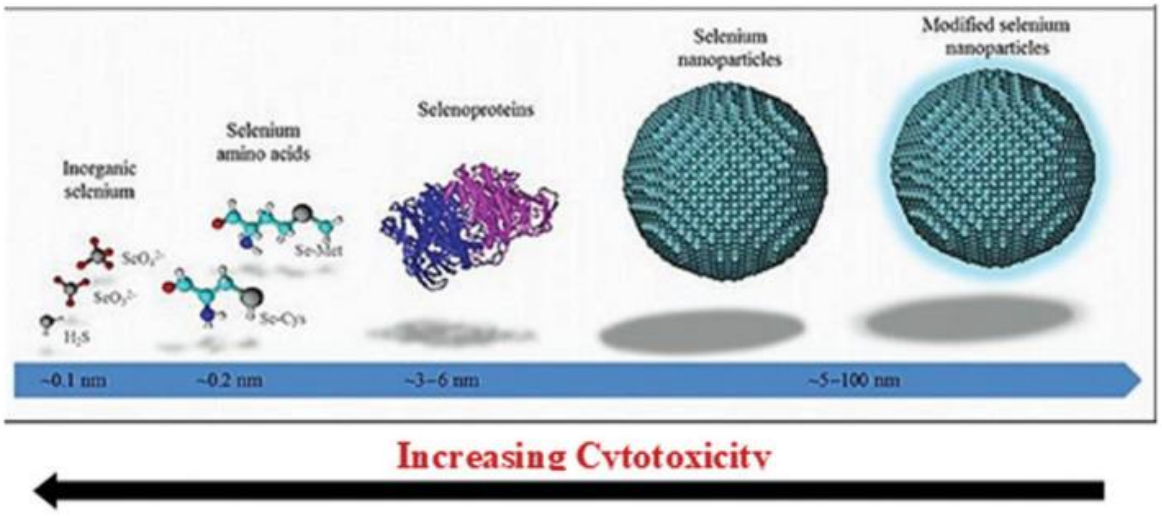

Figure 5 : Alterations of cytotoxic effect of selenium respect to various forms and size [102].

In one study SeNPs and SeO_4^{-2} toxic effects were compared both in tobacco and chilli plants.

According to results observable differences in toxic effects were attributed to uptake mechanisms. SeO_4^{-2} uptake occurs trough active transport through sulfate/phosphate transporters, while SeNPs uptake occurs via passive diffusion through membrane-localized aquaporin channels [103]. The reason why SeNPs have a lower toxicity level compared to other forms of selenium, such as SeO_3^{2-} or SeO_4^{2-} may be due to the gradual release of Se ions from NPs in plant tissue. Thus, selenium (Se) release occurs continuously at a low but constant level; this facilitates demonstration of antioxidant effects, and physiological effects such as promoting organogenesis and the growth of shoots and roots [104]. Moreover, studies have demonstrated that SeNPs enhance plant growth more effectively than inorganic forms of selenium (SeO_3^{2-} or SeO_4^{2-}). This suggests that SeNPs may play a role in the accumulation and secretion of signaling hormones, including ethylene, auxin (AUX), salicylic acid, gibberellins (GA), and cytokinin (CK), which are responsible for regulating plant growth and tissue differentiation [105, 106]. The data presented in this study demonstrate a clear difference from the data obtained from the SeNPs-applied tomato plant study. In the case of tomato plants, the application of SeNPs, which were synthesized using chemical reduction and had diameters ranging from 2 to 20 nm at concentrations of 10 and 20 mg/L, did not result in any toxicity symptoms. Furthermore, these SeNPs led to an increase in plant yield by 21% and 25%, respectively [107]. SeNPs applied to pepper plants were large in size and consequently caused toxic symptoms. However, no toxic effect was observed when the size of SeNPs applied to tomatoes was much smaller. This suggests that besides the size of SeNPs, other characteristics are also key factors in the beneficial or negative effects of SeNPs. It is possible to conclude from these findings that dosage, NP size, and surface structure all play a role in how plants respond to SeNPs.

1.4.1. SeNPs synthesis

Synthesis of SeNPs is possible by several methods. These could be classified into two categories: biological and chemical reduction as illustrated in Figure 6. Biological reduction consists of reduction of several organic or inorganic selenium precursors via biological materials for instance bacteria, fungi, algae, protein molecules, plant extracts, and alteration to non-toxic SeNPs. For example, in several different studies SeNPs synthesis has been reported by using fenugreek extract [108], *E. officinalis* fruit extract[109], microbial polymers [110], *Bacillus sp.* B2 [111], *Saccharomyces cerevisiae var. boulardii* yeast cells

[112], *Penicillium expansum* [113], *Aloe vera* leaf extract [114], *Burkholderia fungorum* [115], and lemon leaf extract [116]. In one study using coffee bean extract to reduce Na_2SeO_3 to Se is another example of an environmentally friendly synthesis. At room temperature, the reaction took only fifteen minutes to finish. The biological approaches for synthesizing nanoparticles are regarded as safe and referred to as "green chemistry" due to their ecologically benign nature. These methods involve natural processes that occur inside biological systems [117].

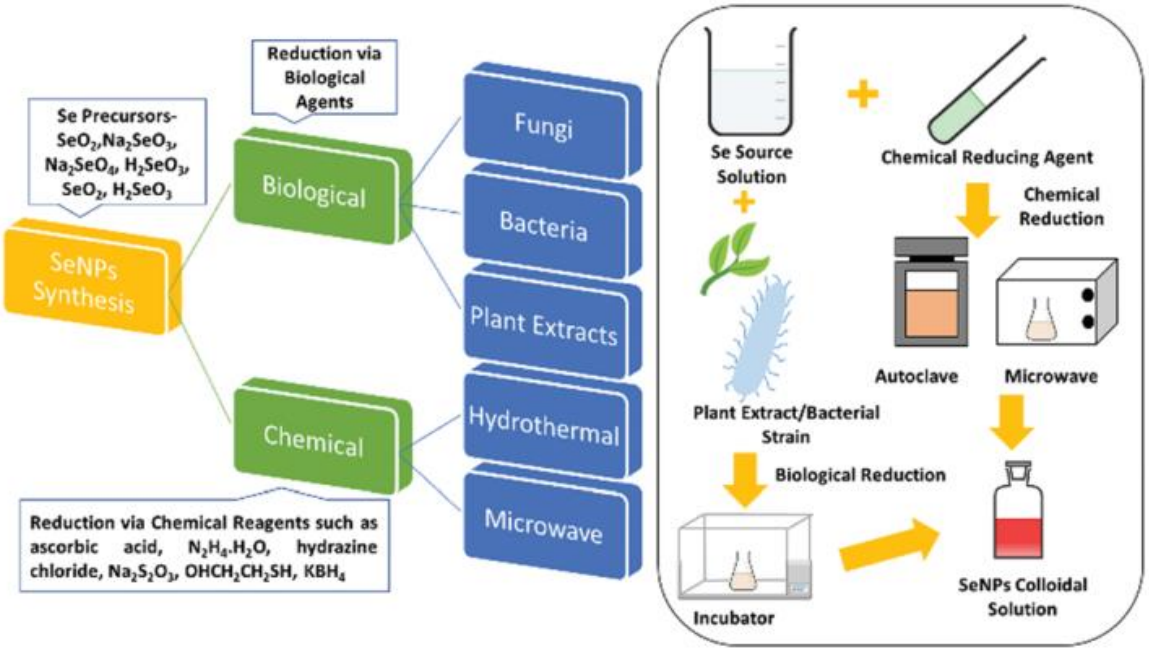

Figure 6 : Several synthesis pathways of selenium nanoparticles [92].

In chemical reduction methods selenium precursors are reduced via reducing agents. Chemical reduction methods are the ones that are abundantly used and simple [118]. These methods generally contain one selenium precursor, one reducing agent and one kind of stabilizing agent. These substances could be either natural or synthetic. According to these substances and the chemical synthesis method the size, zeta potential or toxic effect of SeNPs could differ. For instance, in one study, sodium selenite was reduced by ascorbic acid and polyvinyl alcohol (PVA) used as stabilizing agent to synthesize SeNPs [119]. The size of obtained SeNPs was measured as 70 nm in DLS. In another study, selenious acid as Se precursor was reduced with ascorbic acid using hyperbranched polysaccharide as the stabilizer, to provide highly stable 24 nm SeNPs [120]. Yu et al. indicated that according to their TEM images, monodisperse SeNPs with a size of around 70 nm were produced by reacting selenium dioxide with sodium thiosulfate in the presence of SDS for approximately

4 hours at room temperature [121]. In chemical synthesis due to its uncertainty, the hydrothermal approach is not popular to produce SeNPs. Nonetheless, the existing literature has shown that this approach can produce particles as small as 10–20 nm. Shin et al. were the first to utilize cellulose nanocrystals to reduce Na_2SeO_3 and produce SeNPs with a size ranging from 10 to 20 nm [122]. Hydrazine chloride reduction of Na_2SeO_3 resulted in the synthesis of spherical nanoparticles with an average size of about 15 nm [123]. Moreover, NPs derived from natural materials are reported to cause lower toxicity compared to those produced using chemicals [124]. For instance, ascorbic acid has been used as a reducing agent both provide efficient reduction and because it is naturality provide less toxicity. Also, using natural protein as a stabilizing agent could lead to less toxic effect. For instance, bovine serum albumin (BSA) is a most abundant plasma protein which its tertiary structure, it comprises three homologous domains (domains I, II, and III). [123]. For SeNPs synthesis using natural chemical substances leads to less toxic effect, and relatively small stabilizing agents can provide a smaller NPs size. The impact of nanoparticle size on the absorption of metal-based nanoparticles has been thoroughly investigated in the field of plant biotechnology. According to the research, metal-based nanoparticles smaller than 50 nm can enter plant leaves through the stomatal channel [123]. Thus, synthesized SeNPs smaller than this size are expected to enhance the uptake into plants.

1.5. *Arabidopsis thaliana*

Many recent plant science investigations have preferred to use *Arabidopsis thaliana* as their model organism [125]. It belongs to the mustard family (Cruciferae or Brassicaceae) with a wide natural distribution on earth throughout Europe, Asia, and North America. The full life cycle of *Arabidopsis thaliana*, including seed germination, rosette plant development, main stem bolting, blooming, and initial seed maturity, takes only 6 weeks. Compared to other plant species, all structures of *Arabidopsis thaliana* are relatively small. Its seeds are around 0.5mm in size, flowers are 2 mm length. Depending on the development conditions, seedlings grow into rosette plants with a diameter ranging from 2 to 10 cm [126]. It’s a dicotyledonous plant. *Arabidopsis thaliana* possesses smaller genome size and nuclear volume compared to other advanced flowering plants. Studies stated that a haploid nuclear genome size of *Arabidopsis thaliana* roughly 70,000 kilobase pairs [127]. Therefore, *Arabidopsis thaliana* is a highly preferred model plant in studies of plant genetics. Numerous

mutations and polymorphisms were detected by this preference. However, it is also used in the field of plant biotechnology.

1.6. GFP Plasmid and Linear DNA Cassettes and Imaging in Confocal

GFP of jellyfish *Aequorea victoria* is widely preferred as one of the effective reporters for many molecular studies [128]. For plant biotechnology applications it's also widely used. Especially in plant genetic transformation research, it's one of the most powerful tools due to its providing visible results [129]. GFP can be used as reporter gene both as plasmid (circular) and in linear forms. Designed commercially available plasmids that allow expression of GFP in plant systems contain the GFP protein coding sequence between appropriate promoter and terminator sequences. A successful delivery of GFP gene containing plasmid or linear cassette into a plant cell or tissue results in obtaining GFP expression that provides visualization via several microscopic techniques or light tools [129].

1.7. Scope of Thesis

The main aim of this thesis is investigating chemically synthesized SeNPs gene delivery efficiency in the model plant *Arabidopsis thaliana*. PEI-modified SWNT is used for comparison because it's one of the most widely used NMs in plant biotechnology. Synthesized SeNPs and PEI-SWNTs characterizations and investigation about chemical and physical properties are performed via several techniques. Their toxic effect on *Arabidopsis thaliana* was observed via plant phenotypic reactions to different concentrations. To observe gene delivery, the GFP gene is delivered both in circular plasmid form and linear cassette form, to determine which are most readily expressible in the plant system. To investigate the delivered gene confocal microscopy is used for visualization and the qPCR technique is used to obtain quantitative measures of gene delivery efficiency.

2.MATERIALS & METHODS

2.1. Materials

2.1.1. Chemicals, Kits

Table 2: Chemicals and Kits that was used in the study

Chemical Name	Purchased From
Ammonium nitrate	Sigma-Aldrich (CAS #: 6484-52-2)
Calcium Nitrate 4-hydrate for analysis, ACS	PanReac&AppliChem ITW Reagents (CAS #: 13477-34-4)
Potassium dihydrogen phosphate	Sigma-Aldrich (CAS #: 7778-77-0)
Magnesium Sulfate 7-hydrate for analysis, ACS	PanReac&AppliChem ITW Reagents (CAS #: 10034-99-8)
Potassium chloride	Sigma-Aldrich (CAS #: 7447-40-7)
Boric Acid for analysis, ACS, ISO	PanReac&AppliChem ITW Reagents (CAS #: 10043-35-3)
Manganese (II) sulfate hydrate	Sigma-Aldrich (CAS #: 15244-36-7)
Zinc sulfate heptahydrate	Sigma-Aldrich (CAS #: 7446-20-0)
Copper (II) sulfate pentahydrate	Sigma-Aldrich (CAS #: 7758-99-8)
Ammonium heptamolybdate tetrahydrate	Sigma-Aldrich (CAS #: 12054-85-2)
Ethylenediaminetetraacetic acid, iron (III) monosodium salt,	Thermo Scientific Chemicals (Cat #: 088995.22)

Calcium chloride dihydrate	Sigma-Aldrich (CAS #: 10035-04-8)
Sodium hydroxide	Merck (CAS #: 1310-73-2)
Selenious acid	Sigma-Aldrich (CAS #: 7783-00-8)
Ascorbic acid	AFG Bioscience (CAS #: 50-81-7)
Bovine Serum Albumin	Sigma-Aldrich (CAS #: 9048-46-8)
Nitric acid	Sigma-Aldrich (CAS #: 7697-37-2)
Hydrochloric Acid (37%)	ISOLAB (Cat #: 932.106.2500)
Carbon nanotube, single-walled, carboxylic acid functionalized	Sigma-Aldrich, (Cat #: 652490)
Polyethylenimine, branched	Sigma-Aldrich, (Cat #: 408727)
MES hydrate	Sigma-Aldrich (CAS #: 1266615-59-1)
Magnesium chloride hexahydrate	Sigma-Aldrich (CAS #: 7791-18-6)
N-(3-dimethylaminopropyl)-N′-ethylcarbodiimide hydrochloride	Sigma-Aldrich, (Cat #: E1769)
N-hydroxysulfosuccinimide sodium salt	Sigma-Aldrich (CAS #: 106627-54-7
10× PBS	Pan Biotech (Cat #: P04-53500)
LB Broth (Lennox)	Sigma-Aldrich (Cat #: L3022)
Ampicillin	Sigma-Aldrich (CAS #: 69-52-3)
Tris-Base	NeoFroxx (CAS #: 77-86-1)
Ethylenediamine Tetra acetic Acid (EDTA)	MP Biomedicals (Cat #: 800682)
Boric Acid	MP Biomedicals (Cat #: 194810)
Ethanol Absolute	Merck (CAS #: 64-17-5)

Chloroform	Merck (CAS # :67-66-3)
Isopropanol	BioFrox (CAS#:67-63-0)
Agarose	Prona Biomax (Cat #: HS-8000)
Micropropagation agar	Caisson Labs (CAS #: 9002-18-0)
Nuclease free water	Invitrogen (Ref: 10977-035)
Silwet L-77	PhytoTech (CAS#.27306-78-1)
Murashige&Skoog with Vitamins medium	Caisson (Ref.MSP02-50LT)
Sucrose	ISOLAB (CAS#. 57-50-1)
Tween 20	Merck (CAS#.9005-64-5)
Plasmid isolation kit	EcoSpin Plasmid Isolation Kit (Cat #: EcoPI-50x)
PCR kit	KAPA Taq PCR Kit (KR0352_S – v3.20)
PCR Purification kit	Qiagen QIAquick PCR Purification Kit (Cat #: 28104)
RNA isolation kit	EcoSpin Plant Total RNA Kit (Cat #: E2096)
Nucleogene DNase I treatment part of Nucleogene RNA extraction Kit	Nucleogene QuickEX Total RNA Extraction Kit (Ref.NGE024)
cDNA synthesis kit	NucleoGene cDNA Synthesis Kit (Code: NGMM020)
qPCR kit	SensiFAST™ SYBR® Hi-ROX Kit (Cat #: BIO-92005)

2.1.2. Equipment- Devices

Table 3: Equipment's and devices that was used in the study

Equipment name	Brand
Magnetic stirrer	VELP Scientifica Srl (Italy)
Freeze dryer	Labogene Scanvac CoolSafe Basic Freeze Dryer (UK)
Ultrasonic homogenizer with 6-mm tip	QSONICA (USA)
Ultrasonic Bath	ISOLAB 621.05.003 Model (Germany)
Orbital shaker	Bio Cote Stuart SSL1 (UK)
Centrifuge SORNAL LYNX 6000	Thermofisher scientific (USA)
Centrifuge Allegra X-15R	Beckman Coulter (California, USA)
Centrifuge 5418 R	(Eppendorf, Germany)
pH Meter	(Mettler Toledo, Switzerland)
UV-Visible Spectrophotometer	(Varian, USA)
High Resolution Transmission Electron Microscope	JEM-ARM200F Atomic Resolution Analytical Microscope (Japan)
TGA	Sechimadzu DTG-60H (Japan)
Fluorescent Spectrometer	Agilent Technologies Cary Eclipse Fluorescence Spectrometer (USA)
Dynamic Light Scattering	(Malvern Panalytical, UK)
Fourier Transform Infrared Spectrophotometer (FTIR)	Sechimadzu IRAffinity-1S (Japan)
Biological Safety Cabinets	Thermofisher Scientific Herasafe KS (NSF) Class II, Type A2 (USA)
Growth Cabinet	Nordham Growth Chamber PG24 (Germany)

Shaking Incubator	GFL shaking incubator 3033 (UK)
Nanodrop	Nanodrop 2000c Thermofisher Scientific (USA)
Electrophoresis System	Mupid® One Electrophoresis System Complete Apparatus (Tokyo, Japan)
Bio-Rad Gel Imaging	Bio-Rad (USA)
Bio-Rad PCR	Bio-Rad (USA)
qPCR	Roche Light cycler 480
Confocal Microscopy	Zeiss LSM 710 (Germany)
Light Cycler Multiwell Plate 96 and sealing	Roche (Switzerland)
Microcentrifuge tubes	Expell Microcentrifuge Tubes (Germany)
100,000-MWCO filter units	Merck (Germany)
Falcon tubes 15mL and 50 mL	BluCapp Centrifuge Tubes (Germany)
Pipette tips	Pell PLUS Filter Tips (Mexico)
Extended-length pipette tips	Pell PLUS Filter Tips (Mexico)
Vortex mixer	Bio Cote (UK)
Folded capillary zeta cell	(Malvern Panalytical, UK)
UV cuvette Quartz	ISOLAB (Germany)
Ultra Quartz micro cuvette for fluorescence spectrometer	Shimadzu (Japan)

Microscope slides	Marienfeld (Germany)
Mortar and pestle	ISOLAB (Germany)
60x15 mm petri dish	ISOLAB (Germany)
90x17 mm petri dish	ISOLAB (Germany)
Magenta box	ISOLAB (Germany)
Inoculation loop	ISOLAB (Germany)
Tweezers	ISOLAB (Germany)
Blade	Angel (China)

2.1.3. Bacteria stains and *Arabidopsis thaliana* seeds

Table 4: Bacteria stains and Plant seed which was used in the study.

Bacteria stain /Plant line	**Purchased From**
35s-eGFP-nosT plasmid containing *E. coli* DH5alpha	Addgene (Cat #: 80127)
Col-0	NASC The European Arabidopsis Stock Center (Cat #: N76113)

2.1.4. Software

Table 5: Software which was used in the study.

Software	**Link**
Zeiss ZEN 3.8 Blue	(https://www.zeiss.com/microscopy/us/downloads.html)

2.2. Methods

2.2.1. *Arabidopsis thaliana* Plant Growth

2.2.1.1. Preparing water agar

Water agar was formulated to facilitate the germination of Col-0 seeds effectively. Micropropagation agar (1 gram in 100 mL of water) was heated in a microwave until it began to boil. Subsequently, the solution was poured into small plates in approximately 5 mL aliquots. Once the solution solidified, the plates were covered with Parafilm and stored in a refrigerator at +4°C.

2.2.1.2. Germination of Col-0 seeds

Col-0 seeds, a widely utilized genotype of *Arabidopsis thaliana* (accession 76113), were placed on water agar plates for germination. The plates were covered with parafilm. Subsequently, to initiate the stratification phase, the plates were transferred to a +4°C fridge for a period of 2 days. During this phase, seed dormancy is broken, leading to synchronized germination for all seeds. Following the 2-day stratification period, the seed-containing agar plates were moved to a growth chamber set at 23-24°C with a light intensity of 150 umol/m^2, maintained at 70% humidity level, and subjected to a 12-hour day length. After 3 days in the growth chamber, the seeds had germinated and were ready for transfer to rock wool for further cultivation.

2.2.1.3. Preparation of 0.5x Hoagland solution

A hydroponic nutrient solution should contain all required elements at the right level for healthy plant growth. Hoagland solution is one of the most used hydroponic system nutrient solutions [130]. Table 6 indicates the ingredient solutions and their supplied elements in a 0.5x Hoagland solution. Table 7 displays our modified version of Hoagland solution and

volumes needed for 2 liters of 0.5x Hoagland solution.

Table 6: Hoagland solution ingredients, and their supplied elements, and final concentrations

Macronutrients	Stock (M)	Element	Final concentration in 0.5x
NH_4NO_3	0.5	N	2 mM
Ca $(NO_3)_2.4H_2O$	1	Ca/N	2 mM
KH_2PO_4	0.25	P/K	1 mM
$MgSO_4.7H_2O$	1	Mg/S	0.5 mM
KCl	0.25	K	2 Mm used
Micronutrients (1 X)	Stock (mM)	Element	
KCl	1	Cl	
H_3BO_3	25	B	
$MnSO_4.4H_2O$	2	Mn	
$ZnSO_4.7H_2O$	2	Zn	
$CuSO_4.5H_2O$	0.1	Cu	
$(NH_4)_6Mo_7O_{24}.4H_2O$	0.1	Mo	
FeEDTA	0.02	Fe	

Table 7: Modified version of 0.5X Hoagland solution and, volumes needed for 2L.

	Desired Conc. (mM)	Total element supply	Stock solution conc (mM)	Desired final volume (mL)	Needed volume for 0.5x(mL)
NH4NO3	2	4 mM N	500	2000	8
Ca $(NO_3)_2.4H_2O$	2	4 mM N, 2 mM Ca	1000	2000	4
KH_2PO_4	1	1 mM K, 1mM P	250	2000	8
$MgSO_4.7H_2O$	0.5	0.5 mM Mg, 0.5 mM S	1000	2000	1
KCl	2	2 mM K, 2 mM Cl	250	2000	16
Microelements			Mixed		2
FeEDTA	0.02	0.02 Fe	20	2000	2
CaCl2	1.75	1.75 mM Ca, 3.5 mM Cl	200	2000	17.5

After all, indicated solutions are mixed the solution was filled to 2L with dH_2O. Finally, its pH adjusted to 5.5 by using HCl and NaOH solutions.

2.2.1.4. Planted germinated seeds on rock wools.

Before culturing the germinated Col-0 seeds, the rock wool sections are wetted by using prepared 0.5x Hoagland solution. Wetted square rock wool sections are placed on pots. Then, germinated seeds were put on wet small area of (small clarity of pots) rock wool sections. Cultured Col-0 plants are watered with 0.5x Hoagland nutrient solution 2-3 times a week. After 4 weeks each plant reached its maximum size shortly before the blooming stage. Each application to the Col-0 leaves is performed before blooming, at the 4^{th} week.

2.2.2. Nanoparticles Synthesis and Modifications

2.2.2.1. Preparation of Single Walled Carbon Nanotube

Commercially obtained SWNTs were modified with PEI according to [83] the protocol in literature. Firstly, CNT-COOH suspension was prepared. 30 mg of dry CNT-COOH and 30 mL of nuclease-free water were added to 50-mL conical tube and bath-sonicated for 10 minutes at room temperature. Then, it was continuously sonicated for 30 min at 10% amplitude using a 6-mm probe tip in an ice bath. After the suspension reached room temperature it was centrifuged at maximum speed (approximately 18.000g) for 1 hour at room temperature. After centrifugation, the supernatant was collected that contains individually suspended CNT-COOH. The concentration of suspended CNT-COOH was determined by taking single wavelength absorbance measurement at 632 nm and using extinction coefficient of 0.036 L $mg^{-1}cm^{-1}$. Obtained CNT-COOH suspension was stored at +4◦C. It was bath-sonicated for 30 minutes before using in experiments or measurements. Next, the suspended CNT-COOH was reactivated for reaction with PEI. For proper reaction 500mM MES buffer solution (pH 4.5-5.0) was prepared. The volume containing 2 mg of suspended COOH-SWNTs was calculated and 500 mM MES buffer solution added until 100 mM final concentration was reached. 10 mg N-(3-dimethylaminopropyl)-N′-ethylcarbodiimide hydrochloride (EDC) and 10 mg N-hydroxysulfosuccinimide sodium salt (NHS) was added to 2.5mL of 100 mM MES solution and mixed well until completely dissolved. This solution was prepared fresh for every new reaction because their activity decreases in aqueous solution. This freshly prepared EDC-NHS solution was added dropwise to the 2 mg of suspended CNT-COOH in 100 mM MES buffer. The final reaction mixture was bath-sonicated for 15 minutes at room temperature. Then, the reaction continued for 45 minutes on an orbital shaker at 180 rpm at room temperature. After the reaction was complete, activated CNT-COOH was washed with 0.1× PBS (pH 7.4) three times using pre-washed 100,000-MWCO filters to discard free EDC, NHS, and by-products by centrifuging at 300 g for 8 minutes at 21◦C for 3 times. After washing, the 100,000-MWCO filters part was bath-sonicated which contains activated CNT-COOH for 1 minute while pipetting. Then, filters were placed back to collection tubes and vortexed. After vortex activated CNT-COOH were collected by using a 1,000-µL extended-length pipette tip. Then, 0.1× PBS (pH 7.4) was added to the activated CNT-COOH solution until reaching the initial CNT-COOH

solution volume (before the addition of 500mM MES buffer) and mixture was resuspended by bath sonication for 15 minutes.

In parallel, 40 mg of PEI was added to 5 mL of 0.1× PBS and dissolved fully. Then, the pH of this PEI solution was adjusted to 7.4–7.6 with HCl. Finally, activated CNT-COOHs were added to the PEI solution dropwise. The activated CNT-COOH and PEI reaction occurred overnight (~16 h) at room temperature on an orbital shaker at ~180 rpm. The obtained PEI-SWNTs solutions was washed with nuclease free water six times by using two pre-washed 100,000-MWCO filters. In this washing processes solution centrifuged at 1000 g for 15-20 minutes at 21◦C, before each washing process solution was vortexed. After all washing steps, these two filters were bath-sonicated while pipetting for 1 minute. Then 2 solutions in 2 filters collected in one tube by using extended pipette tips from filters. Then, nuclease-free water was added to the PEI-SWNTs solution until reaching the initial CNT-COOH solution volume (before the addition of 500mM MES buffer). Obtained mixture was resuspended through 15 minutes bath sonication and then 15 minutes probe-tip sonication at 10% amplitude with a 6-mm probe tip in an ice bath. Then the suspension was centrifuged at 16000 g for 1 hour at room temperature and supernatant was collected. Finally, the concentration of PEI-SWNTs was determined with single wavelength measurement at 632 nm and extinction coefficient of 0.036 L mg^{-1} cm^{-1}. Lastly, obtained PEI-SWNTs dispersion was diluted 1:100 and DLS measurement was taken. PEI-SWNTs suspension could be stored at 4°C for further experiments but it should be bath-sonicated for 30 min before cargo loading.

2.2.2.2. Production of SeNPs

Selenium nanoparticle (SeNPs) synthesis contains 100 mM selenious acid (as Se precursor), 0.5 % BSA (as stabilizing agent) and 500 mM ascorbic acid (as reducing agent). Each solution was prepared by using MilliQ water. Firstly, every material that will be used (Erlenmeyer, magnetic fish) was washed with ‘aqua regia’ (3:1 hydrochloric acid/nitric acid)”. Then they were rinsed with pure water. Lastly, they were dried with a paper towel. 100 mM Selenious acid solution was prepared in a 5mL Erlenmeyer and stirred with magnetic fish, also 0.5% (w/v) BSA was added. After adding all ingredients, the mixture was stirred for 15 minutes at room temperature using a relatively fast speed (350 rpm). After 15 minutes stirring and completely dissolving, the stir rate was lowered (100 rpm) and 1 mL 500mM ascorbic acid solution was added at once. In this step, orange color formation was

observed. After adding ascorbic acid mixture was continued to stir at relatively slow rate (100 rpm) for 5-7 minutes. The final mixture should be clear orange. After the reaction ended, obtained SeNPs (as colloidal suspension) was diluted as 1:100 and DLS measurement was taken. After taking measurements, all 2 mL of SeNPs were put in a 15 mL falcon tube and covered with parafilm. Some holes were opened in the parafilm, and the tube was placed at -80◦C overnight. After overnight freezing, SeNPs sample placed to freeze dried for 3 days to fully dry and obtain powder form. Then, powder was weighted in desired ratio and dissolved it by using MilliQ and take DLS measurements and for further characterization.

2.2.3. Characterization of Nanoparticles

Dynamic Light Scattering (DLS), Transmission Electron Microscopy (TEM), Fourier transform infrared spectroscopy (FTIR), and Thermogravimetric analysis (TGA) were employed to characterize the synthesized SeNPs and modified PEI-SWNTs. Furthermore, UV–vis absorption spectroscopy, fluorescent spectroscopy applied to analyze synthesized SeNPs.

2.2.3.1. Dynamic Light Scattering (DLS)

Dynamic Light Scattering (DLS) was employed to determine the hydrodynamic size and surface charge of nanoparticles (NPs). The particle size distribution and zeta potential of both SeNPs and PEI-SWNTs samples were analyzed using DLS. Measurements were conducted in a DTS1070 DLS cuvette at a temperature of 25°C. The viscosity and refractive index were adjusted to match those of water and the DLS cuvette. For DLS measurements, liquid PEI-SWNTs and freshly synthesized colloidal SeNPs were diluted with MilliQ water in a 1:100 ratio, while solid SeNPs, weighing 1 mg, were dispersed in 2 mL of MilliQ water. DLS measurements were performed in triplicate for both size and zeta potential, and the average values were considered as the main results. Size and polydispersity index (PDI) measurements were obtained for triplicate measurements. The particle size and zeta potential were reported as mean values with standard errors.

2.2.3.2. Fourier transform infrared (FT-IR) spectroscopy (FTIR)

Fourier Transform Infrared (FT-IR) spectroscopy was utilized to assess the presence of specific chemical bonds (functional groups) on the surface of nanoparticles within the range of 600–4000 cm^{-1}. The chemical composition of nanomaterials (NMs) was characterized using FTIR. Analysis of all NMs was conducted in powder form, with each sample scanned 20 times at a resolution of 4 cm^{-1} at 600-4000 cm^{-1} region. FTIR measurements were taken from PEI-SWNTs, PEI, SeNPs and BSA solid samples. To take a FTIR measurement PEI-SWNTSs is also lyophilized to get solid concentrated form.

2.2.3.3. UV–vis absorption spectroscopy

UV-vis spectroscopy is widely employed for nanoparticle characterization. By detecting Surface Plasmon Resonance (SPR), this method verifies nanoparticle formation. It offers insights into nanoparticle size, stability, and aggregation tendencies [131]. UV–vis absorption spectra of diluted SeNPs and BSA in Milli-Q were performed in spectrophotometer. Measurements are taken by using a 1 cm path-length quartz cuvette and scanned at a medium scan rate (2 nm per second), 200 to 800 nm.

2.2.3.4. Fluorescent spectroscopy

Metal NPs, such as silver, gold and semi-metallic elements like selenium (Se) could have intrinsic fluorescence and a characteristic spectrum [132]. Even if this is a possibility for SeNPs, fluorescent spectroscopy analysis was conducted. 500 ng/uL SeNPs were prepared using MilliQ water. After that, using fluorescent spectrometer quartz cuvette fluorescent spectroscopy measurement was taken. The excitation wavelength was 220-225 nm and emission spectra were collected from 250 to 600 nm. The excitation slit is adjusted to 10 nm and emission slit is adjusted to 20 nm.

2.2.3.5. Transmission electron microscopy (TEM)

Transmission electron microscopy allows visualization of nanomaterials with high magnification resolution. The studies of morphology and size of the prepared SeNPs and PEI-SWNTs were performed by means of transmission electron microscopy (TEM). The

samples were drop-casted on a carbon-coated TEM copper grids and air dried for imaging.

2.2.3.6. Thermogravimetric analysis (TGA)

By integrating Thermogravimetric Analysis (TGA) thorough investigation into a material's thermal characteristics is achieved. While TGA primarily captures alterations resulting from mass loss, DTA extends the analysis to detect changes in the material even when no mass loss occurs. Thermal stability of SeNPs and PEI-SWNTs, CNT-COOH and PEI are analyzed by TGA. Analysis is performed within argon atmosphere and with heating rate of 10 ºC per min up to 800 ºC.

2.2.4. Production of Deliverable Genetic Materials

2.2.4.1. Plasmid GFP DNA production via E. coli

E. coli DH5α strain containing 35s-eGFP-nosT plasmid was cultured on LB Agar media plates containing 100 μg/mL Ampicillin. They were incubated at 37◦C for 1 day. Formed single colonies were transferred to 5 mL LB Broth that contained 100 μg/mL Ampicillin in 15 mL falcon tubes. These were incubated at 37◦C for 16 hours in shaking incubator (180 rpm shaking). Single wavelength measurements at 600 nm were performed after 16 hours, if absorbance reach 1-1.5 whole bacteria samples were collected. After that plasmid isolation was performed by using EcoSpin Plasmid Isolation Kit. This kit is composed of 3 main steps which are lysis of bacteria, filtering the lysate and enhancing the plasmid DNA remaining by washing steps. Plasmids obtained by applying kit procedures were measured in Nanodrop to determine concentration and purity. A 260/280 ratio approximately equal to 1.8 is typically considered indicative of high purity for DNA. The 260/230 ratio serves as a marker for the presence of extraneous organic compounds. Acceptable 260/230 ratios for DNA typically exist within the range of 2.0 to 2.2. The size of the isolated 35s-eGFP-nosT plasmid (approximately 4 kb long), was also checked using 1% agarose gel and 0.5xTBE buffer used gel electrophoresis.

2.2.4.2. Production of GFP linear DNA cassette via PCR

According to the 35s-eGFP-nosT [1] plasmid map which is represented in Figure 7, to obtain a linear GFP DNA expression cassette in *Arabidopsis thaliana*, M13 reverse and forward primers were used with KAPA Taq PCR Kit. M13 forward and reverse primers sequence is given in table 8.

Table 8: M13 forward and reverse primers sequence

Name of primer	Sequence
M13 forward primer	TGTAAAACGACGGCCAGT
M13 reverse primer	CAGGAAACAGCTATGAC

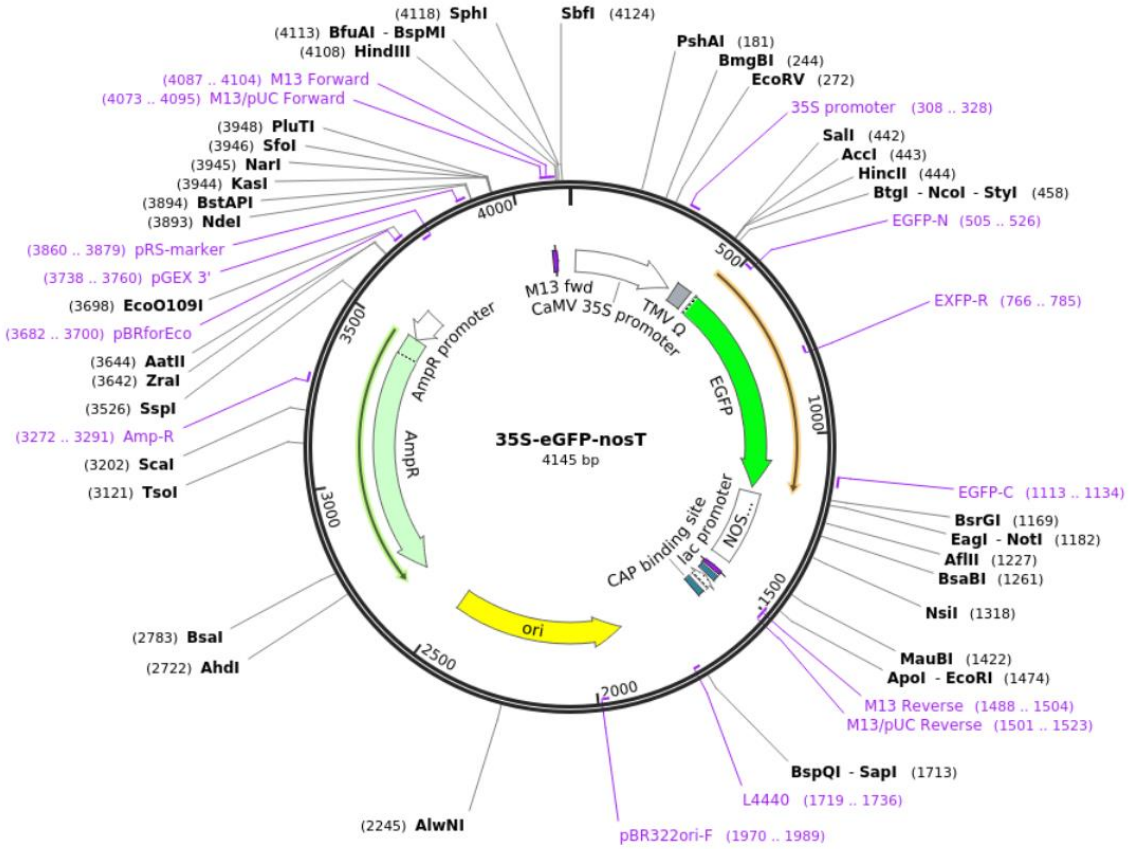

Figure 7: 35s-eGFP-nosT plasmid map. [132[1]

There were some modifications to the recommended KAPA Taq PCR setup as follows:

2 µl → 10x KAPA Taq PCR buffer with MgCl2

0.4 µl → 10 mM KAPA dNTP mix

0.4 µl → 10 µM F primer (M13 Forward for GFP plasmid)

0.4 µl → 10 µM R primer (M13 Reverse for GFP plasmid)

0.1 µl → KAPA Taq polymerase

15.7 µl→ Nuclease-free water

1 µl → plasmid DNA (max 50ng)

The total reaction volume was 20 µL. To ensure the required amount of linear GFP DNA cassette, the PCR master mix was prepared without plasmid DNA as a template. The initial six components were combined to form a master mix, with 19 µL aliquoted into reaction tubes. Subsequently, 1 µL of plasmid DNA was added to each PCR reaction tube.

PCR program:

1. Initial denaturing 95 ^{o}C for 2 min
2. 35 cycles of: 95 ^{o}C for 15; 50 ^{o}C for 30s; 72 ^{o}C for 1.5 min
3. Final extension of 3 min at 72 ^{o}C

The PCR program was established based on the predicted annealing temperatures of the primers and the length of the desired linear GFP DNA cassette. Considering that the desired linear GFP DNA cassette is relatively long (1.5 kb), both the cycle extension time and the final extension time were prolonged. Linear GFP DNA cassettes were produced according to these specified parameters.

2.2.4.3.PCR clean up.

After each PCR protocol obtained PCR products should be cleaned up from unused PCR products, dNTPs, and enzyme. For that reason, each PCR product was cleaned up by using Qiagen QIAquick PCR Purification Kit. Kit contains filter that remains actual long PCR product while discarding other materials. After PCR purification, linear GFP DNA cassette concentration and pureness was determined using nanodrop. Also, to confirm obtained product is linear GFP DNA cassette gel electrophoresis was performed.

2.2.5. Nanoparticles and Plasmid DNA, Linear GFP DNA cassette binding

2.2.5.1. Binding process

Firstly, MES delivery buffer (25 mM MES,15 mM $MgCl_2$ at pH 6) was prepared according to the protocol [83].Nanoparticles were bound to both types of DNA circular plasmid and linear GFP DNA expression cassettes are by the same procedure[83]. To facilitate the binding of DNA to PEI-SWNTS and SeNPs, the desired quantity of these particles was added to MES delivery buffer. The nanomaterials and genetic materials were combined based on mass-to-mass ratios. The desired amount of DNA was placed in a separate Eppendorf tube. Subsequently, the nanomaterials and MES delivery buffer solution were pipetted several times and added dropwise to the tube containing the DNA. After collecting all components in one tube, incubation was conducted for 30 minutes at room temperature. Following incubation, 0.2% Silwet L-77 was added to the solution, serving as a surfactant for application to plant leaves.

2.2.5.2. Binding confirmation via DLS

The most efficient binding ratios of circular plasmids and linear GFP DNA cassette to PEI-SWNTs and SeNPs were determined by conducting zeta potential measurements as described in 2.2.3.1. Various mass-to-mass ratios were tested, and the ratio resulting in the most significant shift to negative zeta potential was selected as the efficient binding ratio. The prepared solutions were diluted in MilliQ water at a 1:100 ratio for DLS measurements.

2.2.6. Application to *Arabidopsis thaliana* Plants

Prepared NPs and DNA bound versions were applied to *Arabidopsis thaliana* plants from roots and leaves separately.

2.2.6.1. Application of PEI-SWNTs and SeNPs to Arabidopsis thaliana leaves

Fresh solutions of DNA-bound PEI-SWNTs and SeNPs were prepared for each application on plant leaves. These application solutions were homogenously spread across the entire leaf surface, focusing on the abaxial region, using 200 µL pipettes with pipette tips that did not damage the leaves. Applications were carried out on the abaxial sides to facilitate passage through the stomata, and they were conducted after watering the plants, typically at noon when photosynthesis is most active. To ensure uniform distribution, 0.2% Silwet surfactant was added to the application solution. A volume of 50 µL of the application solution was provided per fully expanded *Arabidopsis thaliana* leaf. After application, the plants were returned to the growth cabinet for 3 days before being collected for further analysis.

2.2.6.2. Application of PEI-SWNTs and SeNPs to Arabidopsis thaliana roots

To apply the nanomaterials-bound DNA complex solution to *Arabidopsis thaliana* roots, a sterile MS medium was first prepared in magenta boxes. The MS medium, containing only 1% sucrose, was prepared by mixing 2.15 grams of MS vitamin, 5 grams of sucrose, and 450 mL of distilled water, and adjusting the pH to 5.8. Next, 3.5 grams of micropropagation agar was added, and the mixture was filled with distilled water up to 500 mL before autoclaving. The autoclaved MS medium was aliquoted into magenta boxes and allowed to solidify in a biosafety cabinet. The boxes were then closed and covered with parafilm before being stored at +4°C for later use. Secondly, to culture Col-0 seeds on the prepared MS medium, the seeds needed to be sterilized. For the sterilization process, 40 Col-0 seeds were placed in a 1.5 mL microcentrifuge tube. Then, 500 µL of a 50% (v/v) bleach solution containing Tween 20 was added to the tube, and the tube was inverted to suspend the seeds in the bleach solution for 10 minutes. Afterward, the bleach solution was discarded, and 500 µL of sterile distilled water was added to the tube. The tube was closed and inverted to mix, allowing the seeds to settle to the bottom after 1 minute. The rinsing process was repeated 6 times, after which 1 mL of autoclaved distilled water was added to suspend the seeds. To culture them on the MS media, the seeds were poured from the microcentrifuge tube onto the magenta boxes, with each box containing a maximum of 10 Col-0 seeds. After placing the seeds on the media, they were spread using a sterile single-use inoculating loop. The boxes were then placed in the laminar flow hood with the lid partially closed to allow excess water to evaporate over the seeds. Once the seeds were cultured on the MS medium in the magenta

boxes, the boxes were covered with parafilm and stored at +4°C for 3 days in the dark. After 3 days at +4◦C fridge, boxes were transferred to growth cabinet for 5 days at 24 °C with 12 h daylength[133]. After 5 days, Col-0 seeds germinated and developed roots. Once the roots were formed, applications were carried out in a biosafety cabinet using a syringe. The prepared application solutions were applied inside the MS medium. Each experimental group, consisting of 10 Col-0 plants, received 2 mL of the application solution. While not all of the 2 mL application solution remained within the MS medium, the excess solution visibly penetrated the Col-0 roots. Additionally, the Col-0 roots were able to penetrate the MS medium, indicating that the plants could still survive while absorbing the applied solution. Following the application, the boxes were covered with parafilm and placed in the growth cabinet for 3 days. After this period, the roots were placed between microscope slides, and confocal microscope analysis was conducted.

2.2.7. SeNPs and PEI-SWNTs Toxic Symptoms Observation for *Arabidopsis thaliana* leaves

In order to determine toxic threshold for SeNPs and PEI-SWNTs for *Arabidopsis thaliana* leaves, these NMs applied as 4 different concentrations. Silwet L-77 surfactant is also used because of its application to leaves. All dosages were applied to 3 leaves each on 3 different plants. After application, leaves were observed on the first and third day and distinguishable necrosis was noted. Photographs were taken on these days.

2.2.8. Observation of GFP reporter gene

To visualize the expressed GFP protein in *Arabidopsis thaliana* leaves and roots, confocal microscopy was employed. Fresh leaves and roots were harvested for observation three days after the application of NPs. Some of the collected leaves were stored at -80°C for further qPCR analysis.

2.2.8.1. Confocal microscopy

Confocal microscopy was utilized to observe the GFP reporter protein expression in both

leaves and roots. Leaves were gently flattened between two microscope slides individually. In confocal microscopy, the gain values for the TMPT and EGFP channels were determined based on negative control leaves to eliminate auto-fluorescence from plant molecules like chlorophyll, lignin, and also SeNPs fluorescence. The determined gain values for TMPT and EGFP channels were 325 and 450, respectively. For high-resolution imaging, parameters such as a 1 AU pinhole, a frame size of 1024x1024, and a speed of 3, resulting in a 1-minute acquisition time, were used. Three to five images were captured for each experimental group from three different leaves.

For root observation, roots were separated from the plant and placed between two microscope slides. Imaging was conducted using the TMPT and EGFP channels. Gain values were determined based on the 'linear GFP DNA cassette-only' sample group, as roots lack chlorophyll. The determined gain values for TMPT and EGFP channels were 268 and 800, respectively. Imaging parameters included a 1 AU pinhole, a frame size of 512x512, and a speed of 10, resulting in a 10-second acquisition time. Three to five images were taken for each experimental group from five different roots.

2.2.9. Gene Expression Analysis of GFP Applied Plant Leaves.

2.2.9.1. RNA isolation to leaves.

To analyze GFP expression at the mRNA level, total RNA was extracted from the treated leaves. The RNA isolation process is basically separating RNA from DNA and proteins after extraction with an acidic solution. Initially, 300 mg of leaf samples were ground using liquid nitrogen, a mortar, and pestle. RNA isolation was then conducted using the Ecospin Total RNA Isolation kit for stored *Arabidopsis thaliana* leaves. As part of the Nucleogene Plant RNA isolation kit, DNase I treatment was applied to RNA while bound to the silica filter matrix, just before the second washing steps. Although the Ecospin Plant Total RNA Isolation kit does not include DNase treatment, Nucleogene DNase I buffer, and enzyme were utilized after the first washing step. Specifically, 3.5 µL of DNase I mix was added to each filter, and the filters were then incubated at 37°C for 15 minutes. Subsequently, the remaining protocol of the Ecospin kit, including washing steps to remove other materials except RNA, was followed.

2.2.9.2. cDNA synthesis

After RNA isolation from samples, RNA should be converted to cDNA for qPCR analysis. cDNA synthesis for isolating RNA samples were conducted by using Nucleogene 5x cDNA synthesis kit according to manufacturer's protocol. An equal amount of cDNA was synthesized from whole samples. 500 ng RNA was used to synthesize each cDNA. Incubations after reaction mixture prepared was as follow as: 5 minutes at 25°C → 30 minutes at 42°C → 5 minutes at 85°C → Hold at 4°C.

After the reaction was complete, 500 ng of cDNA in a 20 µL reaction volume was diluted with 80 µL of nuclease-free water (NFW). The resulting cDNA was then used directly in qPCR analysis. For each well, 4 µL of cDNA was added, corresponding to approximately 20 ng of cDNA.

2.2.9.3. qPCR Analysis

The analyses were performed using the SYBR qPCR Hi-ROX kit and Roche LightCycler 480 instrument. For each sample, three technical replicates were measured. In each well, 4 µL of cDNA, equivalent to 20 ng of cDNA, was added. The housekeeping gene RPL36 was used for normalization, while GFP served as the gene of interest. Both RPL36 and GFP primers were used for all samples. Table 9 indicates the sequence of these primers. Table 10 represents the amplification program (45 cycle) of qPCR setup.

Table 9: RPL36 and GFP primers sequence

Name of primer	Sequence
RPL36aARTqPCR_Forward primer	GATAGTCTTGCTGCACAGGGAAA
RPL36aARTqPCR_Reverse primer	GGTCTGACCTCCATATCCTGATTG
GFPRTqPCR_Forward Primer	GGTGAACTTCAAGATCCGCC
GFPRTqPCR_Reverse Primer	CTTGTACAGCTCGTCCATGC

Table 10: amplification program of qPCR setup

Target (°C)	Acquisition Mode	Hold (hh: mm: ss)	Ramp Rate (°C/s)
95	None	00:00:10	4.40
60	None	00:00:10	2.20
72	Single	00:00:10	4.40

After the LightCycler process, the Cp values obtained for the three replicates of each sample were averaged. The average Cp value of the wells with RPL36 primers was subtracted from the average Cp value of the wells with GFP primers for each sample group separately, resulting in ΔCp values. Subsequently, the ΔCp value of the negative control sample group was subtracted from the ΔCp values of the other sample groups to obtain ΔΔCp values.
ΔΔCp values exponential to 2 were calculated, and then these values were transferred to a logarithmic scale by taking the base 10 logarithm. This procedure allowed for the analysis of fold change expression levels of the GFP gene relative to the negative control.

2.2.10. Statistical analyses

Statistical analyses were conducted using two-tailed Student's t-test with equal variance. For Confocal microscope images, Zen 3.8 software was used to obtain fluorescent intensity at defined regions.

3.RESULTS and DISCUSSION

3.1 Characterization of Synthesized PEI-SWNTs and SeNPs

PEI modified SWNT and chemically synthesized SeNPs, nanomaterials, are characterized using imaging, spectroscopic and thermal techniques before use as a DNA carrier for plant gene delivery applications.

3.1.1. DLS Results of PEI-SWNTS and Synthesized & Stabilized SeNPs.

The size and surface charge of these nanomaterials (NMs) were characterized by DLS technique. Figure 8 illustrates the size distribution and surface charge of SWNT and PEI-SWNTs. PEI modification to SWNT, by wrapping around, provides positive zeta potential and an increase in size. Before PEI modification size of the CNT-COOH was measured at 114 nm and its surface charge was around -47 mV. The peak of obtained PEI-SWNTs sizes was at 146 nm while the minor peak seen in Figure 8 c corresponds to unbound PEI, and surface charge zeta potential was measured as +61 mV. Obtaining results after PEI functionalization are compatible with literature [134, 135]

The polydispersity index (PDI) value of both versions of SWNT was found at quite a good dispersion status. CNT-COOH's PDI was measured 0.3265±0.03416 and PEI-SWNTs' PDI was measured 0.29887±0.04926 that proves proper dispersion. The PDI value demonstrates the variation in size and aggregation status of sample in the aqueous media while ranging from 0 to 1. Lower PDI values indicate better dispersion and a more homogeneous suspension of measured sample. A PDI index exceeding 0.7 indicates that the tested particle possesses a significantly large hydrodynamic size, rendering it unsuitable for DLS measurement [136].

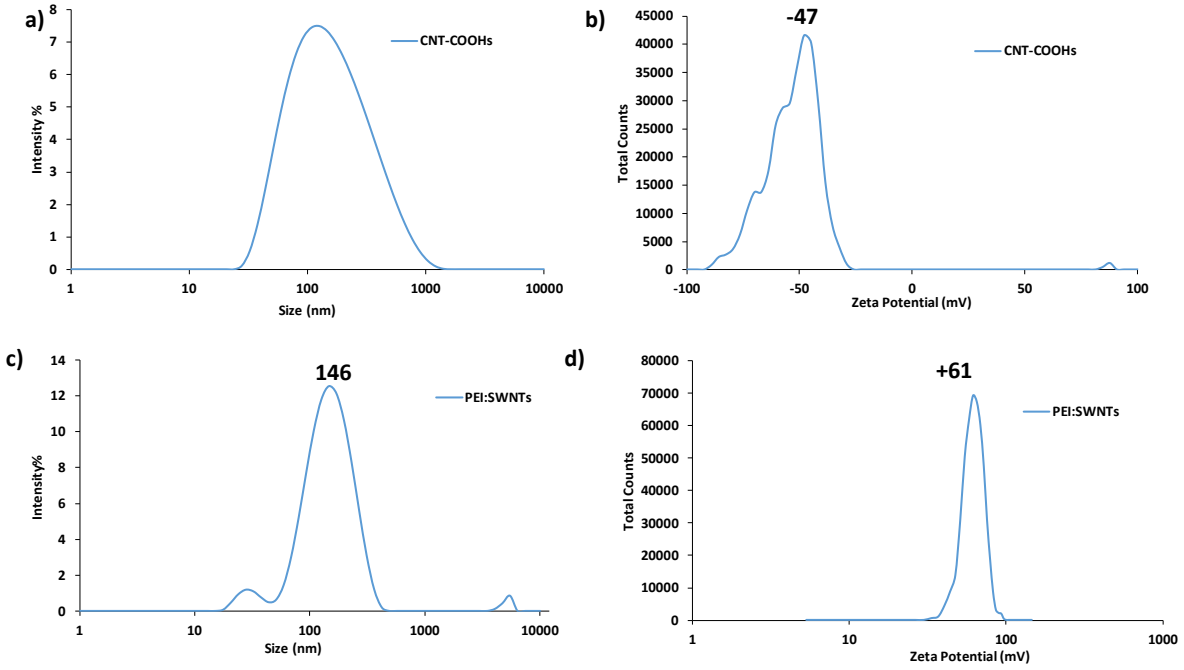

Figure 8: CNT-COOH and PEI-SWNTs DLS analysis and results. Intensity of the scattered light from (a) CNT-COOH and (c) PEI-SWNTs respect to size. Total counts respect to surface zeta potential of (b) CNT-COOH and (d) PEI-SWNTs

On the other hand, SeNPs size and zeta potentials for fresh synthesis and stabilized lyophilized form were also measured in DLS. Figure 9 represents the DLS analysis of freshly synthesized SeNPs size and surface charge. Freshly synthesized SeNPs size was measured as 27 nm while the surface charge was around +11mV. Obtained small size of SeNPs after synthesis is also prove that chemical synthesis methods provide smaller size [92]. The positive surface charge and stable size are due to BSA used as a stabilizing agent [137]. The PDI value of freshly synthesized SeNPs was found to be 0.3178±0.03539 which also indicated proper dispersion. The BSA protein, which is added as a stabilizing agent, prevents agglomeration of SeNPs and provides positive surface charge. Stabilization of the synthesized SeNPs was challenging part, as the colloidal suspension form of SeNPs obtained by chemical synthesis was not stable over time. There is a lot of research on lyophilizing nanoparticles to solve this stability problem. Lyophilization, also termed freeze-drying, involves the sublimation of ice under reduced pressure to extract water from a sample. This approach has proven effective in enhancing the long-term stability of nanoparticles [138]. By lyophilization and obtaining powder form of SeNPs, this challenge was accomplished. By this way both size and zeta potential of SeNPs can be preserved as it was when first synthesized. Figure 10 displays the DLS results of SeNPs after lyophilization and 1 month storage at +4◦C. 1 mg of lyophilized- SeNPs was weighted and dispersed in 1 mL of MiliQ

water. By DLS data obtained PDI values were 0.1991±0.03074 which shows the SeNPs were still properly dispersed.

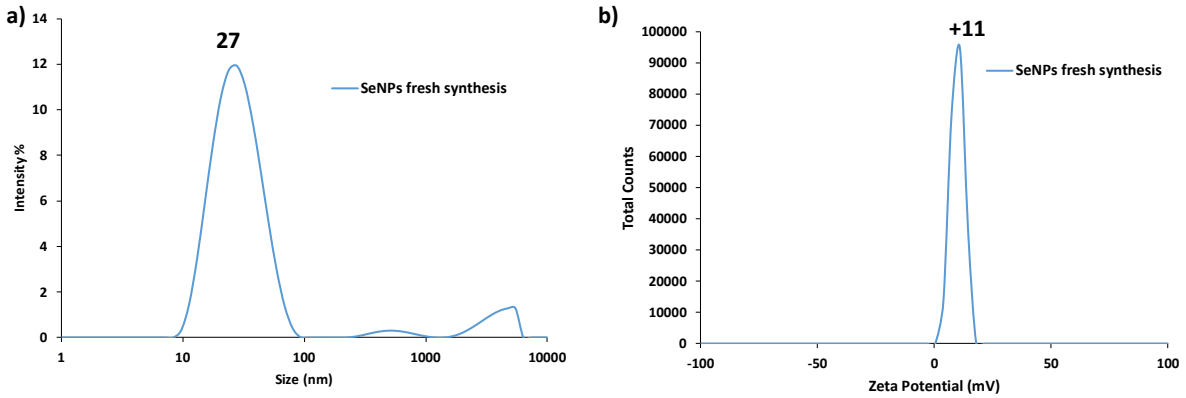

Figure 9: Synthesized SeNPs DLS results. (a) Intensity percentage of fresh synthesized SeNPs size. (b) Total counts of fresh synthesized SeNPs respect to surface charge as zeta potential (mV).

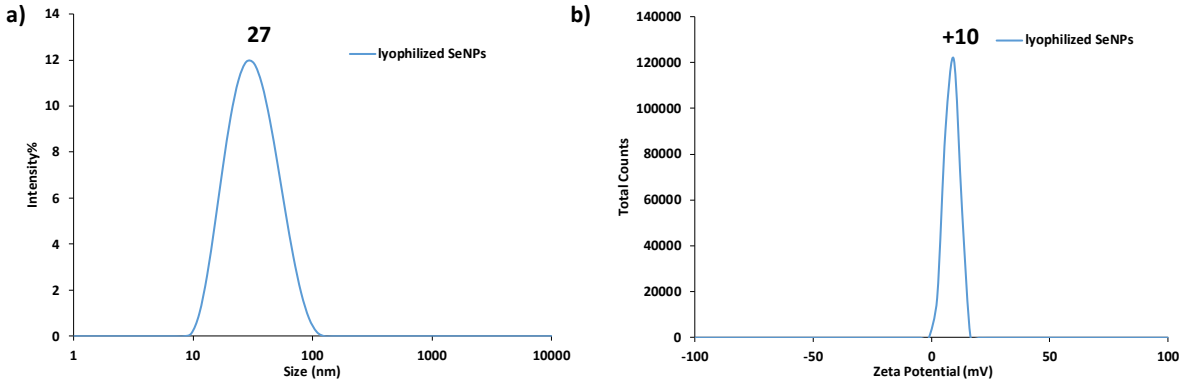

Figure 10: SeNPs DLS analysis after freeze-drying. A) Intensity percentage of lyophilized SeNPs size. b) Total counts of lyophilized SeNPs respect to surface charge as zeta potential (mV).

3.1.2. TEM Images of PEI-SWNTs and SeNPs

TEM images of PEI-SWNTs and SeNPs with increasing magnifications were displayed in Figure 11. As seen, SWNT is in the shape of a long thin tube. According to the obtained images the diameter of the PEI-SWNTs is 6 nm and length is around 140 nm, this is consistent with the DLS size data. SeNPs were in spherical form suggesting that they were fairly homogeneous arrangements of Selenium atoms. The size of SeNPs is around 20 nm according to TEM images. The SeNPs size which is measured in DLS and TEM different because of the methodology of techniques.

DLS gives hydrodynamic size that means its actual size plus the liquid layer around the particle. However, size measured in TEM gives the more actual size of the nanoparticle. For that reason, even the size values were not exactly same at DLS and TEM they are consistent. The size of nanoparticles is an essential parameter for plant tissue passage. Research indicates that metal-based nanoparticles smaller than 50 nm in diameter can penetrate plant leaves through the stomatal pathway [38]. So, approximately 20 nm size SeNPs can pass easily to plant leaves. Besides, PEI-SWNTs can also penetrate to plant cell wall because of its long thin shape [139].

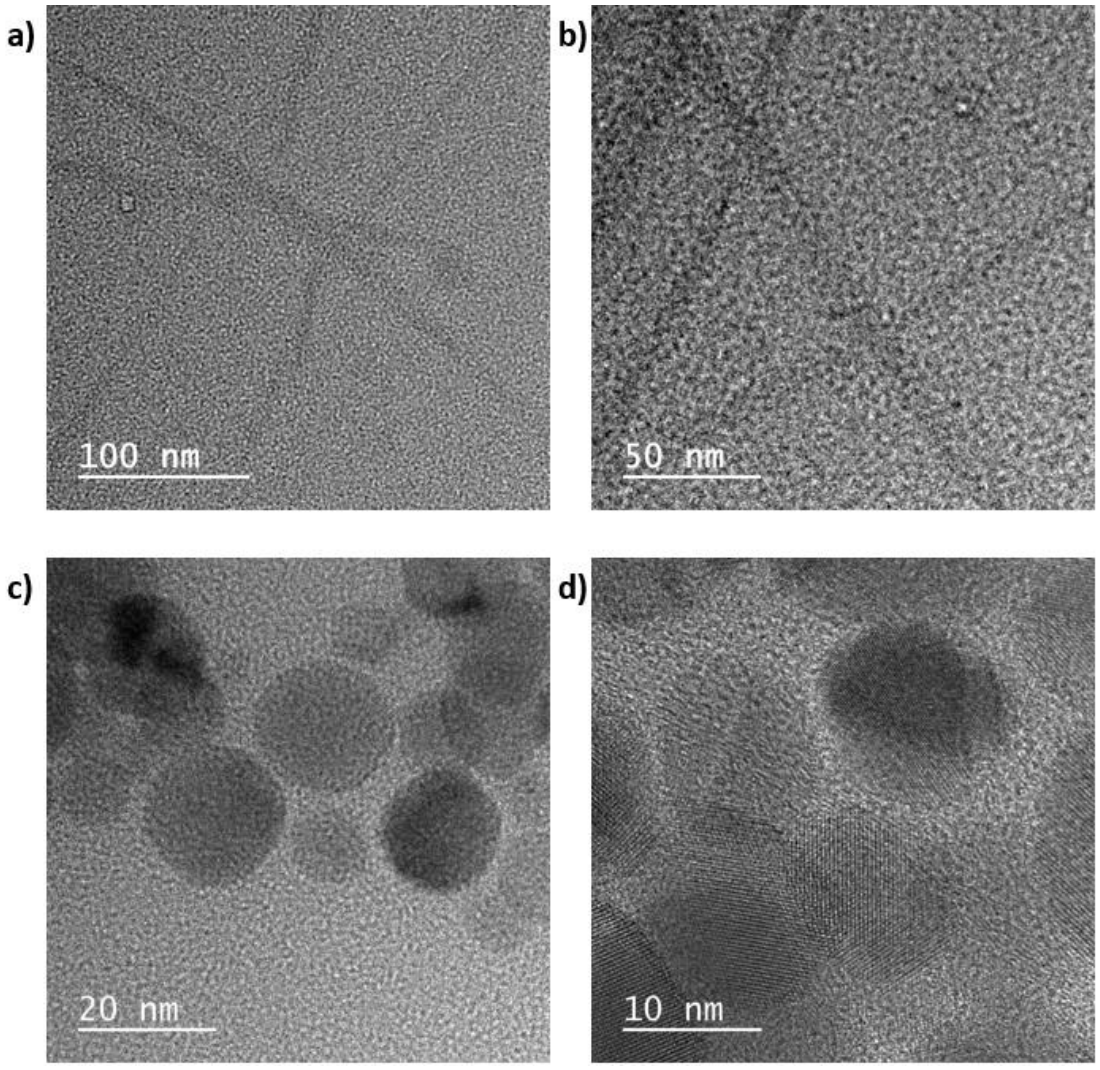

Figure 11: TEM images of PEI-SWNTs and SeNPs. a)PEI-SWNTs TEM image at 100 nm scale. b) PEI-SWNTs TEM images at 50nm. c) Spherical SeNPs TEM image at 20 nm scale. d) SeNPs TEM image at 10 nm scale.

3.1.3. FTIR Results of PEI-SWNTs and SeNPs

One technique for analyzing a variety of materials is FTIR Spectroscopy. These materials can include polymers, organic chemicals, and occasionally even inorganic substances. By scanning samples using infrared light, this analytical method provides determination of the chemical properties of the materials. Figure 12 a indicates the FTIR spectra of PEI and PEI-SWNTs from 600 to 4000 cm^{-1} wavelength. FTIR spectroscopy provided precious information about their chemical structures. In FTIR spectrum of PEI, the peak at 2929 cm-1 corresponds the stretching and bending vibration peaks of CH_2 group in PEI molecule. The 1582 cm^{-1} peak indicates the secondary amine, N-H bend (1650–1550 cm^{-1}), of PEI molecule[140]. Furthermore, the wide peak which is observed at 3,350 cm^{-1} is one of the characteristic peaks of carbon nanotubes in the FTIR spectrum of PEI-SWNTs. This peak is assigned to the vibration stretching of the O–H groups. The peak at 1722 cm^{-1} is related to the stretch of the carboxyl groups of SWNTs [141]. Peaks at 1456 cm^{-1} were attributed to C–O moieties, and those at 1030 cm^{-1} reflected the existence of C–C and C–H functionalities of SWNT. The peak at 1562 cm^{-1} indicates aliphatic nitro compounds which come from PEI. The presence of a peak at 1580 cm^{-1} in the PEI-SWNTs spectrum suggests that it corresponds to the vibration of the amide carbonyl group, indicating a successful bonding of PEI to SWNTs [142].

Figure 12 b represents SeNPs and BSA FTIR spectra. The FTIR spectrum of BSA protein displays two characteristic bands. As anticipated for a protein primarily composed of α-helix structures, the distinctive amide I band of BSA appears at 1641 cm^{-1}[143]. The band observed at 1523 cm^{-1} is indicative of robust primary amine scissoring (N-H bending), while the peak centered at 3278 cm^{-1}can be attributed to primary amines [144]. In SeNPs FTIR spectrum the broad peak at 3278 cm^{-1} is also due to -OH stretching of the aromatic rings of surface bound BSA (N-H) symmetric vibration [145]. In the low wavelength range, there are several different peaks. These correspond to the amide I band at 1664 cm^{-1} (C=O stretch of the ester group), amide II at 1535 cm^{-1} (N-H bending), 1328 cm^{-1} (C-H asymmetric bending in CH2 and CH3 groups), 1205 cm^{-1} (secondary -OH bending) [146]. Moreover, the large and intense band at 1120 cm^{-1} corresponds the superposition of in plane C-H bending, but also the characteristic Se-O stretching vibration, according to the literature [147]. Also, in the finger print region of FTIR spectrum of SeNPs, the peak at 657 cm^{-1} could indicate additional bending vibrations of Se-O bond [148]. From the FTIR spectra, an interaction between SeNPs and BSA protein is further confirmed by the shift in CH (1641 cm^{-1} to 1786

cm^{-1}), and CN (1523 cm^{-1} to 1664 cm^{-1}) peaks. Therefore, FTIR can confirm the fluctuations in non-covalent bonds[149]. This shift, fluctuations, confirm that non-covalent interactions between BSA and SeNPs. It is well known that free amine groups or cysteine residues the protein can bind to SeNPs that lead to the stabilization by surface-bound protein as BSA [117].

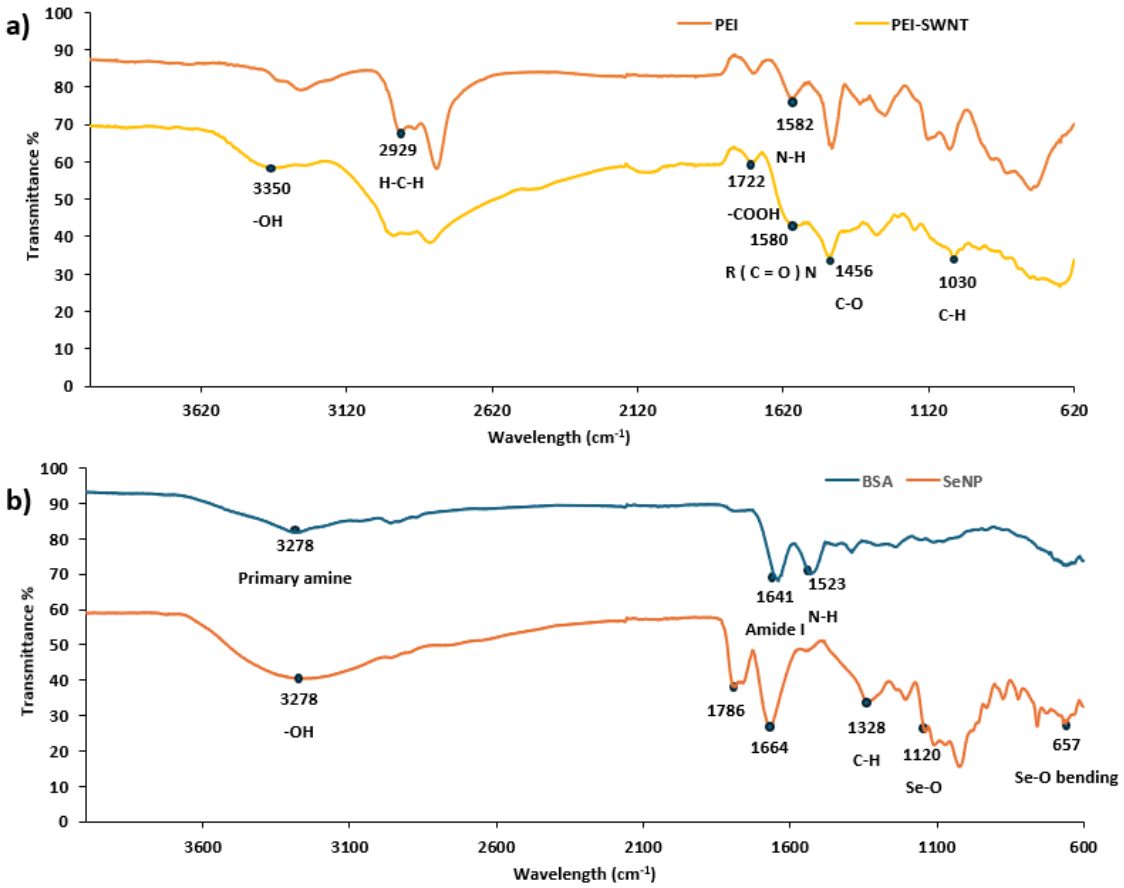

Figure 12: FTIR analysis result of (a)PEI-SWNTs and PEI. (b) SeNPs and BSA.

3.1.4. TGA Results of PEI-SWNTs and SeNPs

The thermal stability of PEI-SWNTs, PEI and CNT-COOH and SeNPs was assessed using TGA and displayed in Figure 13 as percentage weight loss with respect to increasing temperature. Through TGA, the quantity of PEI incorporated into PEI-SWNTs throughout the functionalization process could be measured. Pure PEI was completely vaporized at around 420°C, as seen in Figure 13 a. However, CNT-COOH showed gradual weight loss that reached 15% at 220◦C and 25% at 420◦C. The weight loss of PEI-SWNTs at 420◦C was 28%. The mass of PEI conjugated on PEI-SWNTs was therefore directly corelated with the

additional weight loss of PEI-SWNTs at 420°C relative to CNT-COOH [134]. Consequently, 3% (w/w) of the mass of PEI-SWNTs was ascribed to PEI. The finally obtained PEI-SWNTS thermal stability resembles that of CNT-COOH suggesting that the PEI coating had been destroyed (figure 13 a). The thermal stability of synthesized SeNPs was recorded by TGA from 10 °C to 800 °C at the heating rate of 10 °C/min under a nitrogen atmosphere. BSA-stabilized SeNPs showed 8-10 % weight losses observed until temperature reaches 150 ◦C possibly because of loss of moisture. Then serious weight losses were observed starting from 150 °C and reaching 70% by 500◦C because of SeNPs decomposition [150].

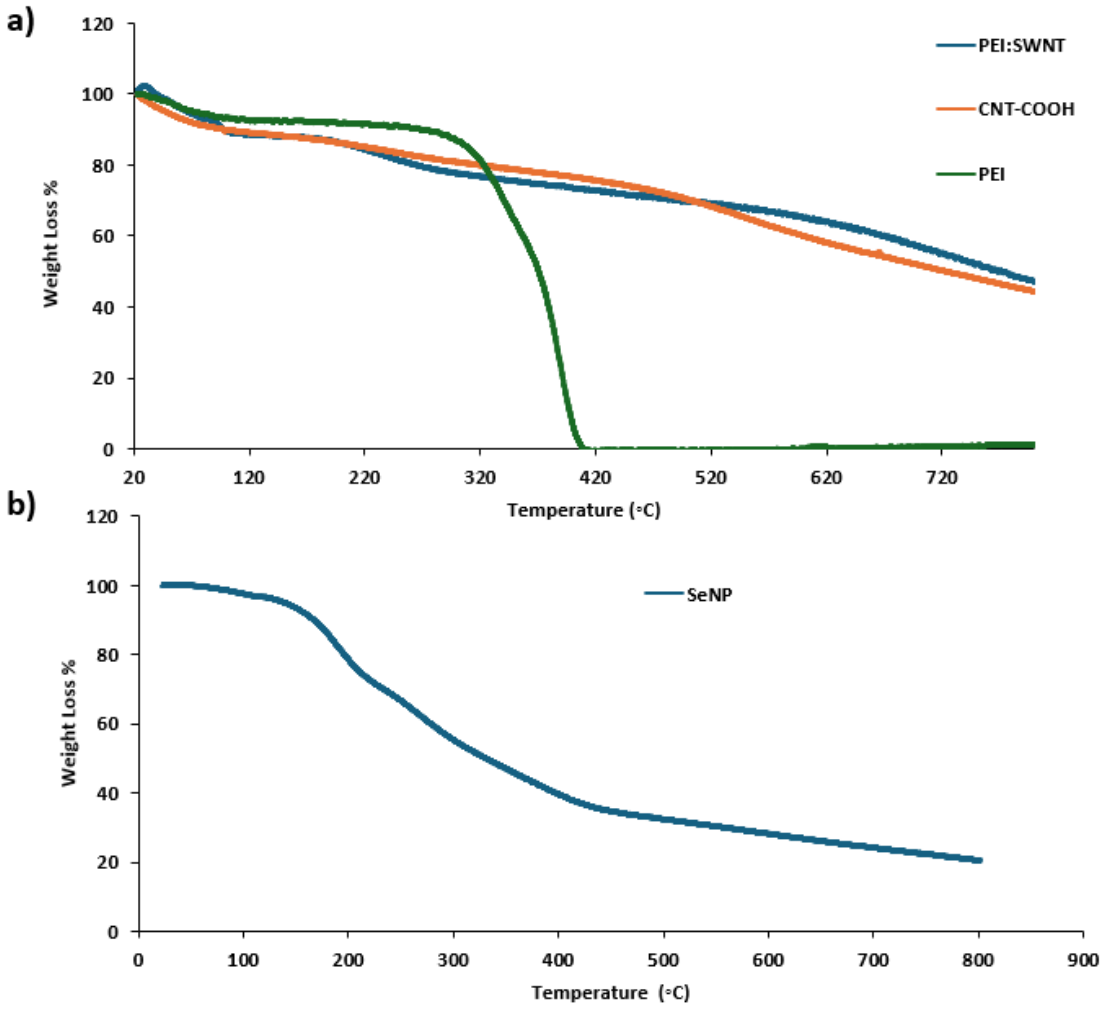

Figure 13: TGA results of a) PEI, SWNT and PEI-SWNTs b) SeNPs in nitrogen atmosphere

3.1.5. UV Absorbance Results of SeNPs

Figure 14 shows the UV-vis absorption spectra of the BSA and BSA-stabilized SeNPs from 200 nm to 800 nm wavelength. As seen, BSA possesses two peaks: one in the lower wavelength region (200-230 nm) and a broader peak in the higher wavelength region (260-290 nm), which is typical of proteins. For SeNPs UV absorption, max absorption was detected at 227 nm, just like BSA. However, as a difference from BSA, SeNPs also have a very broad absorption peak from 300 nm to 600 nm. Several studies have corroborated that the UV absorption peak of selenium nanoparticles is typically found in 200-300 nm spectral region. However, the precise location can vary due to factors such as particle size, shape, material composition, and local surroundings [151]. Numerous studies on the formation of SeNPs have identified multiple different absorption peaks in UV-vis spectra, suggesting the presence of SeNPs. In these studies, the peaks appeared at 290 nm [152],strong absorption band located at 265 nm [117]. It’s mentioned that the UV-visible spectra's characteristics directly correlate with selenium nanoparticles (SeNPs) sizes below 100 nm. Specifically, when the particle size is 100 nm or less, it gives a clear absorption maximum in the UV range [153]. Here according to DLS and TEM result, synthesized SeNPs are also smaller than 100 nm also as mentioned above, it gives clear absorption spectra in 200-300 nm. In Figure 14 the increasing absorption peak at 227nm and 350 nm to 600 nm wide absorption directly correlated with SeNPs. Between 200-300 nm BSA’s absorption peaks are also seen, however, characteristics of SeNPs clearly distinguishes. The light absorbed by SeNPs in the wavelength range of 300 to 550 nanometers may be connected to the existence of selenium in its elemental form at the nano-level. This presence of selenium in its elemental form is likely responsible for the majority of light absorption, attributed to exciton resonance effects. [154, 155].

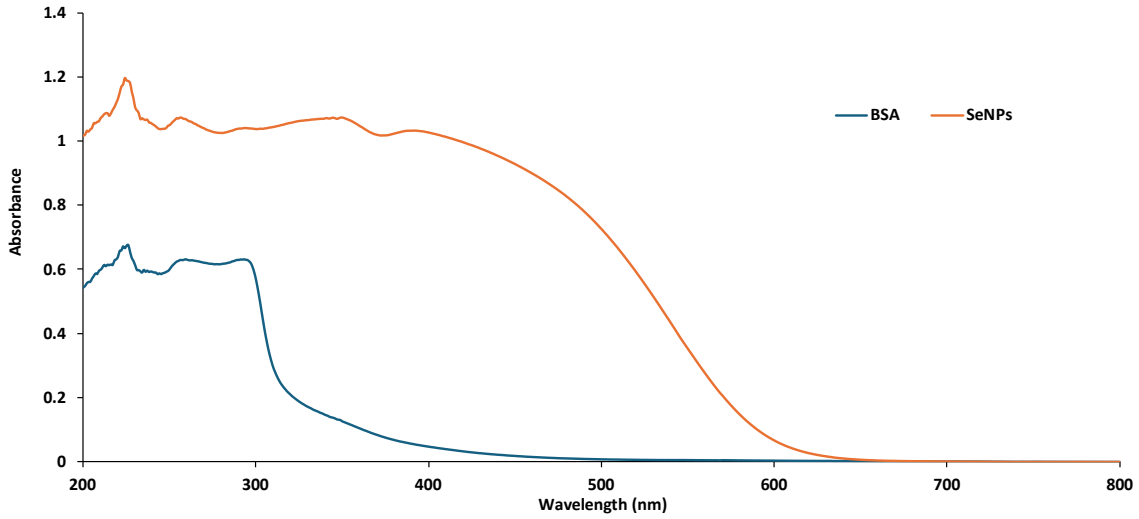

Figure 14: UV Absorbance analysis of SeNPs and BSA.

3.1.6. Fluorescence spectra of SeNPs

When light is applied to selenium nanoparticles, an exciton resonance or transition happens because of the absence of free conduction electrons in the metal [156]. The photoluminescence property of SeNPs is related to physical-chemical mechanisms, also depends on particle size, polydispersity, and the surrounding capping agents [132]. The sources and mechanisms behind light emission in nanoparticles vary significantly depending on whether they are made of metal, semiconductor, or insulator materials. Photoluminescence in metals typically arises from the excitation of d-electrons to the sp-conduction band [157]. Since Se shares several physical-chemical properties with metals, the strong fluorescence emission is observed as seen in Figure 15. The excitation of SeNPs in aqueous solution at 220 nm, the wavelength at maximum absorbance peak taken in UV analysis, led to the detection of fluorescence contributions in the 300–600 nm region. As shown in Figure 15. the peak intensity is at 437 nm and a maximum intensity broad band between 500–700 nm. The fluorescence intensities obtained match the images taken with the Confocal microscope of powder SeNPs. Figure 16. represents the confocal microscope images of powdered SeNPs to analyze its fluorescence at specific wavelengths used in microscopy. All images are taken at the same laser intensity and gain value but different channels that have different excitation status: in DAPI channel at 405 nm, in GFP channel at 475 nm, TAMRA channel at 552 nm. With respect to collected confocal images, SeNPs' fluorescence property reaches maximum at DAPI channel. As seen in Figure 16, the image taken in the DAPI channel gave more intense glowing than the image taken in the GFP and

TAMRA channels. In the DAPI channel, emission is collected from 405 nm to 600 nm. The maximum fluorescence intensity peak at 437 nm taken on the fluorescence spectrometer coincides with this. Secondly, the radiation received from the image is higher than that taken from the GFP channel. This can again be associated with the peak at 488 nm in the fluorescence spectrum because in the GFP channel, the emission spectrum is collected from 488 nm to 600 nm. However, the image taken from the Tamra channel did not receive as much radiation as the others. The total fluorescent intensity measured from randomly selected same sized squares of each images' fluorescent intensities are listed in Table 11.

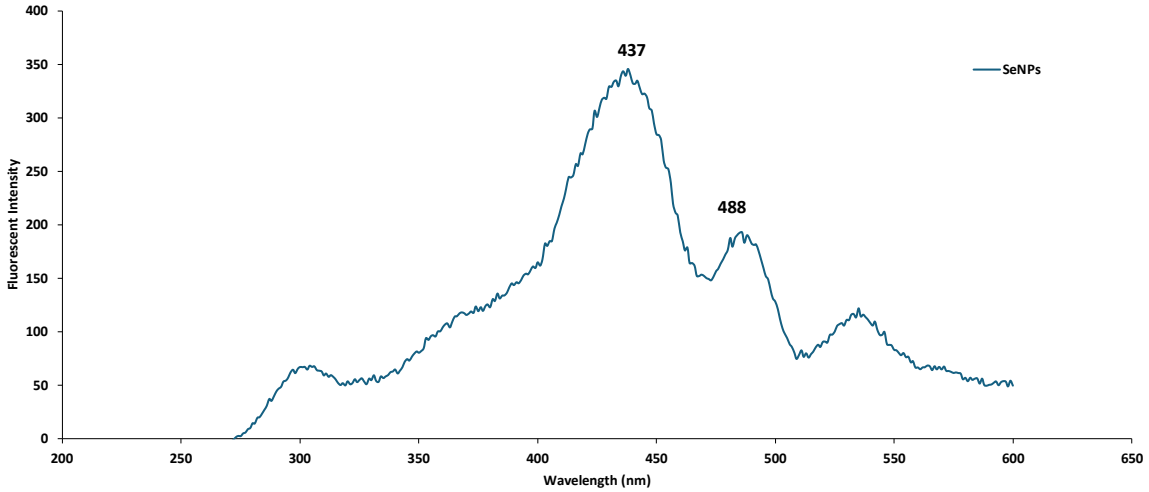

Figure 15: SeNPs fluorescent emission spectrum. Fluorescence intensity scale shown is in arbitrary units (A.U)

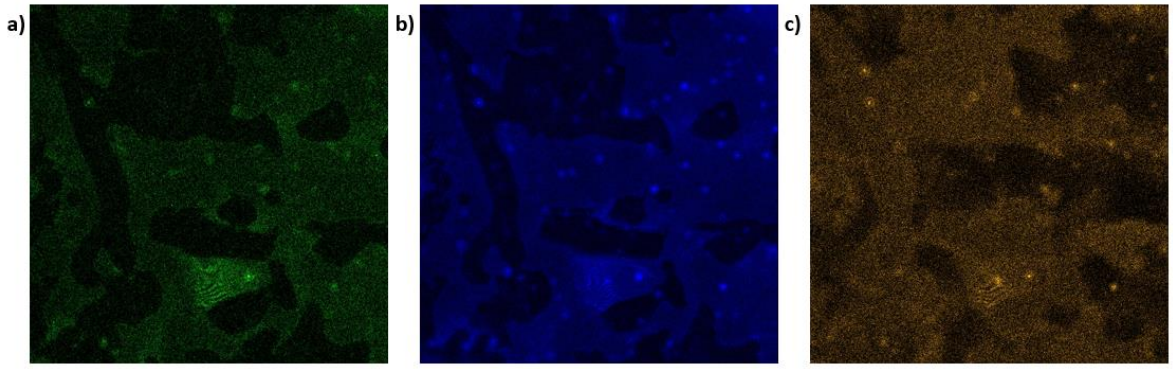

Figure 16: Confocal images of powder form SeNPs at a) EGFP channel b) DAPI channel c) Tamra channel wavelength

Table 11: Fluorescent Intensity values from same sized squares from Confocal images of SeNPs at different channels

Name	Fluorescent intensity
SeNPs in GFP channel	4
SeNPs in DAPI channel	19
SeNPs in TAMRA channel	3

3.2.DNA Binding Confirmation of PEI-SWNTs and SeNPs by Using DLS.

Positive surface charge allows interactions between PEI-SWNTs and negatively charged DNA material. To confirm these interactions and determine DNA binding capacity of NMs, DLS measurement is commonly used [158]. Efficient binding between negatively charged DNA molecules and positively charged NMs is achieved mostly by electrostatic and Van der Waals interactions [159]. In order to determine proper binding ratio for NMs to circular plasmid and linear GFP DNA cassettes, DLS zeta potential measurements are considered. For each specific plasmid or linear GFP DNA cassette these ratios should be optimized for efficient binding. Figure 17 shows binding of PEI-SWNTs to GFP Plasmid DNA (4145 bp) and linear GFP DNA cassette (1562 bp) tried at 3 different ratios (1:3,1:1,3.1). At 1:3 ratio of PEI-SWNTs: GFP Plasmid as expected by binding of negatively charged circular plasmid DNA surface charge shift to negative. However, as seen in Figure 17 a there are still non-bound PEI-SWNTs with a positive zeta potential. At the 1:1 ratio of PEI-SWNTs: GFP Plasmid, surface charge also shifted to less positive values but at 3:1 ratio of PEI-SWNTs: GFP Plasmid more shift was observed according to all 3 technical replicates of measurement. Table 12 indicates all average zeta potential values. Therefore, 3:1 PEI-SWNTs: GFP Plasmid binding ratio was chosen as the optimal binding ratio. For linear GFP DNA cassette binding to PEI-SWNTs 3 different ratios were also tested and the measured zeta potential for those shown in Figure 17 d, e and f. At 1:1 ratio of PEI-SWNTs: Linear GFP DNA cassette, more shift to negative surface charge is found even there are some non-bound PEI-SWNTs peak, choosing that ratio for PEI-SWNTs: Linear GFP DNA cassette binding is more logical. The all-average values of zeta potentials of 3 technical replicates of

measurement are displayed in Table 12. The cell membrane surface has a net negative charge [160], Therefore, it is hypothesized that this might potentially reject molecules with a negative charge. Therefore, achieving a zeta potential that is near to 0 is optimal for the transport of DNA.

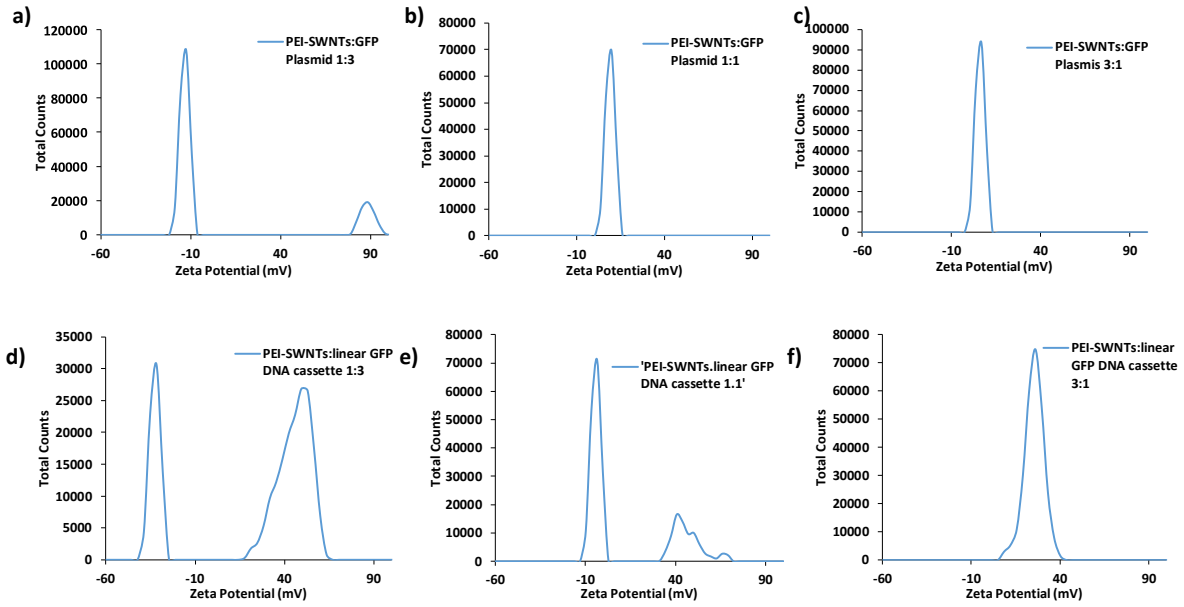

Figure 17 :DLS zeta potential measurements of PEI-SWNTs:GFP plasmid DNA and PEI-SWNTs: linear GFP DNA cassette at different ratio a)PEI-SWNTs:GFP plasmid 1:3 b) PEI-SWNTs:GFP plasmid 1:1 c) PEI-SWNTs:GFP plasmid 3:1 d) PEI-SWNTs: linear GFP DNA cassette 1:3 e) PEI-SWNTs: linear GFP DNA cassette 1:1 f) PEI-SWNTs: linear GFP DNA cassette 3:1

Table 12: DLS zeta potential measurements of PEI-SWNTs and its GFP Plasmid and linear GFP DNA cassette binding versions at different ratios.

Name	Zeta Potential	Standard deviation
PEI: SWNTs	64.36	1.586
PEI: SWNTs: GFP Plasmid 1:3	12.18	4.285
PEI: SWNTs: GFP Plasmid 1:1	8.864	2.055
PEI: SWNTs: GFP Plasmid 3:1	6.03	1.224
PEI-SWNTs: linear GFP DNA cassette 1:3	23.04	0.7812
PEI-SWNTs: linear GFP DNA cassette 1:1	10.42	2.401
PEI-SWNTs: linear GFP DNA cassette 3:1	26.28	2.762

Figure 18 indicates the DLS zeta potential measurements of SeNPs and GFP circular plasmid DNA and linear GFP DNA cassette binding at different ratios. Also, as for PEI-SWNTs, for each specific plasmid or linear GFP DNA cassette these ratios should be optimized for

efficient binding to SeNPs. According to the obtained zeta potential peaks and averages of 3 replicates of measurement which shown in table 13, 3:1 ratio for SeNPs: GFP plasmid DNA and 1:1 ratio for SeNPs: linear GFP DNA cassette DNA was chosen for further experiments. Optimal binding ratios can be achieved at different ratios for each different NMs and biomolecule cargo in various forms. The primary factor behind this is the correlation between the two structures, which is influenced by their surface charge, forms, and size. Circular plasmid DNA and linear DNA used here showed different binding rates with NMs because circular plasmid DNA has less surface to interact with NMs compared to linear DNA.

As for DNA loading capability, both SeNPs and PEI-SWNTs represent the same ratios for plasmid and linear DNA. In most of the DNA delivery applications with NMs use plasmid DNA because naked DNA molecules supposed that fragile, cannot the cell membrane and open to rapid degradation [161]. However, according to plasmid DNA their size as bp could be small and this could facilitate transport. PEI-SWNTs efficiency about plasmid DNA delivery [162] and RNA delivery [134]have stated in literature. Also, SeNPs shows significant efficiencies about RNA delivery in literature [163-165]. In addition, chemically synthesized SeNPs that coated with poly-L-lysine (PLL) in around 120 nm size can effectively deliver and protect plasmid DNA molecule [166]. Nevertheless, linear DNA delivery with both PEI-SWNTs and SeNPs hasn't been investigated. The reason behind this is naked DNA's unprotectedness for delivery. In this research, both plasmid and linear DNA delivery efficiency were investigated. For linear DNA loading capacity, 1.1 ratio between NMs and linear DNA is logical according to plasmid DNA loading capacity. The huge plasmid DNA needs more NMs to safely interact. However, linear forms of DNA have more appropriate surface to make connections with NMs. About plasmid DNA loading capability PEI-SWNTs seems more efficient because the zeta potential shift is highly huge from +64 to +6. The 3.1 ratio of PEI-SWNTs to plasmid DNA is compatible with Demirer's study [83]. SeNPs and plasmid DNA interactions stated that 1.1 ratio as efficient binding in Naidoo et all research [166]. However, in this study SeNPs size around 120 nm, thus could be provide making more interactions. In this study, synthesized SeNPs size around 27 nm, so, plasmid DNA requires more SeNPs to make efficient interactions. On the other hand, the huge plasmid DNA is circular, and SeNPs is also circular so, this could limit their surface electrostatic interactions.

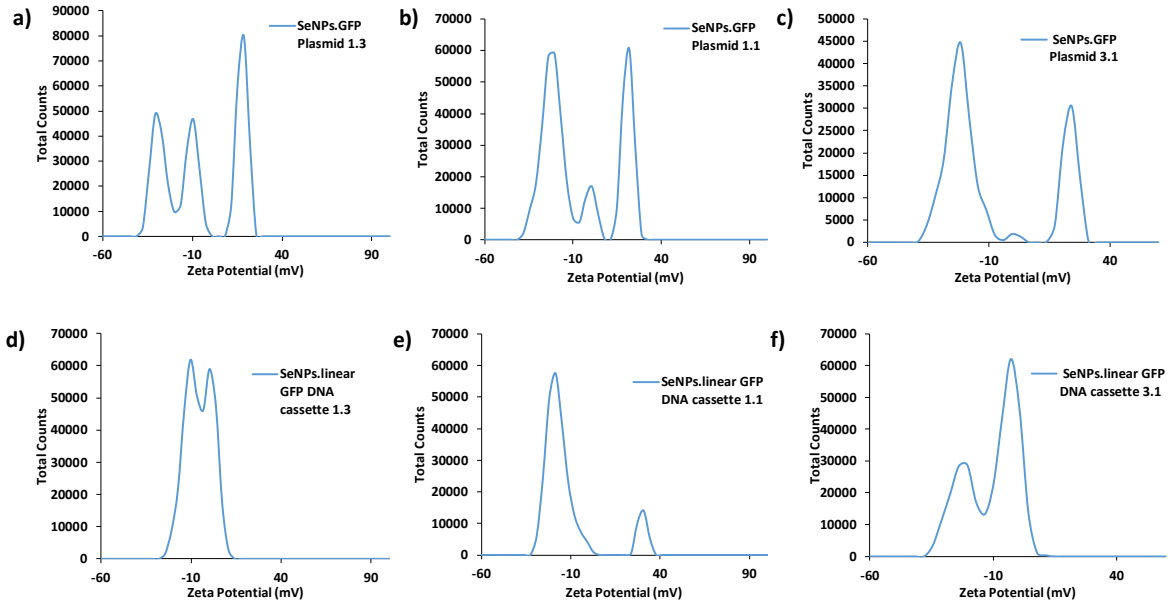

Figure 18 :DLS zeta potential measurements of SeNPs:GFP plasmid DNA and SeNPs: linear GFP DNA cassette DNA at different ratio a) SeNPs:GFP plasmid 1:3 b) SeNPs:GFP plasmid 1:1 c) SeNPs:GFP plasmid 3:1 d) SeNPs:linear GFP DNA cassette 1:3 e) SeNPs:linear GFP DNA cassette 1:1 f)) SeNPs:linear GFP DNA cassette 3:1

Table 13: DLS zeta potential measurements of SeNPs and its GFP plasmid and linear GFP DNA cassette binding versions at different ratios.

Name	Zeta Potential	Standard deviation
SeNPs fresh synthesis	8.491	5.236
SeNPs lyophilized	10.29	4.118
SeNPs: GFP plasmid 1:3	-5.42	0.896
SeNPs: GFP plasmid 1: 1	-7.211	1.572
SeNPs: GFP plasmid 3:1	-9.13	0.6948
SeNPs: linear GFP DNA cassette 1: 3	-6.804	2.057
SeNPs: linear GFP DNA cassette 1: 1	-10.79	1.171
SeNPs: linear GFP DNA cassette 3: 1	-7.553	2.799

3.3. Applications of PEI-SWNTs and SeNPs to *Arabidopsis thaliana* Leaves to Determine Toxic Effects.

PEI-SWNTs and SeNPs were applied to *Arabidopsis thaliana* plants at 4 different

concentrations, as well as a mock application with no NPs. These were 1 ng/uL, 5 ng/uL, 25 ng/uL, and 100 ng/uL for PEI-SWNTs. For SeNPs these concentrations were 100 ng/uL, 500 ng/uL, 1000 ng/uL, and 2500 ng/uL. These ratios were decided according to previous studies. Modified PEI-SWNTs stock concentration was 115 ng/uL which was determined by single wavelength absorbance measurement. The stock concentration of SeNPs (500 ng/uL) was prepared from 1 mg of lyophilized SeNPs dispersed in 2000uL dH_2O. Application to the *Arabidopsis thaliana* plant was performed using MES delivery buffer (pH:6) to *Arabidopsis thaliana* leaves, Silwet L-77 surfactant was used at 0.02 % (v/v) in 1000 uL application mix solution. To each leaf 50 uL application solution mix was applied. For each plant 3 fully expended leaves were chosen for application. In leaves surface application, NMs enter plant system through stomata. Stomata found on the surface of leaves play a vital role in controlling the exchange of water and gases within plants [40]. While certain plant species have stomata on both the top and lower epidermis, the majority of plant species only have stomata on the bottom epidermis [41]. In dicotyledonous plants like as *Arabidopsis thaliana*, when stomata were present on both surfaces of leaves, the number of stomata on the abaxial region (lower side of leaf) was approximately 1.4 times greater than that on the adaxial region (upper side of leaf) [38]. For that reason, applications of PEI-SWNTs were performed at abaxial (lower side) surface of leaves at 3 different 1 month old plants which grown in hydroponic system with Hoagland solution as described in Materials & Methods. The application was made at noon after the plants were watered with Hoagland solution because this is one of the times when the photosynthesis activity of the plants is highest. Changes in the rate of photosynthesis impact gas exchange in plants by influencing the opening and closing of stomata. When photosynthesis rates rise, there is a greater demand for carbon dioxide, this promotes stomata to open wider to facilitate increased gas exchange. In this context, with the application made when photosynthesis activity is high, NMs will enter easily through the opened stomata.

After the first day of application, some leaves were photographed. Figure 19 represents the first day after application leaves. As seen in Figure 19, compared to the negative control leaves PEI-SWNTs cause some necrosis at the end of the leaves at 5 ng/uL even first. At 25 ug/uL and 100 ng/uL PEI-SWNTs applied leaves obvious necrosis is observed even at first day. For SeNPs applied leaves more obvious necrosis start observed at higher level 2500 ng/uL concentration. However, some onset of necrosis was also observed at 1000 ng/uL concentration SeNPs applied leaf. On the first day after application the toxic threshold concentration of PEI-SWNTs for plant leaf is 5 ug/uL. However, for SeNPs this toxic

threshold concentration is 500 ng/uL. This 100 times difference at these concentrations of PEI-SWNTs and SeNPs is a clear proof of 100 times less toxic effect of SeNPs to *Arabidopsis thaliana* plants compared to PEI-SWNTs.

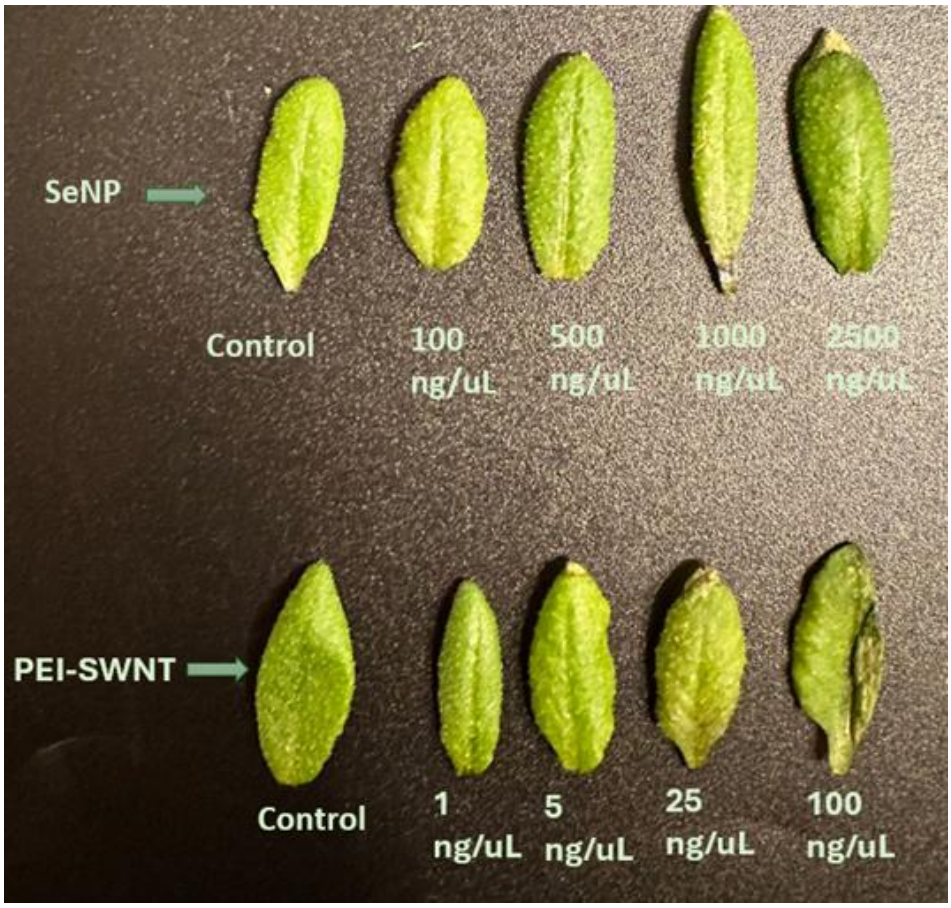

Figure 19: First day after PEI-SWNTs and SeNPs application to *Arabidopsis thaliana* leaves at 5 different concentrations.

After the third day of application again some leaves were photographed. Figure 20 shows some leaves after the 3rd day of application. As seen in Figure 20, results supporting the inferences obtained on the first day after the application were obtained. 5 ng/uL PEI-SWNTs applied leaves necrosis was progressed. 25 ng/uL and 100 ng/uL PEI-SWNTs applied leaves were about to die. However, necrosis at leaves tips which observed at 1000 ng/uL and 2500 ng/uL SeNPs applied leaves seems to remain at the same level. As a result, it was decided that 5 ng/uL PEI-SWNTs was the toxic threshold concentration for *Arabidopsis thaliana* plants, within the results of the 3rd day, which supported the results obtained on the first day. According to the results obtained for SeNPs, the toxic threshold concentration was determined as 500 ng/uL. According to literature, SeNPs in small size don't cause toxic symptoms even it increase yield on plant such as tomato[107]. However, in bigger size SeNPs lead to toxicity in chili plant [103]. This result signifies that size of SeNPs has role in

toxic effect. In this study, the size of SeNPs is small and its synthesis is composed of natural substances such as ascorbic acid and BSA. This also could be effective in its non-toxic effect in *Arabidopsis thaliana* leaves. Selenium elements are not a trace element and beneficial for plants, especially in high concentration. However, in nanoparticle form SeNPs cytotoxic effect is decreases. Selenium release or degradation possibly takes time and in the slow release as low dosage Selenium as an element benefits plant development. Dosage is also another important factor for toxicity, obtaining results indicates that until 500 ng/uL concentration there are no observable toxic effects. On the other hand, PEI-SWNTs cause severe toxic effects especially in higher concentrations. PEI as synthetic polymer could be the main reason for this toxicity. About toxic effect of CNT in plants there are several studies, some of them stated CNT leads toxic symptoms in plat. However, others signify positive effects of CNT in plant applications[167]. Various research states several factors such as concentration, size, plant type, growth stage can contribute to toxicity in plant[168]. Even CNT accepted as non-toxic, PEI functionalization lead toxic effect in PEI-SWNTs applied *Arabidopsis thaliana* leaves.

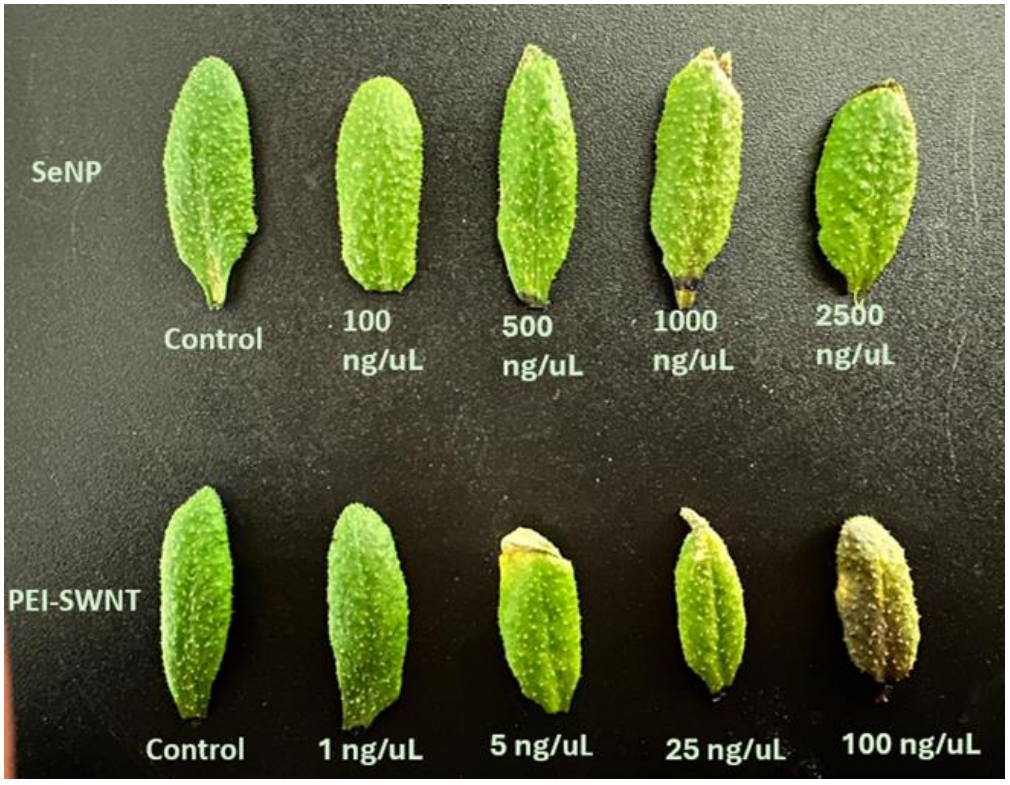

Figure 20: Third day after PEI-SWNTs and SeNPs application to *Arabidopsis thaliana* leaves at 5 different concentrations.

3.4. Obtaining GFP Plasmid DNA and Linear GFP DNA cassette

35s-EGFP-nosT plasmid is a bioengineered plasmid that contains a codon-optimized GFP reporter gene sequence and requires promoter and terminator regions for plant expression of the GFP gene. For Linear GFP DNA cassette production PCR was performed using M13 forward and reverse primers. Primers were decided according to a map of 35s-EGFP-nosT plasmid. The region between these primers also contains promoter and terminator regions. This means produced that the linear GFP DNA cassette can also be expressed in plant organisms. After obtaining those deliverable DNA materials, their expected size was confirmed with gel electrophoresis at 1% agar containing gel by 100 W for 30 minutes run. Figure 21 shows the gel electrophoresis result as gel image, as seen linear GFP DNA cassette is around 1.5kb so it moves more and GFP Plasmid around 4kb so it can move less as expected.

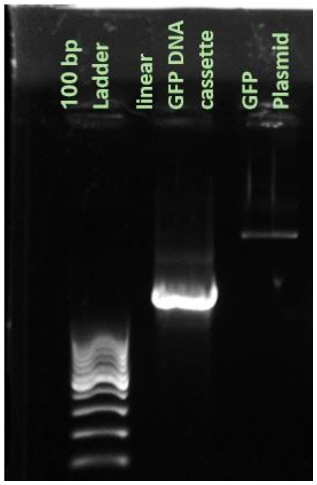

Figure 21: Gel image of linear GFP DNA cassette and GFP Plasmid

3.5. GFP Plasmid and Linear GFP DNA Cassette Bound PEI-SWNTs and SeNPs Application to The *Arabidopsis thaliana* Root.

Nanoparticles can also enter the plant system through root hairs. In order to test SeNPs and PEI-SWNTs gene delivery, *Arabidopsis thaliana* seeds were grown in MS culture. Then DNA bound NMs were applied to this MS culture. Certain research indicates that nanoparticles are taken up by plant roots and primarily penetrate cells via the hydrophilic pathway. However, the narrow pore size significantly limits the entry of nanoparticles into

cells through this route [169]. Endocytosis is another crucial method for NP uptake in plant cells. NPs enter cells through the plasma membrane of plant cells. Research has indicated that plant protoplasts possess the ability to internalize particles smaller than 1 μm by endocytosis; hence, the nanoparticles taken through endocytosis don't have particle size selectivity [170]. As a result of their studies, Liu and colleges suggested that carbon nanotubes were absorbed by endocytosis from the roots of the *Catharanthus roseus* plant [50]. Moreover, nanoparticles can be taken up by plants through interaction with transport proteins present on the outer epidermis [171]. According to these, it was aimed to compare the capacity of SeNPs and PEI-SWNTs in gene transfer from plant roots. For *Arabidopsis thaliana* root PEI-SWNTs, SeNPs and GFP Plasmid, linear GFP DNA cassette application solutions were also prepared with MES delivery buffer. However, unlike leaves Silwet surfactant was not used. 2 mL solutions were applied for each group. In each group approximately 10 MS cultured plants existed. Table 14 represents the root application solutions contents.

Table 14: Root application solutions contents

Name of application group	Nanomaterial amount (ng) in 2 mL	Amount of DNA to be delivered (ng)
Negative Control	-	-
PEI-SWNTs only	4500	-
SeNPs only	4500	-
GFP Plasmid only	-	1500
Linear GFP DNA cassette only	-	4500
PEI-SWNTs: GFP Plasmid	4500	1500
PEI-SWNTs: Linear GFP DNA cassette	4500	4500
SeNPs: GFP Plasmid	4500	1500

After 3 days post-application roots were analyzed by confocal microscopy. Figure 22 represents these confocal images. Many background signals can be obtained from plant tissues in confocal microscopy because of excitation of naturally occurring fluorophores such as lignin in tissues, photoreceptors in cells, and chlorophyll containing organelles [172]. Such structures emit an autofluorescence signal that may obscure the GFP signal that is expected to be detected. For this reason, root tissue was selected for analysis because autofluorescence caused by structures such as photoreceptors and chlorophyll were

eliminated because plant roots don’t have any photoreceptors or chlorophyll. However, autofluorescence from lignin is still present. For this reason, a certain signal was received even from the 'negative control' group without any application. Three confocal images were taken from each application group. These images were generally taken from the root tips. Typical images taken for each group are shown in Figure 22 Since at least some fluorescence signals were received from each group, all samples were examined with the same confocal settings in order to make comparisons, and the fluorescence intensity of the signals from all photographs taken was determined by sampling an equal sized 5 areas from each image. Figure 23 indicates the average mean intensity of 3 confocal images for each sample at same sized squares. According to the applied t-test results, all groups expect ‘PEI-SWNTs only’ have significant florescence signals compared to negative control. As seen in the graph, according to delivered DNA type, only linear GFP DNA cassette cause more GFP protein expression on roots. The reason behind this could be the size and shape of delivered DNA cargo. Plasmid size is bigger than linear one also its circular shape could prevent efficient integration thought out plant tissue. Also, the reason behind probably the applied amount because GFP plasmid amount 3 times lower than linear GFP DNA cassette. For PEI-SWNTs delivery efficiency, it promotes delivery of both types of DNA cargo. The applied t-test initiates that smaller p values (higher significancy) for ‘PEI-SWNTs: linear GFP DNA cassette’ group compared to ‘only linear GFP DNA cassette’ sample group values. However, for GFP plasmid delivery, the significancy also exists compared to ‘GFP plasmid only’ samples group. For SeNPs, there are also additional background signals because of SeNPs’ intrinsic fluorescence property. As seen in Figures 22 and 23, ‘only SeNPs’ applied samples gives relatively high signals compared to negative control. However, even its misleading signals, results indicates that it also promotes DNA cargo delivery especially for linear GFP DNA cassette. Compared to ‘only SeNPs’ sample fluorescent signals, SeNPs bound linear GFP DNA cassette applied to the root sample’s fluorescence gives the lowest p values, which means highly significant. About GFP Plasmid delivery, it seems not effective according to the fluorescent intensities and the applied t-test. The reliable comparison for PEI-SWNTs and SeNPs delivery efficiency for both types of DNA cargo could not be obtained from these results because of the contribution of absorbed SeNPs signals.

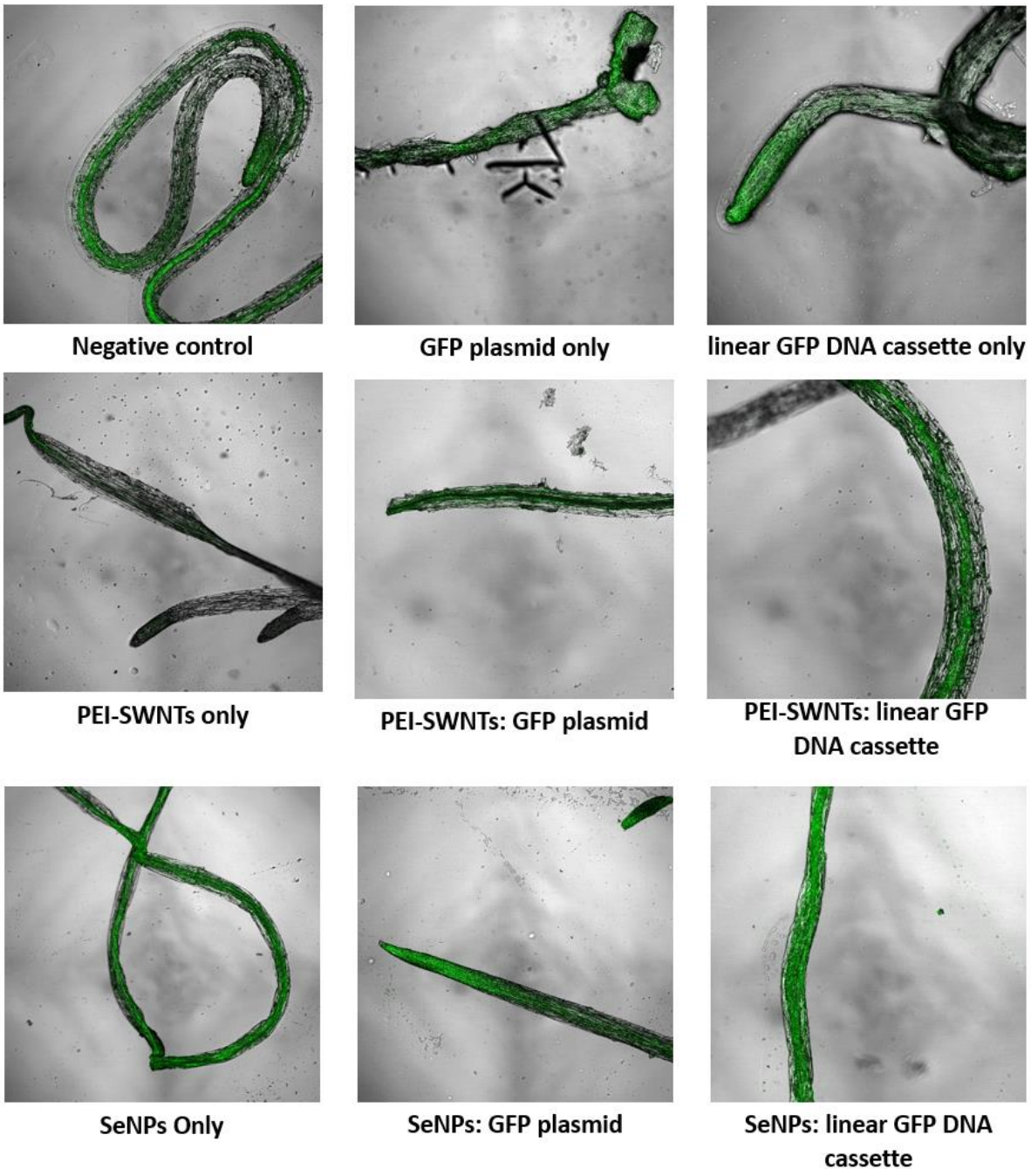

Figure 22 : *Arabidopsis thaliana* roots confocal images 3 days posy applications.

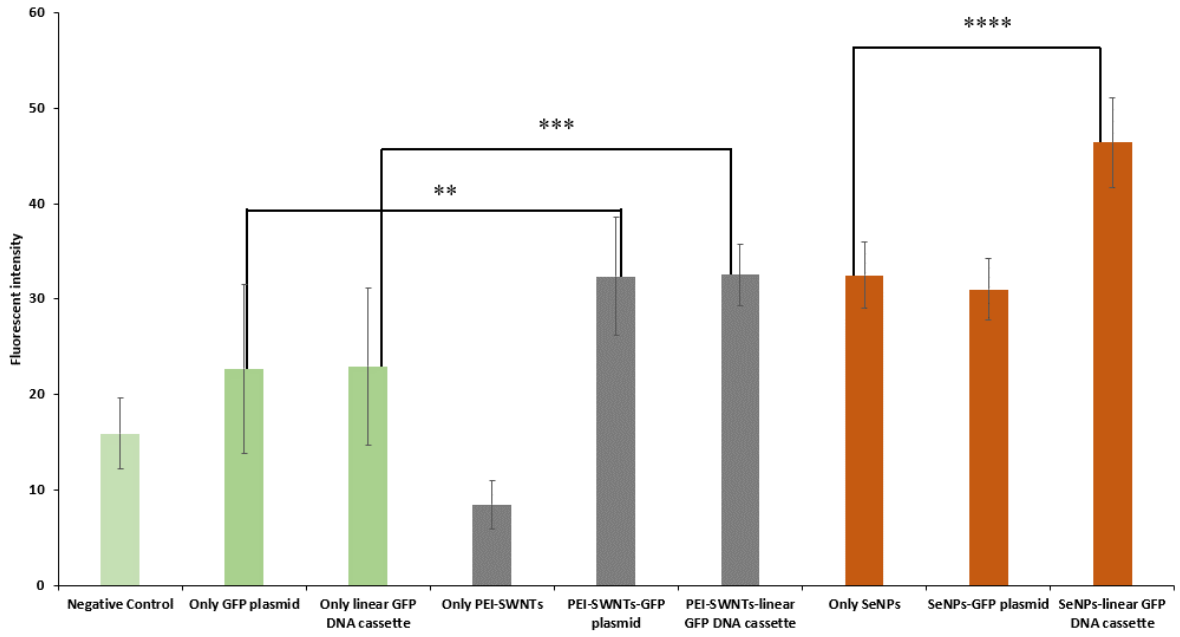

Figure 23: Fluorescent intensity values of 3 images of root samples. (n = 3, *p<0.05; **p< 0.01; ***p<0.001; ****p<0.0001)

3.6. GFP Plasmid and Linear GFP DNA Cassette Bound PEI-SWNTs and SeNPs Application to The *Arabidopsis thaliana* Leaves.

According to the toxicity results from phenotypes of leaves, 4.5ng/uL was chosen as the threshold for PEI-SWNTs. To compare PEI-SWNTs and SeNPs gene delivery efficiency this concentration was applied for both types of NPs. 1 mL of application solutions were prepared with MES delivery buffer. Table 15 represents the leaves application solutions contents. For SeNPs: linear GFP DNA cassette applications the amount was increased as ratio 5x and 10x separately. SeNPs also applied as 4.5ng/uL threshold however its low toxicity provides potential for higher application. For that reason, 5x and 10x times higher concentrations of SeNPs: linear DNA cassette was also applied to leaves. Each sample group was applied to 3 different plants and 5 leaves with 50uL of solution to each. Confocal images are taken from 3 leaves each from 3 different plants.

Table 15: Leaves application solutions contents

Name of application group	Nanomaterial amount (ng) in 1 mL	Amount of DNA to be delivered (ng)	Silwet L-77 (v/v)
Negative Control	-	-	-
PEI-SWNTs only	4500	-	%0.02
SeNPs only	4500	-	%0.02
GFP Plasmid only	-	1500	%0.02
Linear GFP DNA cassette only	-	4500	%0.02
PEI-SWNTs: GFP Plasmid	4500	1500	%0.02
PEI-SWNTs: linear GFP DNA cassette	4500	4500	%0.02
SeNPs: GFP Plasmid	4500	1500	%0.02
SeNPs: linear GFP DNA cassette 1x	4500	4500	%0.02
SeNPs: linear GFP DNA cassette 5x	22500	22500	%0.02
SeNPs: linear GFP DNA cassette 10x	45000	45000	%0.02

Prepared solutions were applied to 1 month old *Arabidopsis thaliana* plants. After 3 days of application, 3 leaves from 3 different plants were collected and placed between 2 microscope slides to take the confocal image for GFP reporter protein signals. 2 channels were used- TMPT and GFP with gain values of 325 and 450 respectively. 1024x1024 was the frame size and the scanning speed was 3. In order to eliminate autofluorescence from leaf structures, confocal parameters were set to give minimal signal in the negative control and the gain value of the GFP channel reduced 2 times compared to the root experiment. On the other hand, acquisition time was increased to get higher resolution images and eliminate the SeNPs florescence signal. The SeNPs' signals elimination is achieved by lower gain values in channels and increasing the acquisition time. By this way, only real GFP protein signals were collected. As seen in Figure 24 there was no signal from in the GFP channel for sample groups in which GFP DNA cargo was not applied. In the TMPT channel which provides

phase-contrast images the mesophyll layer of leaves was observed clearly. Collected GFP signals from related groups were also from this layer. There is a possibility that delivered DNA cargo transported or located at inner levels of leaves or in plant transportation system which could be both xylem and phloem. However, in that circumstance that GFP DNA cargo does not enter plant cell and remains in apoplast (extracellular space outside plant cell membranes) or in xylem the GFP expression does not occur, so any fluorescence signal cannot obtain. According to the confocal images which are presented in Figure 24, GFP expression was enhanced more with PEI-SWNTs: GFP plasmid compared to both 'only GFP Plasmid' and 'SeNPs: GFP Plasmid' samples. The higher positive surface potential of PEI-SWNTS and shape could be cause of this promotion about GFP plasmid delivery. There exists a possibility that thin long positive charged PWI-SWNTs are more proper to circular plasmid DNA binding. The established electrostatic interactions between NPs and DNA cargo also promote efficient delivery until plant cell and proper release inside the cell. PEI-SWNTs and DNA interactions are possibly quite optimal for delivering large circular plasmid to plant cells, and release inside cell. If the release is not occurring the GFP expression does not occur.

On the other hand, considering linear GFP DNA cassette delivery, both SeNPs and PEI-SWNTs seemed to be equally efficient. For 5x and 10x application of SeNPs: linear GFP DNA cassette, there was no significant difference in the signals obtained from the confocal.

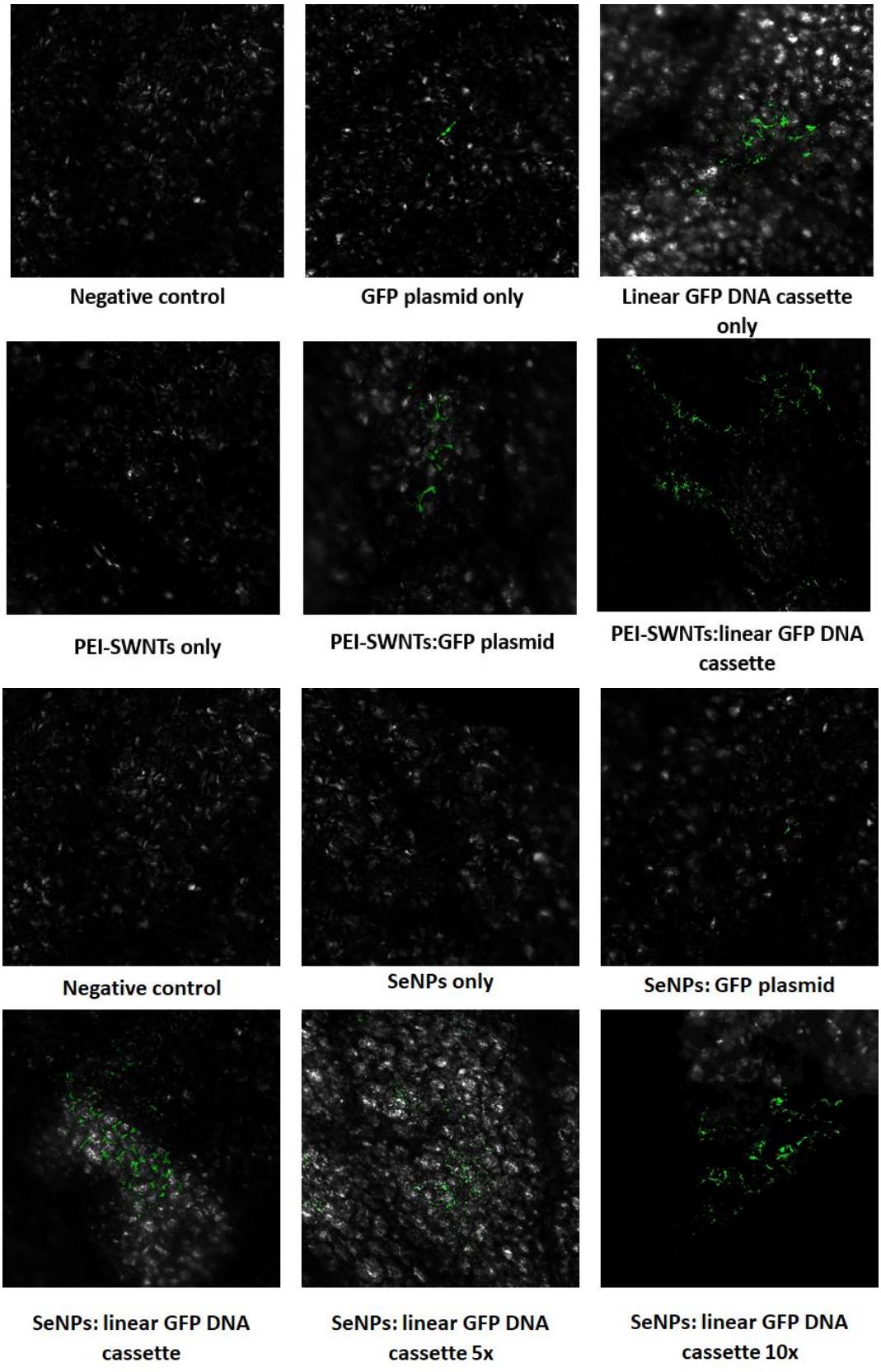

Figure 24: Confocal images of *Arabidopsis thaliana* leaves at 3 days post application

3.6.1. qPCR Analysis for GFP DNA Bound PEI-SWNTs and SeNPs Applied *Arabidopsis thaliana* Leaves.

After 3 days post-application, remaining leaves were harvested and stored at -80◦C for qPCR analysis, to give quantitative comparison of gene delivery for SeNPs and PEI-SWNTs gene delivery. Then, their RNAs were isolated and converted to cDNA. From the obtained cDNA, 20 ng were used to as PCR template into each well. For each experimental group 3 biological replicates were prepared and for each of these the qPCR analysis technical replicate number is also 3. In qPCR, RPL36 was the housekeeping gene and GFP was the target gene. The obtained qPCR results were normalized relative to the negative control group's ΔCt. Figure 25 shows the qPCR analysis results as log10 scale of fold change. The T-test was applied according to the negative control sample group. The obtained qPCR quantitative results and confocal results match reasonably. Thus, the GFP expression increase in the "Only linear GFP DNA cassette" and "PEI-SWNTs: linear GFP DNA cassette" applications significantly ($p<0.05$). In the only GFP plasmid and linear cassette results, the obtaining amplifications possibly come from residual GFP DNA's. Applied DNase I treatment was efficient however there are also a risk for residuals.

Moreover, in the "SeNPs: linear GFP DNA cassette x" and "SeNPs: linear GFP DNA cassette 5x" applications GFP expression significance value increase ($p<0.01$). According to the obtained results, GFP plasmid delivery PEI-SWNTs is more efficient than plasmid alone while SeNPs is not at all. Efficiency of PEI-SWNTs according to "Only GFP plasmid" application about GFP plasmid delivery is 78%. However, SeNPs obviously enhances uptake of the linear GFP DNA cassette more than PEI-SWNTs which gave similar results to the linear DNA cassette alone. PEI.SWNTs enhances linear GFP DNA cassette as 3% compared to "Only linear GFP DNA cassette" applications while SeNPs enhances delivery as 50.06%. Therefore, linear GFP DNA cassette delivery SeNPs 45% more efficient than PEI-SWNTs. For increasing ratios of SeNPs: linear GFP DNA cassette applications, observed GFP expression is also increasing. These indicate that SeNPs could be used for linear DNA cassette cargo efficiently. Also, by using its non-toxic effect even at higher ratios, desired amount of linear DNA cargo could be delivered. The fluorescent intensity results from root application and qPCR results are compatible with SeNPs' plasmid DNA delivery efficiency. According to fluorescent intensity data SeNPs' linear DNA cassette delivery efficiency could not be estimated properly because of SeNPs' fluorescence property. However, results are still concordant that SeNPs are more efficient for linear DNA cassette cargo than PEI-SWNTs. The reason behind that is probably the shape and binding efficiency of SeNPs and

plasmid DNA. PEI-SWNTs, which is long, thin and has a higher positive surface charge, can establish more stable interactions with large and circular plasmid DNA until it delivers the cargo to the cell. However, the interaction of small and less positive surface charged SeNPs, and large circular plasmid DNA is less stable up to this stage. Despite the different surface charges of two circular structures, their interaction is more difficult due to their shapes.

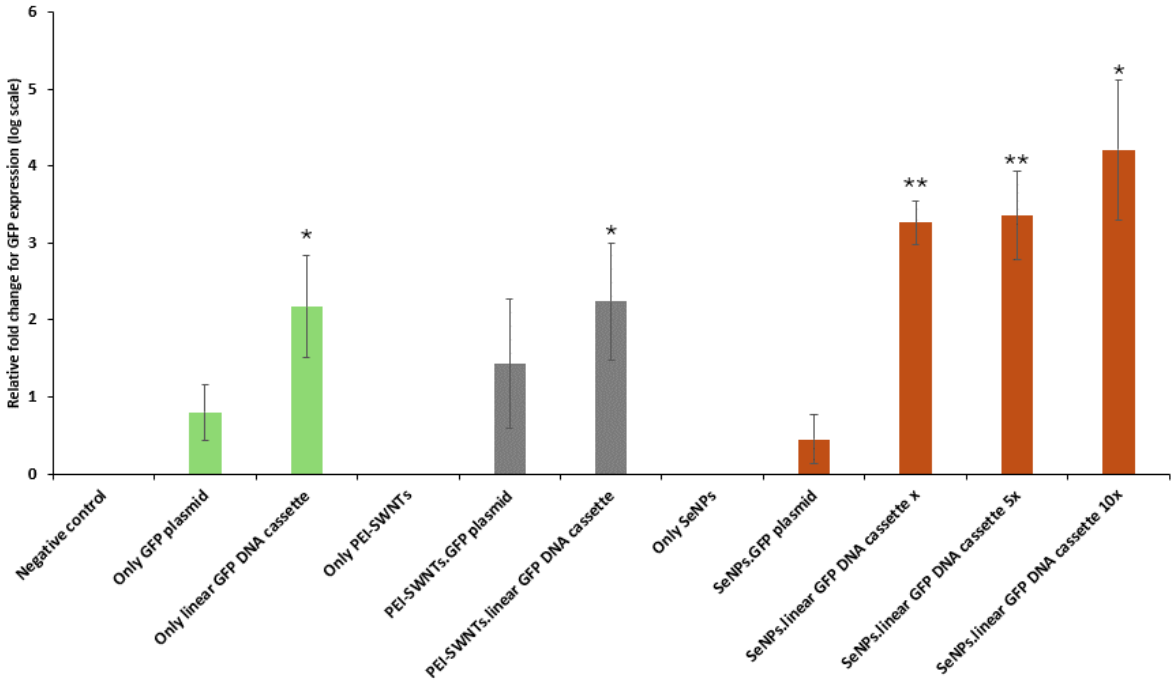

Figure 25 :qPCR analysis results of *Arabidopsis thaliana* leaves after 3 days of application. (n = 3, *p<0.05; **p< 0.01)

4. CONCLUSION

Climate change and the increasing world population are raising the demand for good quality food. However, traditional plant breeding methods are not fully efficient to produce stress- and pathogen-resistant, good nutritional quality plants for agricultural production. Plant biotechnology aims to introduce new and efficient methods for plant genetic engineering to overcome these problems in high yield crop production. One of the main obstacles for plant genetic engineering approaches inefficient and desired gene delivery because of the rigid plant cell wall. If genes which are able to provide genetic manipulation are efficiently delivered to plant cells, desired manipulations could be readily carried out. There are several gene delivery methods for plant systems, but they all have various limitations. Thus, nanoparticle-mediated gene delivery applications have been suggested over decades and have recently also been applied to plant biotechnology. CNTs and their various functionalized forms are one of the most used nanomaterials for gene delivery in plants. However, they cause toxic symptoms in plant tissues. Thus, non-toxic and even beneficial nanoparticle quest are rising for plant gene delivery applications, however, they also should pass though the plant cell wall. To meet this requirement, selenium nanoparticles (SeNPs), which are widely used especially in mammalian cells due to their beneficial effects, were synthesized with relatively natural substances by chemical synthesis method in this study, and the SeNPs efficiency for delivering plasmid and linear GFP DNA cargo from the roots and leaves of *Arabidopsis thaliana*, was investigated. This effect was investigated by comparison with polyethyleneimine functionalized carbon nanotube (PEI-SWNT) mediated delivery. The synthesized SeNPs size is around 20 nm as seen in TEM images, which allows for passage through the plant cell wall while its positive charged surface allows for making interactions with DNA cargo. SeNPs cause 100 times lower toxicity symptoms compared to PEI-SWNTs in leaves applications. GFP DNA delivery allows expressed GFP protein glowing in applied plant tissue by confocal microscopy. Also, GFP expression levels were analyzed with qPCR to get quantitative results. In conclusion, the SeNPs show 45 % more efficiency in linear DNA molecule delivery compared to PEI-SWNTs. In contrast, the SeNPs

were not as effective in plasmid DNA delivery to plant tissue, whereas PEI-SWNTs were more effective. However, despite linear DNA's perceived vulnerability, SeNPs can efficiently deliver it, so, it's possible that it could be protective for its cargo. With further studies, the effectiveness of SeNPs for plant genetic engineering studies in other plant species and whether they protect their cargo can be investigated.

5.BIBLIOGRAPHY

1. Fujii, Y. and Y. Kodama, *In planta comparative analysis of improved green fluorescent proteins with reference to fluorescence intensity and bimolecular fluorescence complementation ability.* Plant Biotechnology, 2015. **32**(1): p. 81-87.
2. Ray, D.K., et al., *Yield trends are insufficient to double global crop production by 2050.* PloS one, 2013. **8**(6): p. e66428.
3. Rosenzweig, C., et al., *Assessing agricultural risks of climate change in the 21st century in a global gridded crop model intercomparison.* Proceedings of the national academy of sciences, 2014. **111**(9): p. 3268-3273.
4. Prohens, J., *Plant breeding: a success story to be continued thanks to the advances in genomics.* Frontiers in plant science, 2011. **2**: p. 51.
5. Datta, A., *Genetic engineering for improving quality and productivity of crops.* Agriculture & Food Security, 2013. **2**: p. 1-3.
6. Venugopal, P.D. and G.P. Dively, *Climate change, transgenic corn adoption and field-evolved resistance in corn earworm.* Royal Society Open Science, 2017. **4**(6): p. 170210.
7. Kissoudis, C., et al., *Enhancing crop resilience to combined abiotic and biotic stress through the dissection of physiological and molecular crosstalk.* Frontiers in plant science, 2014. **5**: p. 90871.
8. Lin, W., et al., *Genetic engineering of rice for resistance to sheath blight.* Bio/technology, 1995. **13**(7): p. 686-691.
9. Patil, V.U., et al., *Genetic engineering for enhanced nutritional quality in potato-a review.* 2017.
10. Jat, S.K., J. Bhattacharya, and M.K. Sharma, *Nanomaterial based gene delivery: a promising method for plant genome engineering.* Journal of Materials Chemistry B, 2020. **8**(19): p. 4165-4175.
11. Zhi, H., et al., *The promising nanovectors for gene delivery in plant genome engineering.* International journal of molecular sciences, 2022. **23**(15): p. 8501.
12. Abdallah, N.A., C.S. Prakash, and A.G. McHughen, *Genome editing for crop improvement: challenges and opportunities.* GM Crops & Food, 2015. **6**(4): p. 183-205.
13. Gelvin, S.B., *Integration of Agrobacterium T-DNA into the plant genome.* Annual review of genetics, 2017. **51**: p. 195-217.
14. Zhang, Y., et al., *Efficient and transgene-free genome editing in wheat through transient expression of CRISPR/Cas9 DNA or RNA.* Nature communications, 2016. **7**(1): p. 12617.
15. Liu, J., et al., *Genome-scale sequence disruption following biolistic transformation in rice and maize.* The Plant Cell, 2019. **31**(2): p. 368-383.
16. Oard, J., *Physical methods for the transformation of plant cells.* Biotechnology advances, 1991. **9**(1): p. 1-11.

17. Yoo, S.-D., Y.-H. Cho, and J. Sheen, *Arabidopsis mesophyll protoplasts: a versatile cell system for transient gene expression analysis.* Nature protocols, 2007. **2**(7): p. 1565-1572.
18. Ma, X., et al., *Highly efficient DNA-free plant genome editing using virally delivered CRISPR–Cas9.* Nature Plants, 2020. **6**(7): p. 773-779.
19. Burch-Smith, T.M., et al., *Efficient virus-induced gene silencing in Arabidopsis.* Plant physiology, 2006. **142**(1): p. 21-27.
20. Mehrotra, S. and V. Goyal, *Agrobacterium-mediated gene transfer in plants and biosafety considerations.* Applied biochemistry and biotechnology, 2012. **168**: p. 1953-1975.
21. Sanford, J.C., *Biolistic plant transformation.* Physiologia Plantarum, 1990. **79**(1): p. 206-209.
22. Kempken, F. and C. Jung, *Genetic modification of plants: agriculture, horticulture and forestry*. Vol. 64. 2009: Springer Science & Business Media.
23. Eeckhaut, T., et al., *Progress in plant protoplast research.* Planta, 2013. **238**: p. 991-1003.
24. Cunningham, F.J., et al., *Nanoparticle-mediated delivery towards advancing plant genetic engineering.* Trends in biotechnology, 2018. **36**(9): p. 882-897.
25. Mohanraj, V. and Y. Chen, *Nanoparticles-a review.* Tropical journal of pharmaceutical research, 2006. **5**(1): p. 561-573.
26. Zeng, X., R. Morgenstern, and A.M. Nyström, *Nanoparticle-directed sub-cellular localization of doxorubicin and the sensitization breast cancer cells by circumventing GST-mediated drug resistance.* Biomaterials, 2014. **35**(4): p. 1227-1239.
27. Salata, O.V., *Applications of nanoparticles in biology and medicine.* Journal of nanobiotechnology, 2004. **2**: p. 1-6.
28. Khan, I., K. Saeed, and I. Khan, *Nanoparticles: Properties, applications and toxicities.* Arabian journal of chemistry, 2019. **12**(7): p. 908-931.
29. Liu, W.-T., *Nanoparticles and their biological and environmental applications.* Journal of bioscience and bioengineering, 2006. **102**(1): p. 1-7.
30. Chaudhry, N., et al., *Bio-inspired nanomaterials in agriculture and food: Current status, foreseen applications and challenges.* Microbial pathogenesis, 2018. **123**: p. 196-200.
31. Duhan, J., et al., *Nanotechnology: the new perspective in precision agriculture. Biotechnol Rep 15: 11–23*. 2017.
32. DeRosa, M.C., et al., *Nanotechnology in fertilizers.* Nature nanotechnology, 2010. **5**(2): p. 91-91.
33. Lv, J., P. Christie, and S. Zhang, *Uptake, translocation, and transformation of metal-based nanoparticles in plants: recent advances and methodological challenges.* Environmental Science: Nano, 2019. **6**(1): p. 41-59.
34. Shang, Y., et al., *Applications of nanotechnology in plant growth and crop protection: a review.* Molecules, 2019. **24**(14): p. 2558.
35. Torabian, S., M. Zahedi, and A.H. Khoshgoftar, *Effects of foliar spray of nano-particles of FeSO4 on the growth and ion content of sunflower under saline condition.* Journal of Plant Nutrition, 2017. **40**(5): p. 615-623.
36. Tripathi, D.K., et al., *Silicon nanoparticles more effectively alleviated UV-B stress than silicon in wheat (Triticum aestivum) seedlings.* Plant Physiology and Biochemistry, 2017. **110**: p. 70-81.
37. Kim, D.H., J. Gopal, and I. Sivanesan, *Nanomaterials in plant tissue culture: the disclosed and undisclosed.* RSC advances, 2017. **7**(58): p. 36492-36505.
38. Wang, X., et al., *Nanoparticles in plants: Uptake, transport and physiological activity in leaf and root.* Materials, 2023. **16**(8): p. 3097.

39. Yang, C., et al., *Antimicrobial nanoemulsion formulation with improved penetration of foliar spray through citrus leaf cuticles to control citrus huanglongbing.* PloS one, 2015. **10**(7): p. e0133826.
40. Ha, N., et al., *Adsorption of nanoparticles suspended in a drop on a leaf surface of Perilla frutescens and their infiltration through stomatal pathway.* Scientific Reports, 2021. **11**(1): p. 11556.
41. Driscoll, S., et al., *Specification of adaxial and abaxial stomata, epidermal structure and photosynthesis to CO2 enrichment in maize leaves.* Journal of experimental botany, 2006. **57**(2): p. 381-390.
42. Peng, C., et al., *Translocation and biotransformation of CuO nanoparticles in rice (Oryza sativa L.) plants.* Environmental Pollution, 2015. **197**: p. 99-107.
43. Rajput, V., et al., *Accumulation of nanoparticles in the soil-plant systems and their effects on human health.* Annals of Agricultural Sciences, 2020. **65**(2): p. 137-143.
44. Mann, C.W., et al., *RNA-based control of fungal pathogens in plants.* International Journal of Molecular Sciences, 2023. **24**(15): p. 12391.
45. Law, S.S.Y., T. Miyamoto, and K. Numata, *Organelle-targeted gene delivery in plants by nanomaterials.* Chemical Communications, 2023. **59**(47): p. 7166-7181.
46. Demirer, G.S., et al., *High aspect ratio nanomaterials enable delivery of functional genetic material without DNA integration in mature plants.* Nature nanotechnology, 2019. **14**(5): p. 456-464.
47. Gumustas, M., et al., *Effect of polymer-based nanoparticles on the assay of antimicrobial drug delivery systems*, in *Multifunctional systems for combined delivery, biosensing and diagnostics*. 2017, Elsevier. p. 67-108.
48. Zhang, H., et al., *Nanoparticle cellular internalization is not required for RNA delivery to mature plant leaves.* Nature nanotechnology, 2022. **17**(2): p. 197-205.
49. Hussain, H.I., et al., *Mesoporous silica nanoparticles as a biomolecule delivery vehicle in plants.* Journal of Nanoparticle Research, 2013. **15**: p. 1-15.
50. Liu, Q., et al., *Carbon nanotubes as molecular transporters for walled plant cells.* Nano letters, 2009. **9**(3): p. 1007-1010.
51. Koo, Y., et al., *Fluorescence reports intact quantum dot uptake into roots and translocation to leaves of Arabidopsis thaliana and subsequent ingestion by insect herbivores.* Environmental science & technology, 2015. **49**(1): p. 626-632.
52. Kurepa, J., et al., *Uptake and distribution of ultrasmall anatase TiO2 Alizarin red S nanoconjugates in Arabidopsis thaliana.* Nano letters, 2010. **10**(7): p. 2296-2302.
53. González-Melendi, P., et al., *Nanoparticles as smart treatment-delivery systems in plants: assessment of different techniques of microscopy for their visualization in plant tissues.* Annals of botany, 2008. **101**(1): p. 187-195.
54. Tripathi, D.K., et al., *An overview on manufactured nanoparticles in plants: uptake, translocation, accumulation and phytotoxicity.* Plant physiology and biochemistry, 2017. **110**: p. 2-12.
55. Zuverza-Mena, N., et al., *Exposure of engineered nanomaterials to plants: Insights into the physiological and biochemical responses-A review.* Plant Physiology and Biochemistry, 2017. **110**: p. 236-264.
56. Sanzari, I., A. Leone, and A. Ambrosone, *Nanotechnology in plant science: to make a long story short.* Frontiers in Bioengineering and Biotechnology, 2019. **7**: p. 120.
57. Gao, M., et al., *Advances in transport and toxicity of nanoparticles in plants.* Journal of Nanobiotechnology, 2023. **21**(1): p. 75.
58. Torney, F., et al., *Mesoporous silica nanoparticles deliver DNA and chemicals into plants.* Nature nanotechnology, 2007. **2**(5): p. 295-300.

59. Martin-Ortigosa, S., et al., *Mesoporous silica nanoparticle-mediated intracellular Cre protein delivery for maize genome editing via loxP site excision.* Plant physiology, 2014. **164**(2): p. 537-547.
60. Martin-Ortigosa, S., et al., *Gold functionalized mesoporous silica nanoparticle mediated protein and DNA codelivery to plant cells via the biolistic method.* Advanced Functional Materials, 2012. **22**(17): p. 3576-3582.
61. Zhao, X., et al., *Pollen magnetofection for genetic modification with magnetic nanoparticles as gene carriers.* Nature plants, 2017. **3**(12): p. 956-964.
62. Finiuk, N., et al., *Investigation of novel oligoelectrolyte polymer carriers for their capacity of DNA delivery into plant cells.* Plant Cell, Tissue and Organ Culture (PCTOC), 2017. **131**: p. 27-39.
63. Naqvi, S., et al., *Calcium phosphate nanoparticle mediated genetic transformation in plants.* Journal of Materials Chemistry, 2012. **22**(8): p. 3500-3507.
64. Burlaka, O., et al., *Plant genetic transformation using carbon nanotubes for DNA delivery.* Cytology and genetics, 2015. **49**(6): p. 349-357.
65. Chang, F.-P., et al., *A simple plant gene delivery system using mesoporous silica nanoparticles as carriers.* Journal of Materials Chemistry B, 2013. **1**(39): p. 5279-5287.
66. Hao, Y., et al., *Magnetic gold nanoparticles as a vehicle for fluorescein isothiocyanate and DNA delivery into plant cells.* Botany, 2013. **91**(7): p. 457-466.
67. Jiang, L., et al., *Systemic gene silencing in plants triggered by fluorescent nanoparticle-delivered double-stranded RNA.* Nanoscale, 2014. **6**(17): p. 9965-9969.
68. Dresselhaus, M.S. and P. Avouris, *Introduction to carbon materials research*, in *Carbon nanotubes: synthesis, structure, properties, and applications*. 2001, Springer. p. 1-9.
69. Cha, C., et al., *Carbon-based nanomaterials: multifunctional materials for biomedical engineering.* ACS nano, 2013. **7**(4): p. 2891-2897.
70. Iijima, S. and T. Ichihashi, *Single-shell carbon nanotubes of 1-nm diameter.* nature, 1993. **363**(6430): p. 603-605.
71. Dresselhaus, M., G. Dresselhaus, and P. Eklund, *Carbon materials.* Science of Fullerenes and Carbon Nanotubes, 1996: p. 15-59.
72. Wang, N., et al., *Single-walled 4 Å carbon nanotube arrays.* Nature, 2000. **408**(6808): p. 50-51.
73. Hamada, N., S.-i. Sawada, and A. Oshiyama, *New one-dimensional conductors: Graphitic microtubules.* Physical review letters, 1992. **68**(10): p. 1579.
74. Burlaka, O.M., et al. *Application of carbon nanotubes for plant genetic transformation*. in *Nanocomposites, Nanophotonics, Nanobiotechnology, and Applications: Selected Proceedings of the Second FP7 Conference and International Summer School Nanotechnology: From Fundamental Research to Innovations, August 25-September 1, 2013, Bukovel, Ukraine*. 2015. Springer.
75. Riley, M.K. and W. Vermerris, *Recent advances in nanomaterials for gene delivery—a review.* Nanomaterials, 2017. **7**(5): p. 94.
76. Cañas, J.E., et al., *Effects of functionalized and nonfunctionalized single-walled carbon nanotubes on root elongation of select crop species.* Environmental Toxicology and Chemistry: An International Journal, 2008. **27**(9): p. 1922-1931.
77. Nakayama-Ratchford, N., et al., *Noncovalent functionalization of carbon nanotubes by fluorescein− polyethylene glycol: supramolecular conjugates with pH-dependent absorbance and fluorescence.* Journal of the American Chemical Society, 2007. **129**(9): p. 2448-2449.
78. Serag, M.F., et al., *Introducing carbon nanotubes into living walled plant cells through cellulase-induced nanoholes.* RSC advances, 2012. **2**(2): p. 398-400.

79. Kwak, S.-Y., et al., *Chloroplast-selective gene delivery and expression in planta using chitosan-complexed single-walled carbon nanotube carriers.* Nature nanotechnology, 2019. **14**(5): p. 447-455.
80. Ochoa-Olmos, O.E., et al., *Transformation of plant cell suspension cultures with amine-functionalized multi-walled carbon nanotubes.* Journal of Nanoscience and Nanotechnology, 2016. **16**(7): p. 7461-7471.
81. Golestanipour, A., et al., *Gene delivery to tobacco root cells with single-walled carbon nanotubes and cell-penetrating fusogenic peptides.* Molecular biotechnology, 2018. **60**: p. 863-878.
82. Ghaghelestany, A.B., A. Jahanbakhshi, and E. Taghinezhad, *Gene transfer to German chamomile (L chamomilla M) using cationic carbon nanotubes.* Scientia Horticulturae, 2020. **263**: p. 109106.
83. Demirer, G.S., et al., *Carbon nanotube–mediated DNA delivery without transgene integration in intact plants.* Nature Protocols, 2019. **14**(10): p. 2954-2971.
84. Yemul, O. and T. Imae, *Synthesis and characterization of poly (ethyleneimine) dendrimers.* Colloid and Polymer Science, 2008. **286**: p. 747-752.
85. Vancha, A.R., et al., *Use of polyethyleneimine polymer in cell culture as attachment factor and lipofection enhancer.* BMC biotechnology, 2004. **4**: p. 1-12.
86. Boussif, O., et al., *A versatile vector for gene and oligonucleotide transfer into cells in culture and in vivo: polyethylenimine.* Proceedings of the National Academy of Sciences, 1995. **92**(16): p. 7297-7301.
87. Akinc, A., et al., *Exploring polyethylenimine-mediated DNA transfection and the proton sponge hypothesis.* The Journal of Gene Medicine: A cross-disciplinary journal for research on the science of gene transfer and its clinical applications, 2005. **7**(5): p. 657-663.
88. Kieliszek, M., *Selenium–fascinating microelement, properties and sources in food.* Molecules, 2019. **24**(7): p. 1298.
89. Bodnar, M., P. Konieczka, and J. Namiesnik, *The properties, functions, and use of selenium compounds in living organisms.* Journal of Environmental Science and Health, Part C, 2012. **30**(3): p. 225-252.
90. Araie, H. and Y. Shiraiwa, *Selenium in algae.* The physiology of microalgae, 2016: p. 281-288.
91. Vinković Vrček, I., *Selenium nanoparticles: Biomedical applications.* Selenium, 2018: p. 393-412.
92. Bisht, N., P. Phalswal, and P.K. Khanna, *Selenium nanoparticles: A review on synthesis and biomedical applications.* Materials Advances, 2022. **3**(3): p. 1415-1431.
93. Maiyo, F. and M. Singh, *Selenium nanoparticles: Potential in cancer gene and drug delivery.* Nanomedicine, 2017. **12**(9): p. 1075-1089.
94. Bano, I., et al., *Uses of selenium nanoparticles in the plant production.* Agronomy, 2021. **11**(11): p. 2229.
95. Feng, R., C. Wei, and S. Tu, *The roles of selenium in protecting plants against abiotic stresses.* Environmental and experimental botany, 2013. **87**: p. 58-68.
96. Garza-García, J.J., et al., *The role of selenium nanoparticles in agriculture and food technology.* Biological trace element research, 2022: p. 1-21.
97. Schiavon, M., et al., *Selenium fertilization alters the chemical composition and antioxidant constituents of tomato (Solanum lycopersicon L.).* Journal of Agricultural and Food Chemistry, 2013. **61**(44): p. 10542-10554.
98. Schiavon, M. and E.A. Pilon-Smits, *The fascinating facets of plant selenium accumulation–biochemistry, physiology, evolution and ecology.* New Phytologist, 2017. **213**(4): p. 1582-1596.

99. White, P.J., *Selenium metabolism in plants.* Biochimica et Biophysica Acta (BBA)-General Subjects, 2018. **1862**(11): p. 2333-2342.
100. Mangiapane, E., A. Pessione, and E. Pessione, *Selenium and selenoproteins: an overview on different biological systems.* Current Protein and Peptide Science, 2014. **15**(6): p. 598-607.
101. Cheng, B., et al., *Multiomics understanding of improved quality in cherry radish (Raphanus sativus L. var. radculus pers) after foliar application of selenium nanomaterials.* Science of The Total Environment, 2022. **824**: p. 153712.
102. Skalickova, S., et al., *Selenium nanoparticles as a nutritional supplement.* Nutrition, 2017. **33**: p. 83-90.
103. Sotoodehnia-Korani, S., et al., *Selenium nanoparticles induced variations in growth, morphology, anatomy, biochemistry, gene expression, and epigenetic DNA methylation in Capsicum annuum; an in vitro study.* Environmental Pollution, 2020. **265**: p. 114727.
104. Domokos-Szabolcsy, E., et al., *Accumulation of red elemental selenium nanoparticles and their biological effects in Nicotinia tabacum.* Plant Growth Regulation, 2012. **68**: p. 525-531.
105. Hussein, H.-A.A., et al., *Evaluation of cytotoxicity, biochemical profile and yield components of groundnut plants treated with nano-selenium.* Biotechnology Reports, 2019. **24**: p. e00377.
106. Juárez-Maldonado, A., et al., *Nanoparticles and nanomaterials as plant biostimulants.* International journal of molecular sciences, 2019. **20**(1): p. 162.
107. Hernández-Hernández, H., et al., *Impact of selenium and copper nanoparticles on yield, antioxidant system, and fruit quality of tomato plants.* Plants, 2019. **8**(10): p. 355.
108. Ramamurthy, C., et al., *Green synthesis and characterization of selenium nanoparticles and its augmented cytotoxicity with doxorubicin on cancer cells.* Bioprocess and biosystems engineering, 2013. **36**: p. 1131-1139.
109. Gunti, L., R.S. Dass, and N.K. Kalagatur, *Phytofabrication of selenium nanoparticles from Emblica officinalis fruit extract and exploring its biopotential applications: antioxidant, antimicrobial, and biocompatibility.* Frontiers in microbiology, 2019. **10**: p. 451408.
110. Abinaya, M., et al., *Microbial exopolymer-capped selenium nanowires–Towards new antibacterial, antibiofilm and arbovirus vector larvicides?* Journal of Photochemistry and Photobiology B: Biology, 2019. **192**: p. 55-67.
111. Bharathi, S., et al., *Extracellular synthesis of nanoselenium from fresh water bacteria Bacillus sp., and its validation of antibacterial and cytotoxic potential.* Biocatalysis and agricultural biotechnology, 2020. **27**: p. 101655.
112. Borowska, M., E. Pawlik, and K. Jankowski, *Investigation of interaction between biogenic selenium nanoparticles and human serum albumin using microwave plasma optical emission spectrometry operating in a single-particle mode.* Monatshefte für Chemie-Chemical Monthly, 2020. **151**: p. 1283-1290.
113. Hashem, A.H., et al., *Biomedical applications of mycosynthesized selenium nanoparticles using Penicillium expansum ATTC 36200.* Biological trace element research, 2021: p. 1-11.
114. Fardsadegh, B. and H. Jafarizadeh-Malmiri, *Aloe vera leaf extract mediated green synthesis of selenium nanoparticles and assessment of their in vitro antimicrobial activity against spoilage fungi and pathogenic bacteria strains.* Green Processing and Synthesis, 2019. **8**(1): p. 399-407.

115. Khoei, N.S., et al., *Insights into selenite reduction and biogenesis of elemental selenium nanoparticles by two environmental isolates of Burkholderia fungorum.* New biotechnology, 2017. **34**: p. 1-11.
116. Prasad, K.S., et al., *Biosynthesis of Se nanoparticles and its effect on UV-induced DNA damage.* Colloids and Surfaces B: Biointerfaces, 2013. **103**: p. 261-266.
117. El-Deeb, B., et al., *Biological synthesis and structural characterization of selenium nanoparticles and assessment of their antimicrobial properties.* American Scientific Research Journal for Engineering, Technology, and Sciences, 2018. **45**(1): p. 135-170.
118. Nie, T., et al., *Facile synthesis of highly uniform selenium nanoparticles using glucose as the reductant and surface decorator to induce cancer cell apoptosis.* Journal of Materials Chemistry B, 2016. **4**(13): p. 2351-2358.
119. Tran, P.A., et al., *Low cytotoxic trace element selenium nanoparticles and their differential antimicrobial properties against S. aureus and E. coli.* Nanotechnology, 2015. **27**(4): p. 045101.
120. Zhang, Y., J. Wang, and L. Zhang, *Creation of highly stable selenium nanoparticles capped with hyperbranched polysaccharide in water.* Langmuir, 2010. **26**(22): p. 17617-17623.
121. Yu, S., et al., *The inhibitory effect of selenium nanoparticles on protein glycation in vitro.* Nanotechnology, 2015. **26**(14): p. 145703.
122. Shin, Y., et al., *Synthesis and stabilization of selenium nanoparticles on cellulose nanocrystal.* Materials Letters, 2007. **61**(21): p. 4297-4300.
123. Abbasian, R. and H. Jafarizadeh-Malmiri, *Green approach in gold, silver and selenium nanoparticles using coffee bean extract.* Open Agriculture, 2020. **5**(1): p. 761-767.
124. Xia, Y.-Y., *Synthesis of selenium nanoparticles in the presence of silk fibroin.* Materials Letters, 2007. **61**(21): p. 4321-4324.
125. Meyerowitz, E.M., *Arabidopsis thaliana.* Annual review of genetics, 1987. **21**(1): p. 93-111.
126. Meinke, D.W., et al., *Arabidopsis thaliana: a model plant for genome analysis.* Science, 1998. **282**(5389): p. 662-682.
127. Sparrow, A., H. Price, and A. Underbrink, *A survey of DNA content per cell and per chromosome of prokaryotic and eukaryotic organisms: some evolutionary considerations.* 1972.
128. Sheen, J., et al., *Green-fluorescent protein as a new vital marker in plant cells.* The plant journal, 1995. **8**(5): p. 777-784.
129. Stewart, C., *The utility of green fluorescent protein in transgenic plants.* Plant cell reports, 2001. **20**: p. 376-382.
130. Hoagland, D.R. and D.I. Arnon, *The water-culture method for growing plants without soil.* Circular. California agricultural experiment station, 1950. **347**(2nd edit).
131. Khalid, K., R. Ishak, and Z.Z. Chowdhury, *UV–Vis spectroscopy in non-destructive testing*, in *Non-Destructive Material Characterization Methods*. 2024, Elsevier. p. 391-416.
132. Khalid, A., et al., *Intrinsic fluorescence of selenium nanoparticles for cellular imaging applications.* Nanoscale, 2016. **8**(6): p. 3376-3385.
133. Parkinson, S.J., et al., *Polymer nanoparticles pass the plant interface.* Nature Communications, 2022. **13**(1): p. 7385.
134. Huang, Y.-P., et al., *Delivery of small interfering RNAs in human cervical cancer cells by polyethylenimine-functionalized carbon nanotubes.* Nanoscale research letters, 2013. **8**: p. 1-11.

135. Moradian, H., et al., *Poly (ethyleneimine) functionalized carbon nanotubes as efficient nano-vector for transfecting mesenchymal stem cells.* Colloids and Surfaces B: Biointerfaces, 2014. **122**: p. 115-125.
136. Danaei, M., et al., *Impact of particle size and polydispersity index on the clinical applications of lipidic nanocarrier systems.* Pharmaceutics, 2018. **10**(2): p. 57.
137. Manojlović-Stojanoski, M., et al., *The effects of BSA-stabilized selenium nanoparticles and sodium selenite supplementation on the structure, oxidative stress parameters and selenium redox biology in rat placenta.* International Journal of Molecular Sciences, 2022. **23**(21): p. 13068.
138. Gatto, M.S. and W. Najahi-Missaoui, *Lyophilization of Nanoparticles, Does It Really Work? Overview of the Current Status and Challenges.* International Journal of Molecular Sciences, 2023. **24**(18): p. 14041.
139. Smirnova, E., et al., *Multi-walled carbon nanotubes penetrate into plant cells and affect the growth of Onobrychis arenaria seedlings.* Acta Naturae (англоязычная версия), 2011. **3**(1 (8)): p. 99-106.
140. Xu, R., et al., *Preparing sodium alginate/polyethyleneimine spheres for potential application of killing tumor cells by reducing the concentration of copper ions in the lesions of colon cancer.* Materials, 2019. **12**(9): p. 1570.
141. Liu, S., et al., *Characteristics of aniline and nitrobenzene adsorption on single-walled, multi-walled and graphitized multi-walled carbon nanotubes.* Current Science, 2019. **117**(4): p. 683-689.
142. Hu, H., et al., *Polyethyleneimine functionalized single-walled carbon nanotubes as a substrate for neuronal growth.* The Journal of Physical Chemistry B, 2005. **109**(10): p. 4285-4289.
143. Retnakumari, A., et al., *Molecular-receptor-specific, non-toxic, near-infrared-emitting Au cluster-protein nanoconjugates for targeted cancer imaging.* Nanotechnology, 2009. **21**(5): p. 055103.
144. Nairi, V., et al., *Interactions between bovine serum albumin and mesoporous silica nanoparticles functionalized with biopolymers.* Chemical Engineering Journal, 2018. **340**: p. 42-50.
145. Boroumand, S., et al., *Selenium nanoparticles: synthesis, characterization and study of their cytotoxicity, antioxidant and antibacterial activity.* Materials Research Express, 2019. **6**(8): p. 0850d8.
146. Safaei, M., et al., *Optimization of green synthesis of selenium nanoparticles and evaluation of their antifungal activity against oral Candida albicans infection.* Advances in Materials Science and Engineering, 2022. **2022**: p. 1-8.
147. Kannan, S., et al., *Synthesis of selenium nanorods with assistance of biomolecule.* Bulletin of Materials Science, 2014. **37**: p. 1631-1635.
148. Fritea, L., et al., *Green biosynthesis of selenium nanoparticles using parsley (Petroselinum crispum) leaves extract.* Studia Universitatis" Vasile Goldis" Arad. Seria Stiintele Vietii (Life Sciences Series), 2017. **27**(3): p. 203-208.
149. Palanisamy, A. and V. Veerappan, *Impact of pH and Sucralose on the Non-Covalent Interaction of Ovalbumin: FT-IR Analysis.* 2023.
150. Zhang, W., et al., *Synthesis and antioxidant properties of Lycium barbarum polysaccharides capped selenium nanoparticles using tea extract.* Artificial cells, nanomedicine, and biotechnology, 2018. **46**(7): p. 1463-1470.
151. Joshi, M., A. Bhattacharyya, and S.W. Ali, *Characterization techniques for nanotechnology applications in textiles.* 2008.
152. Hemalatha, T., et al., *Preparation and characterization of hydroxyapatite-coated selenium nanoparticles and their interaction with osteosarcoma (SaOS-2) cells.* Acta Metallurgica Sinica (English Letters), 2014. **27**: p. 1152-1158.

153. Visha, P., et al., *Biosynthesis and structural characteristics of selenium nanoparticles using Lactobacillus acidophilus bacteria by wet sterilization process.* International Journal of Advanced Veterinary Science and Technology, 2015. **4**(1): p. 178-183.
154. Kerker, M., *The scattering of light and other electromagnetic radiation*. 2016: Elsevier.
155. Islam, S.K., M.A. Sohel, and J.R. Lombardi, *Coupled exciton and charge-transfer resonances in the Raman enhancement of phonon modes of CdSe quantum dots (QDs).* The Journal of Physical Chemistry C, 2014. **118**(33): p. 19415-19421.
156. Nayak, V., et al., *Potentialities of selenium nanoparticles in biomedical science.* New Journal of Chemistry, 2021. **45**(6): p. 2849-2878.
157. Piacenza, E., et al., *Tunable photoluminescence properties of selenium nanoparticles: biogenic versus chemogenic synthesis.* Nanophotonics, 2020. **9**(11): p. 3615-3628.
158. Yiu, H.H., et al., *Comprehensive study of DNA binding on iron (II, III) oxide nanoparticles with a positively charged polyamine three-dimensional coating.* Langmuir, 2013. **29**(36): p. 11354-11365.
159. Paillusson, F., et al., *Effective interaction between charged nanoparticles and DNA.* Physical Chemistry Chemical Physics, 2011. **13**(27): p. 12603-12613.
160. Nishino, M., et al., *Measurement and visualization of cell membrane surface charge in fixed cultured cells related with cell morphology.* PLoS One, 2020. **15**(7): p. e0236373.
161. Song, H., et al., *Plasmid DNA delivery: nanotopography matters.* Journal of the American Chemical Society, 2017. **139**(50): p. 18247-18254.
162. Behnam, B., et al., *Non-covalent functionalization of single-walled carbon nanotubes with modified polyethyleneimines for efficient gene delivery.* International journal of pharmaceutics, 2013. **454**(1): p. 204-215.
163. Wang, C., et al., *Silencing of MEF2D by siRNA loaded selenium nanoparticles for ovarian cancer therapy.* International journal of nanomedicine, 2020: p. 9759-9770.
164. Xia, Y., et al., *siRNA-loaded selenium nanoparticle modified with hyaluronic acid for enhanced hepatocellular carcinoma therapy.* International journal of nanomedicine, 2018: p. 1539-1552.
165. Maiyo, F. and M. Singh, *Polymerized selenium nanoparticles for folate-receptor-targeted delivery of anti-luc-siRNA: Potential for gene silencing.* Biomedicines, 2020. **8**(4): p. 76.
166. Naidoo, S., et al., *Poly-L-lysine–lactobionic acid-capped selenium nanoparticles for liver-targeted gene delivery.* International Journal of Molecular Sciences, 2022. **23**(3): p. 1492.
167. Mathew, S., D. Tiwari, and D. Tripathi, *Interaction of carbon nanotubes with plant system: A review.* Carbon Letters, 2021. **31**(2): p. 167-176.
168. Dasgupta-Schubert, N., et al., *Plant responses to nano and micro structured carbon allotropes: water imbibition by maize seeds upon exposure to multiwalled carbon nanotubes and activated carbon.* Advances in nano research, 2017. **5**(3): p. 245.
169. Li, L., et al., *Effective uptake of submicrometre plastics by crop plants via a crack-entry mode.* Nature sustainability, 2020. **3**(11): p. 929-937.
170. Ma, X. and J. Yan, *Plant uptake and accumulation of engineered metallic nanoparticles from lab to field conditions.* Current opinion in environmental science & health, 2018. **6**: p. 16-20.
171. Grillo, R., et al., *Foliage adhesion and interactions with particulate delivery systems for plant nanobionics and intelligent agriculture.* Nano Today, 2021. **37**: p. 101078.
172. Andrew, W. and B. Nicholas, *Distinguishing GFP from cellular auto fluorescence.* Analytical Biochemistry, 2001. **291**: p. 175-197.